DEVELOPMENT OF A NANOMATERIAL-TISSUE PATCH FOR VASCULAR AND CARDIAC RECONSTRUCTION

A Dissertation Presented to the

Faculty of the Graduate School

at the University of Missouri

In Partial Fulfillment

Of the Requirements for the Degree

Doctor of Philosophy

---

by

ALLISON M. OSTDIEK

Dr. Sheila A. Grant, Dissertation Supervisor

DECEMBER 2014

The undersigned, appointed by the Dean of the Graduate School, have examined the dissertation entitled

DEVELOPMENT OF A NANOMATERIAL-TISSUE PATCH FOR VASCULAR AND CARDIAC RECONSTRUCTION

Presented by Allison M. Ostdiek

A candidate for the degree of Doctor of Philosophy

And hereby certify that in their opinion it is worthy of acceptance.

_____

Dr. Sheila Grant
Department of Biological Engineering

_____

Dr. Raghuraman Kannan
Department of Radiology

_____

Dr. Craig Franklin
Department of Veterinary Pathobiology

_____

Dr. Catherine Hagan
College of Veterinary Pathobiology

_____

Dr. W. Kirt Nichols
Department of Vascular Surgery

DEDICATIONS

This dissertation is dedicated to my grandmother, Lorraine.

You always asked the important questions, even when they were the hard ones.

ACKNOWLEDGEMENTS

First, I would like to thank my advisor, Dr. Sheila Grant, for her amazing mentorship and support. Being part of the Grant Lab has shown me how well research functions when directed by a positive, effective leader. I would like to acknowledge Dr. Craig Franklin for facilitating an excellent residency program that allowed me to explore my research interests and for his support of this project. In addition I would like to acknowledge the members of my committee, Dr. Catherine Hagan for her help with pathology and imaging, Dr. Kannan for his knowledge of nanoparticles and federal guidelines, and Dr. Nichols for his input on current medical technologies. Everyone on the committee has been overwhelmingly helpful and available with their time.

Next, I would like to acknowledge the members of the Grant Lab. I came into this lab with minimal knowledge on how to characterize biomaterials and all were willing to teach me. Dave Grant is an excellent lab manager and always able to troubleshoot problems. Matt Cozad and Carrie Schmitt first made me welcome in the lab and answered every question I asked, even the obvious ones. Sarah Smith has been a great lab and office mate and can always be counted on to remind me of the important things. Aaron Wood has helped with my animal studies and as a resource for characterization methods.

The *in vivo* work I did would not have been possible without a great team. Dr. Raja Gopaldas worked with us to develop studies and materials, and performed the vascular aspects of the surgeries. Jan Ivey helped organize all of

the *in vivo* work and without her resources and time the project would have never moved forward. Dr. Cindy Besch-Williford and the histology department at IDEXX bioresearch spent hours with me to find the best staining techniques and the MU Cytology Core did a fantastic job with the confocal imaging.

I would like to acknowledge all the contributions made by the Comparative Medicine Program and the Office of Animal Resources. Drs. Scott Korte, Erin O'Connor, and Beth Ahner contributed a great deal of time helping with anesthesia and explantation. Dr. Sarah Hansen is a valuable resource for anesthesia and ultrasound. The other residents in the program and numerous vet students also contributed to this project through help with surgery and veterinary care. Dana Weir and the husbandry staff took excellent care of the animas.

Funding for the project has come from the NIH T32 training grant, Food for the Twenty-First Century Grant, and from the Departments of Bioengineering and Surgery.

Finally I would like to thank my family and friends, which has come to include all of the aforementioned people. Kevin Milligan not only edited the majority of this dissertation, but supported me on the days the research wasn't going very smoothly. My parents and sister have always encouraged my education. Thank you all for your constant support, without it none of this would have been possible. And of course, the pigs.

Table of Contents

List of Figures

Figure

List of Tables

Table

DEVELOPMENT OF A NANOMATERIAL-TISSUE PATCH FOR VASCULAR AND CARDIAC RECONSTRUCTION

Allison M. Ostdiek

Dr. Sheila Grant, Dissertation Supervisor

ABSTRACT

It is a universally acknowledged truth that biomaterials are an essential part of current medical therapies. Biomaterials comprised of decellularized tissue mimic natural tissue by providing a natural extracellular matrix. Gold nanoparticles have been shown to improve wound healing by decreasing free radicals at the site and hinder collagenase binding sites, thus improving the durability of the material. This dissertation examines decellularized porcine arterial tissue conjugated with gold nanoparticles for use as a vascular and cardiac repair. The material was characterized through numerous *in vitro* tests, including biocompatibility assays, cell proliferation assays, mechanical testing, histology, and scanning electron microscopy. It was further investigated through two *in vivo* studies allowing for closer examination of the body's interaction with the material. The results of these tests show a material that is comparable to natural tissue with regard to biocompatibility and mechanical strength. The material is feasible in a vascular environment and shows better *in vivo* biocompatibility and superior cell reintegration when compared with current biomaterials used in vascular repair. Further studies are needed to evaluate the

patch in a diseased environment to better understand the role of the gold nanoparticles. This material has the potential to create a new class of biomaterials for use in cardiovascular work.

Chapter One

LITERATURE REVIEW

1.1 Challenges Facing Cardiovascular Biomaterials

Cardiovascular diseases are a major cause of morbidity and mortality in Western civilization [1-3]. Cardiac and vascular repair materials are used to treat problems such as trauma, aneurysms, congenital heart defects, and blood vessel wall defects [4-7]. The current variety of materials being used has a litany of problems, and there is a need to find an optimal biomaterial that can be used for these repairs through better understanding of the relationship between blood components and biomaterials.

1.1.1 The Blood Vessel

1.1.1.1 Normal Vascular Structure

In order to understand the process of vascular repair we must first understand the basic structure of a normal artery. There are three layers in the large and medium arteries, consisting of the intima, media, and adventia. These layers are present in the smaller vessels as well, but less defined. The innermost layer, or intima, has a lining of endothelial cells attached to connective tissue. These endothelial cells are the layer that contacts the blood [2]. The importance

of the endothelial cell layer cannot be overstated, as endothelial cells have been noted to be more than a passive barrier cell, but rather a cell that can both create and distribute copious important compounds that effect numerous bodily reactions. Furchgott and Zadwaski first observed that the endothelial cell played a much more active role than previously considered, and from there the realization of the importance of the endothelial cell has grown exponentially. The work they began expanded to show that the endothelial cell synthesizes compounds that include molecules such as growth factors, vasoactive factors, coagulation and platelet adherence modulators, and chemotactic factors. The cells mediate vasodilation, vasoconstriction, and overall help maintain homeostasis of the extracellular matrix within the vessel wall [8-13].

The media, or middle layer, is a concentric organization of smooth muscle cells (SMCs) and bands of elastic tissue. The luminal endothelial cells affect the SMCs through the release of mitogens such as epidermal growth factor and platelet derived growth factor and also cause relaxation of the smooth muscle cells via acetylcholine [8, 14, 15]. In 1979 Chamley-Campbell et al. showed that the smooth muscle cells have two main phenotypes which represent SMCs that contract and SMCs that synthesize extracellular matrix (ECM), with overlap of the two phenotypes in individual cells [16]. These SMCs lie in an interstitial matrix that also contains type 1 and type 3 collagen with fibronectin and chondroitin sulfate. Also present are lamellae containing large amounts of elastin [17]. SMCs play an important role in the formation of ECM during both angiogenesis

and vascular healing. The media heavily influences blood pressure and vascular resistance. Changes in the smooth muscle layer can lead to vascular stenosis, hypertension, ischemia, and vasospasm [8].

The outer layer is the adventitia which is made up of a collagenous extracellular matrix that has fibroblasts and other cells, and adds rigidity to the vessel. It surrounds the tunica media and plays a critical role in the overall homeostasis of the vessel. The adventitia is the interface between the body, the media, and the intima and contains important immune cells such as T-cells, B-cells, and mast cells while also containing lymphatic vessels and autonomic nerves [18-22]. The presence of these indicates that the adventitia helps to regulate the vessel's lumen size by controlling medial smooth muscle tone and wall remodeling responses, including the formation of microvessels that feed the inner vessel layers [18, 23]. All three vascular layers depend upon one another to create a healthy working vascular environment.

1.1.1.2 Vascular Repair

The manner in which vascular tissue repairs itself is a major hurdle in the design of successful biomaterials. Vessels have a delicate homeostasis. Thromboembolism formation and subsequent vessel narrowing and occlusion are the more immediate troublesome healing responses to vessel injury. The initial response to injury is platelet deposition and the initiation of the coagulation

cascade. This response begins when the endothelium of the vessel is interrupted either through loss of cells or the addition of foreign materials. The exposure of the collagen due to the injury of the endothelial cells leads to the exposure of collagen fibrils which in turn begins the process of primary hemostasis - platelet adhesion and thrombus formation through activation of the intrinsic pathway - and the secretion of agonists such as adenosine phosphate, serotonin, and thromboxane [24, 25]. As the cascade continues, more platelets are activated, and adhere to the vessel wall in layers, eventually leading to the formation of thrombin and the beginning of secondary hemostasis. Secondary hemostasis leaves a platelet plug within the vessel at the site of the initial damage [26]. The thrombus decreases the cross sectional area available for the blood to flow through, in turn causing yet more platelet interactions with the vessel walls and the formation of larger clots. Eventually these clots can occlude the entire vessel or break off to cause ischemic attacks elsewhere in the body. These can clots occur with both injuries to the vessel and when the blood comes into contact with a foreign object, such as an implanted biomaterial.

Thromboembolisms and vessel occlusions are immediate problems with vascular injury and healing. The longer term consequence is an overzealous wound healing response known as intimal hyperplasia. Intimal hyperplasia is the term for intimal thickening caused by increased amounts of cells and ECM in the vessel caused by injury, inflammation, and increased wall stress [17, 27]. There are numerous compounding mechanisms that create intimal hyperplasia, though

some of the causes of cell signaling changes leading to stimulation of proliferation are yet unknown [28]. Intimal hyperplasia begins with platelet deposition and coagulation, followed by increased SMC migration and proliferation and an increase in the laying down of ECM. The initial mechanisms begin with the changes in the normal endothelial mechanisms. Alterations in endothelial derived substances likely result in a decreased ability to regulate coagulation and an increase in SMC activity [29]. The SMCs of adult arteries rarely need to proliferate, but are able to quickly divide in response to vascular injury [30]. As previously discussed, vascular SMCs have two main phenotypes: those that contract and those that synthesize ECM. In normal vessels the synthesis of the extracellular matrix is balanced by continuous degradation. However in injury more SMCs are needed to divide and regenerate, and there is a change in the active genes which leads to basement membrane components such as laminin to be down regulated while increasing interstitial matrix components like type 1 collagen, elastin, and fibronectin [17, 31-33]. Over time the synthesis of excessive ECM results in a hyperplasia, a decreased vessel lumen, and stenosis of the vessel.

1.1.2 Blood – Material Interactions

1.1.2.1 Material Surface Interaction

Vascular repair materials present unique challenges due to the highly variable environment into which they are implanted. Vascular biomaterials are in constant contact with blood which requires them to have particular characteristics in order to be biocompatible. When placed in a vessel they trigger the intrinsic pathway causing coagulation and the inflammatory stage of the wound healing response. The differences in coagulation reactions to native endothelial and artificial surfaces have been studied for over 100 years [34]. The objective of examining the blood-biomaterial interaction is to understand the effects the biomaterial has on the components of the blood and the subsequent thrombogenicity of the material, or how it induces the coagulation response [35]. The blood response is affected by the texture, composition, and charge of the graft surface as well as the structure and chemical composition of the entire graft [36]. A reaction to the material can cause a wide variety of problems, including thrombi partially or totally blocking blood vessels, and the formation of emboli that can cause strokes [37]. The surface chemistry of the material must promote cell attachment, proliferation, and migration to allow for ingrowth of host cells through a predictable interaction while also being biocompatible [38, 39].

A foreign material implanted into the body is not thromboresistant like the native endothelium and cannot secrete factors to actively aid in

thromboresistance [35, 40, 41]. The initial contact of blood to the biomaterial triggers the adsorption of proteins such as fibrinogen, albumin, and factor XII to the surface which in turn promote the adhesion and aggregation of platelets [34]. Many of the consequences seen after this are due to the interactions of the blood with the adsorbed protein layer [35, 42]. The immune response includes the initiation of the extrinsic and intrinsic coagulation cascades and formation of thromboemboli as previously described. The body also responds as it would to any foreign material with an inflammatory response including neutrophils, macrophages, and multi-nucleated giant cells [43]. As these cells attack the material they attempt to ingest it, and when they cannot, the body sometimes walls off the material. This can lead to chronic inflammation and other implant issues.

Another major aspect to the blood-material interaction is the flow mechanics within the vessel. Different types of vascular materials have different levels of compliance. A more compliant graft may match mechanical and flow parameters better than a less compliant material [44]. Changes in the flow of the blood lead to some of the problems previously described and contribute yet more challenges to a blood contacting biomaterial such as atherosclerosis and vascular plaques [45]. Normal blood plasma behaves like a Newtonian fluid, flowing through the arteries in a pulsatile fashion, and thus the force applied to the fluid is related to the velocity gradient within the fluid with consideration to the viscosity [46]. When the flow through the vessel is altered due to injury or repair

with a biomaterial the stress placed on the wall of the adjacent artery is changed. Over time the body adapts to these changes by remodeling the artery. Increased flow rates will cause a larger diameter vessel with the same arterial structure while decreased flow will see a thickening of the intimal layer [47]. Changes to the medial layer include the proliferation of SMCs and changes in the organization of the elastin and collagen structure. Long term hypertension caused by changes in the size of the vessel, including vascular wall repair, lead to a generalized thickening of the media [47, 48].

Variation in flow and thus shear stress on the artery can lead to intimal hyperplasia and has been seen when using vascular grafts of differing diameters [49]. With vascular biomaterials we can see thrombosis and intimal hyperplasia leading to stenosis. When stenosis occurs the shear stress on the walls of the arteries changes with intense turbulence downstream of the stenosis and can lead to further platelet adhesions and thrombi [50]. In addition to all of the physiological responses there is added stress to the biomaterial that can lead to weakening and early failure of the implant. The consequences of altering the vascular flow emphasize the need for vascular biomaterials that can mimic the native tissue.

1.2 Current Materials for Cardiovascular Repair

Cardiac and vascular materials are utilized to treat trauma and aneurysms, repair congenital defects, and patch defects in vessel and cardiac walls [4-7]. Materials used currently for vascular and cardiac repairs tend to fall into two categories: Those created from synthetic materials and those with a biologic origin. Both have strengths and weaknesses. Surface modifications to both synthetic and biologic materials are also being explored as a way to enhance biocompatibility. There are numerous characteristics for an ideal vascular graft, all of which entail making the graft as close to a native vessel as possible. The first set of requirements are those of any implant: biocompatibility, easy sterilization, stable and convenient to store for long periods of time, and ease if implantation. The more specific requirements for a vascular graft include having the same composition, structural, and mechanical properties. It should mimic the native extracellular matrix, sustain and guide new cell growth, avoid intimal hyperplasia, resist infection, and degrade after new tissue has formed [1-3, 44, 51, 52].

1.2.1 Synthetic Repair Materials

Vascular materials have been created from synthetic polymers, such as expanded polytetrafluoroethylene (ePTFE), and polyethylene terephthalate (PET). These synthetic polymers provide excellent mechanical strength and *in*

vivo durability, but lack biocompatibility leading to intimal hyperplasia, thrombus formation, calcium deposition, and increased rates of infection [7, 53-63].

Synthetic polymers cause an immune reaction in the body that can be extremely problematic when they come into contact with blood. Normally when a synthetic material is implanted the immune response sends phagocytic cells to the area to try and remove the foreign material. This creates an inflammatory response that becomes chronic as the material remains in the body for years. Biomaterial surface activated coagulation occurs more frequently with synthetic materials. They completely lack any biomolecules such as those created by endothelial cells. As previously discussed, this absence causes high levels of platelet adhesion and the downstream consequences. A material's thrombogenicity can result in failure and major *in vivo* complications such as pseudoaneurysm formation [37, 64-66].

The synthetics lack a "natural" extracellular matrix (ECM) and subsequently lack the molecules and growth factors present in biologic tissue that signal the body to start re-integrating cells into the matrix. They can induce a low level of inflammation due to a foreign body response that will result in late graft failure [36]. They have higher infection rates than biologic materials and show a greater tendency towards forming biofilms. These infections can later lead to increased material removal and mortality rates [67, 68]. Overall, synthetic materials lead to numerous unappealing reactions within the native tissue.

1.2.2 Biologic Repair Materials

Current cardiovascular biologic patch materials include autologous and cadaver vessels and natural extracellular matrices from animals. Biologic materials allow for the host cells to infiltrate the implant and remodel it into a functional living tissue [69, 70]. These materials better approximate characteristics of the native tissue than synthetic materials, and can be engineered to include the host's own cells. However, since they are organic they tend to be weaker than the synthetic materials, and break down faster within the body. Certain types can also cause immune reactions if they are not treated correctly. Biologic materials tend to fall into three categories: autologous grafts, tissue engineered grafts, and decellularized xenografts, with some overlap.

In humans the gold standard for most vascular repair situations is the autologous graft. When a person's own tissue is used to graft a vessel there is little chance of immune rejection. However, in many cases patients do not have viable tissue available for use, and resulting in a secondary surgical site. In particular, when veins are used to replace arteries the grafts do not always thicken to the strength of arteries and can develop stenosis or failure later on. Cadaver tissues have also been cryopreserved and implanted into patients with the hopes that the endothelial cells of the allograft would remain viable and help improve patency [71]. However Sachs et al. showed that frozen cryopreserved

veins lose endothelium and fibrolytic activity five days after grafting [72]. The traditional allografts express major histocompatibility complex antigens I and II, which lead to immune reactions and thrombosis in these grafts [73]. Cadaver tissue is also of limited availability and can transmit diseases [74].

One of the most popular areas of biologic materials research is the use of a natural extracellular matrix (ECM) as a base material for scaffolding. This process has been used with multiple tissues, including small intestine submucosa [75, 76], heart valves [77-80], blood vessels [81-83], urinary bladder [84], bovine pericardium, and many others [85]. ECM tissues serve as scaffolds for cell attachment, migration, and proliferation. They provide the added benefits of having growth factors and RGD-peptides present, as well as other unknown factors that seem to aid in the repopulation and revascularization processes [86]. Xenografts closely mimic the host tissue's original mechanical and structural properties and have a lower infection rate [87]. The structural and functional molecules differ in each tissue and organ. Therefore, different organ and tissue ECMs vary in structure and in biomolecules [85].

The bioactive factors remain behind after decellularization, which is a process necessary to remove the immunogenic components present. The decellularization process is vital to the creation of ECM grafts. The goal is to remove all cellular components while leaving the ECM and cell associated proteins, such as actin, tubulin, and myosin [88, 89]. There are several methods of decellularization being explored which include ionic and non-ionic detergents

and enzymes. The ionic detergents, such as sodium dodecyl sulfate, remove nuclear remnants, but may disrupt the native tissue structure and cause a decrease in glycosaminoglycans. Non-ionic detergents, such as Triton X-100 also remove nuclear remnants, but have had mixed reports of decreasing the tensile strength of the scaffold [90, 91]. Zwitterionic detergents have been shown to improve the efficacy of the non-ionic detergents without causing further damage to the ECM. Enzymatic treatments cleave the nuclear remnants, but can be hard to remove from the tissue and cause an immune response [92]. A protocol that removes the nuclear remnants and does not disrupt the ECM is the ideal basis for a vascular graft.

Another method of modifying ECM to optimize a biomaterial is crosslinking. Crosslinking was originally used to decrease the resorption rate of the material *in vivo* [87]. Crosslinking can be done to strengthen the scaffold as well as create larger pore sizes for cells to grow into. Crosslinking collagen molecules has been shown to promote resistance to protease degradation [93]. This increases the *in vivo* durability of the material. Traditionally, glutaraldehyde has been used as a crosslinker with natural tissue. However it is cytotoxic at high levels and is a bridge forming crosslinker. Other chemical crosslinkers include disocyanates, acylazide, and 1-ethyl-3-(3-dimethyl aminopropyl) carbodiimide (EDC). EDC is a zero-length crosslinker that directly links the collagen molecules to one another. Some studies have shown EDC crosslinking creates a more biologically stable scaffold [94, 95]. Using crosslinking to create

a larger pore size can allow cells to colonize the scaffold. In some ECMs the collagen fibers are woven too tightly for the natural cells to grow into. With a larger pore size the cells and nutrients can spread into the scaffold [96]. Crosslinking is a promising way to optimize biologic tissues.

1.2.3 Surface Modifications

Surface modifications to biologic and synthetic materials can increase blood compatibility [97]. Proteins rapidly adsorb onto biomaterial surfaces when they are implanted. Subsequent interactions with host fluids and tissues are mostly determined by this attached protein layer [35, 42]. Various methods of controlling the amount and types of blood components being adsorbed onto biomaterial surfaces are being explored. Surface modifications that elute particular bioactive molecules such as heparin have shown promise in controlling the body's response to the repair material. In one study, Zhou et al. added vascular endothelial growth factor (VEGF) and heparin to a decellularized scaffold to encourage endothelial cell ingrowth and decrease coagulation. VEGF is a chemoattractant for endothelial cells and also helps inhibit intimal hyperplasia. The heparin helps maintain graft patency. The study showed a higher cell proliferation rate and a smaller hyperplastic intimal area with the added VEGF and heparin [98]. Another type of surface modification that can improve biocompatibility is the use of nanoparticles.

1.3 Nanoparticles

Nanoparticles have a broad array of biomedical applications, such as imaging, drug delivery, and diagnostics [99-101]. Protein interactions occur within the body on a nanoscale and control numerous important cell functions such as cellular proliferation, migration, and ECM production, all of which have significant effects on the success and failure of biomaterials [102, 103]. By capitalizing on these effects, we can generate vastly improved nanocomposite biomaterials.

1.3.1 Uses in Biomaterials

Recent research delves into cellular responses to nanomaterials present on biomaterials [104]. Nanoparticles have many biomaterial applications, since they are the size of some of the proteins essential for cellular functions and signaling. Biomolecules interact with a biomaterial surface based on its surface chemical composition. This protein surface interaction is part of what makes nanoparticles so appealing: they can directly influence these proteins. Another important aspect to the surface – material interaction is the adsorption of proteins to the surface of the material. Nanoparticles can improve cellular function as they have been shown to create a more hydrophilic material and maintain more crystal grains and atoms on the surface of the material. The larger number of

grains contributes to protein adsorption and unfolding by increasing surface roughness, area, and energy [102, 105]. By affecting these interactions they can change the body's reaction to the implantation of a foreign material and influence cellular signaling cascades [106, 107]. An excellent example of this is the use of silver nanoparticles as antimicrobial coatings [108]. Gold nanoparticles are one of many being investigated for their effects *in vivo*.

1.3.2 Gold Nanoparticles

Gold nanoparticles (AuNPs) are being used in numerous medical applications such as drug delivery, imaging, biosensors, diagnostics, gene therapy, and nanocomposite biomaterials due to their biocompatibility, optical properties, and conjugation capabilities [100, 101, 104, 109-111]. Gold is a noble metal that is biologically inert. AuNPs have been used for the immobilization of proteins, enzymes, and antibodies [112]. These multiple positive effects of AuNPs arise from the protein – gold interactions that effect cell signaling. Recent research has shown that AuNPs can augment antimicrobial properties of biomaterials as well as increase cell proliferation [112-116]. Hsu et al. showed significantly lower bacterial adhesion to materials with AuNPs attached [114]. This indicates that the presence of AuNPs on a material may prevent the formation of biofilms while also encouraging the body to heal and remodel properly. Other studies have also corroborated the bacteriostatic properties of

AuNPs, a major benefit for biomaterials [115]. Studies show that materials conjugated with AuNPs have improved cell adhesion, protein adsorption, thermal and mechanical properties while showing reduced foreign body reaction, monoctye activation, inflammatory response, and bacterial adhesion when compared to the same material without AuNPs [117, 118]. Using human gingival fibroblasts, Hsu et al. showed the addition of AuNPs to polyurethane increased cellular proliferation and attachment [112]. Another benefit to AuNPs is their ability to increase the stability of biomaterials by slowing their degradation *in vivo*. Grant et al. showed that AuNPs hinder collagenase binding sites [119]. This hindrance slows the enzymes the body sends to break down the foreign material, which allows time for proper remodeling. Several studies have shown that AuNPs conjugated with biomaterials have significantly improved thermal and mechanical properties and improved biostability [112, 117, 120, 121]. With this increased stability, biomaterials conjugated with AuNPs will be able to provide a stronger basis for tissue reconstruction while also being more biocompatible to the host. AuNPs are a strong candidate for future nanocomposite materials.

The biocompatibility of gold nanoparticles has been highly debated. The current literature shows AuNPs to be biocompatible and non-cytotoxic *in vitro* and *in vivo* while suggesting that cellular response is dependent on numerous factors such as nanoparticles concentration, size, and synthesis, and the cell line used in culture [122]. Current research trends show that the cytotoxicity of the AuNPs depends greatly on the size used and may be due to variability in uptake

kinetics between smaller and larger particles, concluding that smaller particles have more negative effects [110]. Conner et al., and Shukla et al. found in 2005 that AuNPs larger than 18 nm show little cytotoxicity, even if they are up taken into a cell [123-125]. The concentration of the gold nanoparticles has also been a concern, but conjugated 20 nm AuNP concentrations up to 5mM have shown no adverse effects on mice fibroblast cells [113, 116]. Overall, gold nanoparticles are biocompatible and have positive effects when used in a biomedical setting.

1.4 Conclusions

There is a unique set of challenges facing cardiac and vascular bioengineered materials *in vivo*. Current research shows that we have numerous materials with varying negative and positive characteristics. The positive characteristics from the materials need to be taken under consideration and combined into a material that is ideally suited to interface with blood. More research is needed to create, characterize, and optimize a composite material using currently available methods that will be strong, durable, antithrombogenic, biocompatible, and mechanically similar to the native tissue.

1.5 References

[1] Bordenave L, Menu P, Baquey C. Developments towards tissue-engineered, small-diameter arterial substitutes. Expert review of medical devices. 2008;5:337-47.

[2] Ratcliffe A. Tissue engineering of vascular grafts. Matrix Biol. 2000;19:353-7.

[3] Tu JV, Pashos CL, Naylor CD, Chen E, Normand S-L, Newhouse JP, et al. Use of Cardiac Procedures and Outcomes in Elderly Patients with Myocardial Infarction in the United States and Canada. New England Journal of Medicine. 1997;336:1500-5.

[4] David TE. The use of pericardium in acquired heart disease: a review article. The Journal of heart valve disease. 1998;7:13-8.

[5] David TE, Armstrong S. Surgical repair of postinfarction ventricular septal defect by infarct exclusion. Seminars in thoracic and cardiovascular surgery. 1998;10:105-10.

[6] Fishman NH. Left ventricular aneurysm repair. The Annals of thoracic surgery. 1998;65:602-3.

[7] Robinson KA, Li J, Mathison M, Redkar A, Cui J, Chronos NAF, et al. Extracellular Matrix Scaffold for Cardiac Repair. Circulation. 2005;112:I-135-I-43.

[8] Furchgott RF, Zawadzki JV. The obligatory role of endothelial cells in the relaxation of arterial smooth muscle by acetylcholine. Nature. 1980;288:373-6.

[9] Furchgott RF. Role of endothelium in responses of vascular smooth muscle. Circulation research. 1983;53:557-73.

[10] Furchgott RF, Vanhoutte PM. Endothelium-derived relaxing and contracting factors. The FASEB Journal. 1989;3:2007-18.

[11] De Mey J, Vanhoutte P. Heterogeneous behavior of the canine arterial and venous wall. Importance of the endothelium. Circulation research. 1982;51:439-47.

[12] De Mey J, Vanhoutte P. Role of the intima in cholinergic and purinergic relaxation of isolated canine femoral arteries. J Physiol. 1981;316:347-55.

[13] Heyligers JM, Arts CH, Verhagen HJ, de Groot PG, Moll FL. Improving small-diameter vascular grafts: from the application of an endothelial cell lining to the
construction of a tissue-engineered blood vessel. Annals of vascular surgery. 2005;19:448-56.

[14] Monsen C, Adams P, Badimon L, Chesebro J, Fuster V. Platelet-vessel wall interactions in the development of restenosis after coronary angioplasty. Zeitschrift fur Kardiologie. 1986;76:23-8.

[15] Hanke H, Strohschneider T, Oberhoff M, Betz E, Karsch KR. Time course of smooth muscle cell proliferation in the intima and media of arteries following experimental angioplasty. Circulation research. 1990;67:651-9.

[16] Chamley-Campbell J, Campbell GR, Ross R. The smooth muscle cell in culture. Physiol rev. 1979;59:1-61.

[17] Newby AC, Zaltsman AB. Molecular mechanisms in intimal hyperplasia. The Journal of Pathology. 2000;190:300-9.

[18] Majesky MW, Dong XR, Hoglund V, Mahoney WM, Daum G. The Adventitia: A Dynamic Interface Containing Resident Progenitor Cells. Arteriosclerosis, Thrombosis, and Vascular Biology. 2011;31:1530-9.

[19] Smith JD, Bryant SR, Couper LL, Vary CP, Gotwals PJ, Koteliansky VE, et al. Soluble transforming growth factor-β type II receptor inhibits negative remodeling, fibroblast transdifferentiation, and intimal lesion formation but not endothelial growth. Circulation research. 1999;84:1212-22.

[20] Rey FE, Pagano PJ. The reactive adventitia fibroblast oxidase in vascular function. Arteriosclerosis, Thrombosis, and Vascular Biology. 2002;22:1962-71.

[21] Galkina E, Kadl A, Sanders J, Varughese D, Sarembock IJ, Ley K. Lymphocyte recruitment into the aortic wall before and during development of atherosclerosis is partially L-selectin dependent. The Journal of experimental medicine. 2006;203:1273-82.

[22] Tieu BC, Lee C, Sun H, LeJeune W, Recinos A, Ju X, et al. An adventitial IL-6/MCP1 amplification loop accelerates macrophage-mediated vascular inflammation leading to aortic dissection in mice. The Journal of clinical investigation. 2009;119:3637-51.

[23] Gutterman DD. Adventitia-dependent influences on vascular function. American Journal of Physiology-Heart and Circulatory Physiology. 1999;277:H1265-H72.

[24] Marcus AJ. Platelets and their disorders. Disorders of hemostasis 3rd ed Philadelphia, PA: WB Saunders. 1996:79-137.

[25] Marcus A, Safier L. Thromboregulation: multicellular modulation of platelet reactivity in hemostasis and thrombosis. The FASEB Journal. 1993;7:516-22.

[26] Kroll MH, Schafer AI. Biochemical mechanisms of platelet activation. Blood. 1989;74:1181-95.

[27] Zwolak RM, Adams MC, Clowes AW. Kinetics of vein graft hyperplasia: association with tangential stress. Journal of Vascular Surgery. 1987;5:126-36.

[28] Fishman J, Ryan G, Karnovsky M. Endothelial regeneration in the rat carotid artery
and the significance of endothelial denudation in the pathogenesis of myointimal thickening. Lab Invest. 1975;32:339-51.

[29] Weber KT. Vascular Wound Healing and Restenosis Following Revascularization. In: Weber KT, editor. Wound Healing in Cardiovascular Disease. Armonk , NY: Futura Publishing Company; 1995. p. 137-47.

[30] Clowes AW, Reidy M, Clowes M. Kinetics of cellular proliferation after arterial injury. I. Smooth muscle growth in the absence of endothelium. Lab Invest. 1983;49:327-33.

[31] Thyberg J, Blomgren K, Roy J, Tran PK, Hedin U. Phenotypic modulation of smooth muscle cells after arterial injury is associated with changes in the distribution of laminin and fibronectin. Journal of Histochemistry & Cytochemistry. 1997;45:837-46.

[32] Chamley-Campbell JH, Campbell GR. What controls smooth muscle phenotype? Atherosclerosis. 1981;40:347-57.

[33] Campbell GR, Campbell JH. Smooth muscle phenotypic changes in arterial wall homeostasis: implications for the pathogenesis of atherosclerosis. Experimental and molecular pathology. 1985;42:139-62.

[34] Bloom AL. Haemostasis and thrombosis: Churchill Livingstone; 1994.

[35] Courtney J, Lamba N, Sundaram S, Forbes C. Biomaterials for blood-contacting applications. Biomaterials. 1994;15:737-44.

[36] Greisler HP. Interactions at the blood/material interface. Annals of vascular surgery. 1990;4:98-103.

[37] Sefton MV, Gemmel CH, Gorbet MB. What really is blood compatibility? Journal of Biomaterials Science -- Polymer Edition. 2000;11:1165.

[38] Zhao Y, Zhang Z, Wang J, Yin P, Wang Y, Yin Z, et al. Preparation of decellularized and crosslinked artery patch for vascular tissue-engineering application. J Mater Sci Mater Med. 2011;22:1407-17.

[39] Lu Q, Ganesan K, Simionescu DT, Vyavahare NR. Novel porous aortic elastin and collagen scaffolds for tissue engineering. Biomaterials. 2004;25:5227-37.

[40] Mason R, Sharp D, Chuang H, Mohammad S. The endothelium: roles in thrombosis and hemostasis. Archives of pathology & laboratory medicine. 1977;101:61-4.

[41] Mason R, Mohammad S, Saba H, Chuang H, Lee E, Balis J. Functions of endothelium. Pathobiology annual. 1979;9:1.

[42] Brash J, Sharma C, Szycher M. Role of plasma protein adsorption in the response of blood to foreign surfaces: Technomic Publishing Co.: Lancaster, PA; 1991.

[43] Velnar T, Bailey T, Smrkolj V. The wound healing process: an overview of the cellular and molecular mechanisms. Journal of International Medical Research. 2009;37:1528-42.

[44] Wang X, Lin P, Yao Q, Chen C. Development of small-diameter vascular grafts. World J Surg. 2007;31:682-9.

[45] Zhao SZ, Xu XY, Hughes AD, Thom SA, Stanton AV, Ariff B, et al. Blood flow and vessel mechanics in a physiologically realistic model of a human carotid arterial bifurcation. Journal of Biomechanics. 2000;33:975-84.

[46] Wootton DM, Ku DN. Fluid Mechanics of Vascular Systems, Diseases, and Thrombosis. Annual Review of Biomedical Engineering. 1999;1:299-329.

[47] Glagov S, Zarins C, Giddens D, Ku DN. Hemodynamics and atherosclerosis. Insights and perspectives gained from studies of human arteries. Archives of pathology & laboratory medicine. 1988;112:1018-31.

[48] Rodbard S. Negative feedback mechanisms in the architecture and function of the connective and cardiovascular tissues. Perspectives in biology and medicine. 1969;13:507-27.

[49] Salam T, Lumsden A, Suggs W, Ku D. Low shear stress promotes intimal hyperplasia thickening. J vasc invest. 1996;2:12-22.

[50] Barstad R, Kierulf P, Sakariassen K. Collagen induced thrombus formation at the apex of eccentric stenoses--a time course study with non-anticoagulated human blood. Thrombosis and haemostasis. 1996;75:685-92.

[51] Zhang WJ, Liu W, Cui L, Cao Y. Tissue engineering of blood vessel. Journal of cellular and molecular medicine. 2007;11:945-57.

[52] Zwirner K, Thiel C, Thiel K, Morgalla MH, Konigsrainer A, Schenk M. Extracellular brain ammonia levels in association with arterial ammonia, intracranial pressure and the use of albumin dialysis devices in pigs with acute liver failure. Metab Brain Dis. 2010;25:407-12.

[53] Awad IA, Little JR. Patch angioplasty in carotid endarterectomy. Advantages, concerns, and controversies. Stroke; a journal of cerebral circulation. 1989;20:417-22.

[54] Bond R, Rerkasem K, Naylor AR, AbuRahma AF, Rothwell PM. Systematic review of randomized controlled trials of patch angioplasty versus primary closure and different types of patch materials during carotid endarterectomy. Journal of Vascular Surgery. 2004;40:1126-35.

[55] Chang Y, Tsai C-C, Liang H-C, Sung H-W. In vivo evaluation of cellular and acellular bovine pericardia fixed with a naturally occurring crosslinking agent (genipin). Biomaterials. 2002;23:2447-57.

[56] Cho SW, Park HJ, Ryu JH, Kim SH, Kim YH, Choi CY, et al. Vascular patches tissue-engineered with autologous bone marrow-derived cells and decellularized tissue matrices. Biomaterials. 2005;26:1915-24.

[57] Cho S-W, Park HJ, Ryu JH, Kim SH, Kim YH, Choi CY, et al. Vascular patches tissue-engineered with autologous bone marrow-derived cells and decellularized tissue matrices. Biomaterials. 2005;26:1915-24.

[58] Marien Bj RJDSCSLWWMJO. Bovine pericardium vs dacron for patch angioplasty after carotid endarterectomy: A prospective randomized study. Arch Surg. 2002;137:785-8.

[59] Muto A, Nishibe T, Dardik H, Dardik A. Patches for carotid artery endarterectomy: Current materials and prospects. Journal of Vascular Surgery. 2009;50:206-13.

[60] Rerkasem K, Rothwell PM. Systematic Review of Randomized Controlled Trials of Patch Angioplasty Versus Primary Closure and Different Types of Patch Materials During Carotid Endarterectomy. Asian Journal of Surgery. 2011;34:32-40.

[61] Rhodes VJ. Expanded polytetrafluoroethylene patch angioplasty in carotid endarterectomy. Journal of Vascular Surgery.22:724-31.

[62] Schmidt CE, Baier JM. Acellular vascular tissues: natural biomaterials for tissue repair and tissue engineering. Biomaterials. 2000;21:2215-31.

[63] Xue L, Greisler HP. Biomaterials in the development and future of vascular grafts. J Vasc Surg. 2003;37:472-80.

[64] Litwinski RA, Wright K, Pons P. Pseudoaneurysm Formation following Carotid Endarterectomy: Two Case Reports and a Literature Review. Annals of vascular surgery. 2006;20:678-80.

[65] Knight BC, Tait WF. Dacron Patch Infection Following Carotid Endarterectomy: A Systematic Review of the Literature. European Journal of Vascular and Endovascular Surgery. 2009;37:140-8.

[66] Frost MC, Reynolds MM, Meyerhoff ME. Polymers incorporating nitric oxide releasing/generating substances for improved biocompatibility of blood-contacting medical devices. Biomaterials. 2005;26:1685-93.

[67] Bergamini TM, Bandyk DF, Govostis D, Kaebnick HW, Towne JB. Infection of vascular prostheses caused by bacterial biofilms. Journal of Vascular Surgery. 1988;7:21-30.

[68] Mertens RA, O'Hara PJ, Hertzer NR, Krajewski LP, Beven EG. Surgical management of infrainguinal arterial prosthetic graft infections: review of a thirty-five-year experience. Journal of Vascular Surgery. 1995;21:782-91.

[69] Bolland F, Korossis S, Wilshaw S-P, Ingham E, Fisher J, Kearney JN, et al. Development and characterisation of a full-thickness acellular porcine bladder matrix for tissue engineering. Biomaterials. 2007;28:1061-70.

[70] Southgate J, Cross W, Eardley I, Thomas DFM, Trejdosiewicz LK. Bladder reconstruction—from cells to materials. Proceedings of the Institution of Mechanical Engineers, Part H: Journal of Engineering in Medicine. 2003;217:311-6.

[71] Madden R, Lipkowitz G, Benedetto B, Kurbanov A, Miller M, Bow L. Decellularized cadaver vein allografts used for hemodialysis access do not cause

allosensitization or preclude kidney transplantation. American Journal of Kidney Diseases. 2002;40:1240-3.

[72] Sachs SM, Ricotta JJ, Scott D, DeWeese JA. Endothelial integrity after venous cryopreservation. Journal of Surgical Research. 1982;32:218-27.

[73] Benedetto B, Lipkowitz G, Madden R, Kurbanov A, Hull D, Miller M, et al. Use of cryopreserved cadaveric vein allograft for hemodialysis access precludes kidney transplantation because of allosensitization. Journal of Vascular Surgery. 2001;34:139-42.

[74] Fishman JA, Greenwald MA, Grossi PA. Transmission of Infection With Human Allografts: Essential Considerations in Donor Screening. Clinical Infectious Diseases. 2012;55:720-7.

[75] Badylak SF, Lantz GC, Coffey A, Geddes LA. Small intestinal submucosa as a large diameter vascular graft in the dog. Journal of Surgical Research. 1989;47:74-80.

[76] Kropp BP, Eppley BL, Prevel C, Rippy M, Harruff R, Badylak S, et al. Experimental assessment of small intestinal submucosa as a bladder wall substitute. Urology. 1995;46:396-400.

[77] Bader A, Schilling T, Teebken OE, Brandes G, Herden T, Steinhoff G, et al. Tissue engineering of heart valves–human endothelial cell seeding of detergent acellularized porcine valves. European journal of cardio-thoracic surgery. 1998;14:279-84.

[78] Grauss RW, Hazekamp MG, Oppenhuizen F, van Munsteren CJ, Gittenberger-de Groot AC, DeRuiter MC. Histological evaluation of decellularised porcine aortic valves: matrix changes due to different decellularisation methods. European journal of cardio-thoracic surgery. 2005;27:566-71.

[79] Kasimir M, Rieder E, Seebacher G, Silberhumer G, Wolner E, Weigel G, et al. Comparison of different decellularization procedures of porcine heart valves. The International journal of artificial organs. 2003;26:421-7.

[80] Rieder E, Kasimir M-T, Silberhumer G, Seebacher G, Wolner E, Simon P, et al. Decellularization protocols of porcine heart valves differ importantly in efficiency of cell removal and susceptibility of the matrix to recellularization with human vascular cells. The Journal of thoracic and cardiovascular surgery. 2004;127:399-405.

[81] Conklin B, Richter E, Kreutziger K, Zhong D-S, Chen C. Development and evaluation of a novel decellularized vascular xenograft. Medical engineering & physics. 2002;24:173-83.

[82] Dahl SL, Koh J, Prabhakar V, Niklason LE. Decellularized native and engineered arterial scaffolds for transplantation. Cell transplantation. 2003;12:659-66.

[83] Uchimura E, Sawa Y, Taketani S, Yamanaka Y, Hara M, Matsuda H, et al. Novel method of preparing acellular cardiovascular grafts by decellularization with poly (ethylene glycol). Journal of Biomedical Materials Research Part A. 2003;67:834-7.

[84] Freytes DO, Badylak SF, Webster TJ, Geddes LA, Rundell AE. Biaxial strength of multilaminated extracellular matrix scaffolds. Biomaterials. 2004;25:2353-61.

[85] Badylak SF, Freytes DO, Gilbert TW. Extracellular matrix as a biological scaffold material: Structure and function. Acta Biomater. 2009;5:1-13.

[86] Walles T, Herden T, Haverich A, Mertsching H. Influence of scaffold thickness and scaffold composition on bioartificial graft survival. Biomaterials. 2003;24:1233-9.

[87] Milthorpe BK. Xenografts for tendon and ligament repair. Biomaterials. 1994;15:745-52.

[88] Crapo PM, Gilbert TW, Badylak SF. An overview of tissue and whole organ decellularization processes. Biomaterials. 2011;32:3233-43.

[89] Daly AB, Wallis JM, Borg ZD, Bonvillain RW, Deng B, Ballif BA, et al. Initial binding and recellularization of decellularized mouse lung scaffolds with bone marrow-derived mesenchymal stromal cells. Tissue Engineering Part A. 2011;18:1-16.

[90] Williams C, Liao J, Joyce E, Wang B, Leach J, Sacks M, et al. Altered structural and mechanical properties in decellularized rabbit carotid arteries. Acta biomaterialia. 2009;5:993-1005.

[91] Amiel GE, Komura M, Shapira O, Yoo JJ, Yazdani S, Berry J, et al. Engineering of blood vessels from acellular collagen matrices coated with human endothelial cells. Tissue engineering. 2006;12:2355-65.

[92] Gilbert TW, Sellaro TL, Badylak SF. Decellularization of tissues and organs. Biomaterials. 2006;27:3675-83.

[93] Jarman-Smith ML, Bodamyali T, Stevens C, Howell JA, Horrocks M, Chaudhuri JB. Porcine collagen crosslinking, degradation and its capability for fibroblast adhesion and proliferation. Journal of Materials Science: Materials in Medicine. 2004;15:925-32.

[94] Ma L, Gao C, Mao Z, Zhou J, Shen J. Enhanced biological stability of collagen porous scaffolds by using amino acids as novel cross-linking bridges. Biomaterials. 2004;25:2997-3004.

[95] Duan X, Sheardown H. Crosslinking of collagen with dendrimers. J Biomed Mater Res A. 2005;75:510-8.

[96] Salem AK, Stevens R, Pearson RG, Davies MC, Tendler SJ, Roberts CJ, et al. Interactions of 3T3 fibroblasts and endothelial cells with defined pore features. Journal of biomedical materials research. 2002;61:212-7.

[97] Courtney J, Yu J, Sundaram S. Immobilisation of macromolecules for obtaining biocompatible surfaces. Immobilised Macromolecules: Application Potentials: Springer; 1993. p. 175-93.

[98] Zhou M, Liu Z, Wei Z, Liu C, Qiao T, Ran F, et al. Development and validation of small-diameter vascular tissue from a decellularized scaffold coated with heparin and vascular endothelial growth factor. Artif Organs. 2009;33:230-9.

[99] Hainfeld J, Slatkin D, Focella T, Smilowitz H. Gold nanoparticles: a new X-ray contrast agent. 2014.

[100] Sperling RA, Rivera Gil P, Zhang F, Zanella M, Parak WJ. Biological applications of gold nanoparticles. Chemical Society Reviews. 2008;37:1896-908.

[101] Freese C, Gibson MI, Klok H-A, Unger RE, Kirkpatrick CJ. Size-and coating-dependent uptake of polymer-coated gold nanoparticles in primary human dermal microvascular endothelial cells. Biomacromolecules. 2012;13:1533-43.

[102] Christenson EM, Anseth KS, van den Beucken JJ, Chan CK, Ercan B, Jansen JA, et al. Nanobiomaterial applications in orthopedics. Journal of orthopaedic research. 2007;25:11-22.

[103] Webster TJ, Schadler LS, Siegel RW, Bizios R. Mechanisms of enhanced osteoblast adhesion on nanophase alumina involve vitronectin. Tissue Engineering. 2001;7:291-301.

[104] Whelove OE, Cozad MJ, Lee BD, Sengupta S, Bachman SL, Ramshaw BJ, et al. Development and in vitro studies of a polyethylene terephthalate-gold nanoparticle scaffold for improved biocompatibility. Journal of biomedical materials research Part B, Applied biomaterials. 2011;99:142-9.

[105] Webster TJ, Ergun C, Doremus RH, Siegel RW, Bizios R. Specific proteins mediate enhanced osteoblast adhesion on nanophase ceramics. J Biomed Mater Res. 2000;51:475-83.

[106] Balasundaram G, Webster TJ. A perspective on nanophase materials for orthopedic implant applications. Journal of Materials Chemistry. 2006;16:3737-45.

[107] Kay S, Thapa A, Haberstroh KM, Webster TJ. Nanostructured polymer/nanophase ceramic composites enhance osteoblast and chondrocyte adhesion. Tissue Engineering. 2002;8:753-61.

[108] Li J, Wang J, Shen L, Xu Z, Li P, Wan G, et al. The influence of polyethylene terephthalate surfaces modified by silver ion implantation on bacterial adhesion behavior. Surface and Coatings Technology. 2007;201:8155-9.

[109] Lim Z-ZJ, Li J-EJ, Ng C-T, Yung L-YL, Bay B-H. Gold nanoparticles in cancer therapy. Acta Pharmacologica Sinica. 2011;32:983-90.

[110] Gu Y-J, Cheng J, Lin C-C, Lam YW, Cheng SH, Wong W-T. Nuclear penetration of surface functionalized gold nanoparticles. Toxicology and applied Pharmacology. 2009;237:196-204.

[111] Everts M, Saini V, Leddon JL, Kok RJ, Stoff-Khalili M, Preuss MA, et al. Covalently linked Au nanoparticles to a viral vector: potential for combined photothermal and gene cancer therapy. Nano Letters. 2006;6:587-91.

[112] Hsu SH, Tang CM, Tseng HJ. Biocompatibility of poly(ether)urethane-gold nanocomposites. J Biomed Mater Res A. 2006;79:759-70.

[113] Castaneda L, Valle J, Yang N, Pluskat S, Slowinska K. Collagen cross-linking with Au nanoparticles. Biomacromolecules. 2008;9:3383-8.

[114] Hsu S-h, Tang C-M, Tseng H-J. Gold nanoparticles induce surface morphological transformation in polyurethane and affect the cellular response. Biomacromolecules. 2007;9:241-8.

[115] Rai A, Prabhune A, Perry CC. Antibiotic mediated synthesis of gold nanoparticles with potent antimicrobial activity and their application in antimicrobial coatings. Journal of Materials Chemistry. 2010;20:6789-98.

[116] Qu Y, Lü X. Aqueous synthesis of gold nanoparticles and their cytotoxicity in human dermal fibroblasts–fetal. Biomedical Materials. 2009;4:025007.

[117] Hsu Sh, Chou CW, Tseng SM. Enhanced thermal and mechanical properties in polyurethane/Au nanocomposites. Macromolecular Materials and Engineering. 2004;289:1096-101.

[118] Chou CW, Hsu SH, Wang PH. Biostability and biocompatibility of poly(ether)urethane containing gold or silver nanoparticles in a porcine model. J Biomed Mater Res A. 2008;84:785-94.

[119] Grant SA, Spradling CS, Grant DN, Fox DB, Jimenez L, Grant DA, et al. Assessment of the biocompatibility and stability of a gold nanoparticle collagen bioscaffold. J Biomed Mater Res A. 2013.

[120] Hsu S-h, Chou C-W. Enhanced biostability of polyurethane containing gold nanoparticles. Polymer degradation and stability. 2004;85:675-80.

[121] Deeken CR, Bachman SL, Ramshaw BJ, Grant SA. Characterization of bionanocomposite scaffolds comprised of mercaptoethylamine-functionalized gold nanoparticles crosslinked to acellular porcine tissue. J Mater Sci Mater Med. 2012;23:537-46.

[122] Boisselier E, Astruc D. Gold nanoparticles in nanomedicine: preparations, imaging, diagnostics, therapies and toxicity. Chem Soc Rev. 2009;38:1759-82.

[123] Shukla S, Priscilla A, Banerjee M, Bhonde RR, Ghatak J, Satyam PV, et al. Porous gold nanospheres by controlled transmetalation reaction: A novel material for application in cell imaging. Chemistry of Materials. 2005;17:5000-5.

[124] Shukla R, Bansal V, Chaudhary M, Basu A, Bhonde RR, Sastry M. Biocompatibility of gold nanoparticles and their endocytotic fate inside the cellular compartment: A microscopic overview. Langmuir. 2005;21:10644-54.

[125] Connor EE, Mwamuka J, Gole A, Murphy CJ, Wyatt MD. Gold nanoparticles are taken up by human cells but do not cause acute cytotoxicity. Small. 2005;1:325-7.

Chapter Two

INTRODUCTION TO RESEARCH

2.1 Significance of Research

Cardiac and vascular materials are used to treat trauma and aneurysms, repair congenital defects, and patch defects in vessel and cardiac walls [1-4]. Finding a suitable material for these repairs included research in both biologic and synthetic materials, yet failed to yield a material that mimics the mechanics and biocompatibility of the natural tissue while not causing host complications. Current synthetic and biologic scaffolds can cause negative host reactions such as inflammation, calcification, and infection [5-10]. The significance of this research was to create, characterize, and optimize an improved gold nanomaterial tissue patch for vascular and cardiac repairs. The material is created from porcine vascular tissue and conjugated with gold nanoparticles to improve biocompatibility, mechanical properties, cellular integration, while resisting calcification, intimal hyperplasia, and thromboembolism formation.

2.2 Research Objectives

The overarching objective of this research was to characterize and optimize decellularized porcine arterial tissue as a vascular and cardiac repair material. The initial stage was *in vitro* testing of the material, which examined the

basic characteristics and biocompatibility of the material. The second stage consisted of two *in vivo* studies. The first investigated several different versions of the experimental material to understand how it behaved *in vivo* and to compare it to a currently used material. The second study was a long-term study that investigated the material in a high pressure setting to better understand the material's strengths and the host's long-term reaction to its presence.

The purpose of the initial *in vitro* work was to provide basic information about the mechanical strength and biocompatibility of the material, and to compare different surface modifications. Published decellularization protocols were used to create a material composed of a non-immunogenic extracellular matrix (ECM) that would retain the characteristics of the native tissue. There are numerous surface modifications being researched to create more favorable surface-blood interactions and to improve biocompatibility. Gold nanoparticles have been shown *in vitro* to enhance cellular proliferation, reduce bacterial adhesion, and reduce reactive oxygen species, and were an obvious choice to help optimize the material [11-14]. The various modifications were examined via light microscopy and scanning electron microscopy (SEM) to determine if all the nuclear remnants were being cleared during the decellularization process, and to ensure the ECM was not being maimed during decellularization and crosslinking. The SEM also determined that the nanoparticles were still conjugated to the material after sterilization. Two different biocompatibilty studies were performed with two cell lines to determine if any of the processing or the presence of the gold nanoparticles would cause changes in cell proliferation or result in

cytotoxicty. Finally, mechanical studies determined the material's strength when compared to the native tissue.

The results from the *in vitro* work led to two *in vivo* studies with swine. In the first study, several differently modified patches were placed on one carotid artery with a commercially available material on the contralateral artery in each animal. This study allowed for comparison between the various patch modifications, as well as between the experimental and commercial materials. The study also offered two time points in order to study the long and short-term healing responses to the material. The second study placed the experimental material conjugated with gold nanoparticles over an artificially created defect in the thoracic aorta. The objective of this study was to see how the material performed in a high pressure environment in the long-term. The study lasted six months; enough time to determine if any common adverse effects such an intimal hyperplasia would arise.

The results of these experiments showed that we have created a nanocomposite material with numerous advantageous qualities. Our material retains its natural structure through processing, shows excellent biocompatibility in cell culture assays, and has mechanical strength equivalent to the native tissue while retaining its natural structure. The *in vivo* work shows that the material is feasible in a vascular environment and has a favorable interface with blood. These studies showed that the material allows for excellent cellular infiltration and resists neo-intimal hyperplasia and calcification. Overall, this

research proves the creation of a novel nanocomposite material tailored to a vascular and cardiac environment.

2.3 References

[1] David TE. The use of pericardium in acquired heart disease: a review article. J Heart Valve Dis. 1998;7:13-8.

[2] David TE, Armstrong S. Surgical repair of postinfarction ventricular septal defect by infarct exclusion. Seminars in thoracic and cardiovascular surgery. 1998;10:105-10.

[3] Fishman NH. Left ventricular aneurysm repair. Ann Thorac Surg. 1998;65:602-3.

[4] Robinson KA, Li J, Mathison M, Redkar A, Cui J, Chronos NAF, et al. Extracellular Matrix Scaffold for Cardiac Repair. Circulation. 2005;112:I-135-I-43.

[5] Awad IA, Little JR. Patch angioplasty in carotid endarterectomy. Advantages, concerns, and controversies. Stroke. 1989;20:417-22.

[6] Bond R, Rerkasem K, Naylor AR, AbuRahma AF, Rothwell PM. Systematic review of randomized controlled trials of patch angioplasty versus primary closure and different types of patch materials during carotid endarterectomy. Journal of Vascular Surgery. 2004;40:1126-35.

[7] Cho SW, Park HJ, Ryu JH, Kim SH, Kim YH, Choi CY, et al. Vascular patches tissue-engineered with autologous bone marrow-derived cells and decellularized tissue matrices. Biomaterials. 2005;26:1915-24.

[8] Lee WK, Park KD, Kim YH, Suh H, Park JC, Lee JE, et al. Improved calcification resistance and biocompatibility of tissue patch grafted with sulfonated PEO or heparin after glutaraldehyde fixation. Journal of biomedical materials research. 2001;58:27-35.

[9] Matsagas M, Bali C, Arnaoutoglou E, Papakostas J, Nassis C, Papadopoulos G, et al. Carotid Endarterectomy with Bovine Pericardium Patch Angioplasty: Mid-Term Results. Annals of vascular surgery. 2006;20:614-9.

[10] Muto A, Nishibe T, Dardik H, Dardik A. Patches for carotid artery endarterectomy: Current materials and prospects. Journal of Vascular Surgery. 2009;50:206-13.

[11] Castaneda L, Valle J, Yang N, Pluskat S, Slowinska K. Collagen cross-linking with
Au nanoparticles. Biomacromolecules. 2008;9:3383-8.

[12] Hsu S-h, Tang C-M, Tseng H-J. Gold nanoparticles induce surface morphological transformation in polyurethane and affect the cellular response. Biomacromolecules. 2007;9:241-8.

[13] Rai A, Prabhune A, Perry CC. Antibiotic mediated synthesis of gold nanoparticles with potent antimicrobial activity and their application in antimicrobial coatings. Journal of Materials Chemistry. 2010;20:6789-98.

[14] Whelove OE, Cozad MJ, Lee BD, Sengupta S, Bachman SL, Ramshaw BJ, et al. Development and in vitro studies of a polyethylene terephthalate-gold nanoparticle scaffold for improved biocompatibility. J Biomed Mater Res B Appl Biomater. 2011;99:142-9.

Chapter Three

PRELIMINARY CHARACTERIZATION STUDIES

3.1 Introduction

The development of a novel biomaterial requires many preliminary characterization studies, some of which are extremely basic steps that must be undertaken to ensure the biomaterial is worth further pursuit. This chapter contains experiments that were not necessary for publication, but useful initial studies. There are several ways we created and tested biocompatibility in our biomaterial. In order to create a biocompatible material all of the native cells must be removed from the tissue through decellularization. This process will decrease the immune response when implanted in the host and is particularly important with xenograft materials [1, 2]. Crosslinking is another aspect of creating a strong biomaterial and can improve the stability of the biomaterial by forming covalent bonds between the collagen fibers. As discussed in Chapter 1.3.2, the use of AuNPs may augment antimicrobial properties of biomaterials as well as increase cell proliferation [3-7]. The broad hypothesis for the experiments done here was that the use of crosslinking and the addition of AuNPs would not hinder murine fibroblast growth. The secondary hypothesis was to test the biocompatibility of bovine carotid artery and compare the mechanical properties of bovine and porcine tissue. These initial studies were to determine the best animal to harvest tissue from looking at porcine and bovine tissue and to ensure

that the material was biocompatible at a very basic level through the use of a very common cell line.

3.2 Materials and Methods

3.2.1 Chemicals

Unconjugated gold nanoparticles (20 nm and 100nm diameter were purchased from Ted Pella, Inc. (Redding, CA) The following chemicals were purchased from Sigma Aldrich (St. Louis, MO): ethylenediaminetetraacetic acid (EDTA), tributyl phosphate, 2-mercaptoethylamine, phosphate buffered saline (PBS), 1-ethyl-3-(3-dimethylaminopropyl)carbodiimide (EDC), N,N-dimethylformamide (DMF), 2-(N-Morpholino)ethanesulfonic acid hydrate (MES), Triton™ X-100 (4-(1,1,3,3-Tetramethylbutyl)phenyl-polyethylene glycol, t-Octylphenoxypolyethoxyethanol, Polyethylene glycol tert-octylphenyl ether), peracetic acid, trypan blue stain, papaya latex, and L-cysteine hydrochloride. Acetone and sodium chloride (NaCl) were purchased from Acros Organics USA (Morris Plains, NJ). ATCC-formulated Eagle's Minimum Essential Medium (EMEM), horse serum, penicillin-streptomycin solution, and Dulbecco's Phosphate Buffered Saline (DPBS) were obtained from American Type Culture Collection (ATCC) (Manassas, VA). Disodium ethylenediaminetetraacetate (Na2EDTA) and 1X TE buffer were purchased from Fisher Scientific (Pittsburgh, PA) and Invitrogen Corporation (Carlsbad, CA), respectively. Ethanol was bought

from University of Missouri ChemStores (Columbia, MO) and N-Hydroxysuccinimide (NHS) from Pierce Protein Research Products (Rockford, IL).

3.2.2 Tissue Harvest and Decellularization

Porcine aortas were harvested immediately following euthanasia of swine after a laboratory exercise at the University Of Missouri School Of Medicine. Bovine carotid arteries were collected from the University of Missouri abattoir at the time of euthanasia. Tissue was immersed in distilled water to immediately start the decellularization process. Decellularization was performed using a protocol adapted from previously published arterial decellularization protocols. [8, 9] Arteries were cleaned of blood and any excess surrounding tissue and then immersed in distilled water for 24 hours at 4 ° C to rupture cell membranes. Next, the vessels were treated with 0.025% trypsin EDTA (ATCC) diluted in Dulbecco's phosphate buffered saline (dPBS; ATCC) for 24 hours at 37 °C. The tissue was then put into a solution of 1% Triton X-100 (Sigma) and 0.1% ammonium hydroxide (Fisher) in distilled water for 72 hours at 4 °C to remove nuclear components and lyse cell membranes and cytoplasmic proteins. The tissue was immersed in a solution of Eagle's Minimum Essential Medium (EMEM; ATCC) 10% (v/v) horse serum and PennStrep (200 U/mL) to deactivate any remaining trypsin for 24 hours at 37 °C. Tissue was washed for 24 hours in distilled water at 4 °C and for 48 hours in PBS at 4 °C, changing the PBS to fresh

solution at 24 hours. All of these steps were done with mechanical agitation on a stir plate.

3.2.3 Crosslinking and Sterilization

Specific experimental groups are listed with their respective experiments. As these were just initial studies the groups varied, but all had the same basic preparations. Tissue was crosslinked using a protocol publish by Deeken et al. [10]. The crosslinking solution was composed of a 50:50 (v/v) solution of acetone and PBS (pH=7.4) with 2mM EDC and 5mM NHS. The EDC was dissolved in a small volume of MES with 0.5M NaCl (pH 6.) and the NHS in a small volume of DMF. The solutions were immediately mixed together and added to the acetone/PBS solution. Treatment groups requiring crosslinking were reacted with this solution at ambient temperature for 15 minutes to activate the carboxyl groups present on the collagen molecules. After 15 minutes the crosslinking solution was withdrawn and 20 nm ($2.8x10^{12}$ particles/mL) AuNPs were added at a concentration of 4 times the stock solution. They were amine functionalized and added to their respective experimental tissue with PBS. The solely crosslinked tissue group was put into PBS after 15 minutes. All groups were incubated for 24 hours with gentle agitation followed by two 24 hours rinses in PBS. Specimens were sterilized by incubating tissue in an aqueous solution of 0.1 %(v/v) peracetic acid with 1.0M NaCl for 30 minutes followed by two 24 hour sterile PBS rinses. All steps were performed at ambient temperature with shaking.

3.2.4 Cell Culture

L-929 murine fibroblast cells (ATCC – Manassas, VA) were cultured in EMEM supplemented with 10% (v/v) horse serum and 200 U/mL penicillin-streptomycin solution in an incubator at 37 °C and 5% CO2. Primary umbilical vein endothelial cells, normal, human, pooled (ATCC PCS-100-013) were cultured Vascular Cell Basal Medium (ATCC PCS-100-030) supplemented with Microvascular Endothelial Cell Growth Kit-BBE (ATCC PCS-110-040) and Penicillin (10 u/mL) –streptomycin (10 µg/mL)-amphotericin B (25 ng/mL) solution (ATCC PCS-999-002).

3.2.5 Biocompatibility of Porcine Tissue with Fibroblasts

Experimental Groups:

1) Decellularized tissues (Decell): porcine aortic tissues that underwent the decellularization protocol. n=21

2) Crosslinked tissues (XLink): decellularized porcine aortic tissues that were crosslinked as previously described. n=19

3) 4x 20nm AuNP tissues (4x AuNP): decellularized porcine aortic tissues that were crosslinked with 20 nm gold nanoparticles at four times the stock solution ($2.8x10^{12}$ particles/mL) in combination with EDC and NHS. n=20

Cell proliferation Reagent WST-1 (Roche Diagnostics Corporation, Indianapolis, IN) was used to compare the biocompatibility of the experimental groups. Each group had an n as described above and an additional two

scaffolds that were not seeded for use as standards. Culture medium with the WST-1 reagent and no cells served as the blank. The 1 cm tissue discs were incubated in individual wells of a 48 well plate at 37 °C and 5% CO2 in EMEM for 24 hours at 37 °C before being seeded with 3 x 10^4 L-929 murine fibroblasts/well. After 2 days the scaffolds were moved to new 48-well plates to ensure cellular attachment to the scaffolds only. All scaffolds were incubated for 3 days at 37 °C and 5% CO2 with half the media in each well replaced every 24 hours. WST-1 reagent was then added to each well and the plates were incubated for 6 hours. 100 µl was removed, placed into a 96-well microplate, and read by a BIO-Rad Model 680 Microplate Reader (Bio-Rad Laboratories Hercules, CA). The percent viability was calculated by normalizing the resulting values by the average absorbance of the decellularized group. The amount of formazan created in the reaction between metabolically active cells and the tetrazolium salts correlated with the number of metabolically active cells and was quantified using UV-Vis absorbance measurements with higher absorbance values representing more metabolically active cells and greater biocompatibility.

3.2.6 Cell Proliferation of Fibroblasts on Porcine Tissue

Experimental Groups:

1) Decellularized tissues (Decell): porcine aortic tissues that underwent the decellularization protocol. n=6

2) Crosslinked tissues (XLink): decellularized porcine aortic tissues that were crosslinked as previously described. n=6

3) 4x 20nm AuNP tissues (4x AuNP): decellularized porcine aortic tissues that were crosslinked with 20 nm gold nanoparticles at four times the stock solution ($2.8x10^{12}$ particles/mL) in combination with EDC and NHS. n=6

Quant-iT™ PicoGreen® dsDNA Reagent (Invitrogen Corporation, Carlsbad, CA) was used to assess cell proliferation (n = 6 per group at each time point). This assay allows for quantification of dsDNA content which can be directly correlated to the amount of cellular growth on the scaffold. The 1 cm tissue discs were incubated in individual wells of a 48 well plate at 37 °C and 5% CO2 in EMEM for 24 hours at 37 °C before being seeded with 3×10^4 L-929 murine fibroblasts/well. All scaffolds were incubated at 37 °C and 5% CO2 for the 7, 10, and 14 day time points. After 2 days the scaffolds were moved to new 48-well plates to ensure cellular attachment to the scaffolds only. The media was changed out every other day. At 7 and 10 days post cell seeding the appropriate scaffolds were removed, rinsed with 5mL sterile PBS, placed in 1.5 mL microcentrifuge tubes, and frozen at - 70 C. Samples were lypholized for 24 hours and then the dry mass of each scaffold was determined. Each sample was subjected to a papain digestion buffer of 125 µg/mL on a buffer of sterile PBS with 5mM cysteine-HCl and 5mL Na2 EDTA for 24 hours at 60 °C. Each sample was put in 4 mL cuvettes then diluted with 1X TE buffer and the PicoGreen dsDNA reagent. The cuvettes were incubated at in the dark at ambient temperature for 5 minutes. Fluorescence readings were taken at 520 nm using 480 nm excitation on a FluoroMax-3 spectrofluorometer (HORIBA Jobin Yvon, Inc., Edison, NJ). A

Lambda DNA standard curve was used to determine the DNA concentrations for the samples. Each concentration was normalized by the dry mass of the sample.

3.2.7 Biocompatibility of Bovine Tissue with Endothelial Cells

Experimental Groups:

1) Decellularized tissues (Decell): bovine carotid arteries that underwent the decellularization protocol. n=9

2) Crosslinked tissues (XLink): decellularized bovine carotid arteries that were crosslinked as previously described. n=9

3) 4x 100nm AuNP tissues (4x AuNP): decellularized bovine carotid arteries that were crosslinked with 20 nm gold nanoparticles at four times the stock solution ($2.8x10^{12}$ particles/mL) in combination with EDC and NHS. n=9

Cell proliferation Reagent WST-1 was used to compare the biocompatibility of bovine carotid tissue. Each group had an n=9 and an additional scaffold that was not seeded for use as a standard. Culture medium with the WST-1 reagent and no cells served as the blank. The tissue discs were incubated at 37 °C and 5% CO2 in Vascular Cell Basal Medium (ATCC PCS-100-030) supplemented with Microvascular Endothelial Cell Growth Kit-BBE (ATCC PCS-110-040) and Penicillin (10 u/mL) –streptomycin (10 µg/mL)-amphotericin B (25 ng/mL) solution (ATCC PCS-999-002) for 24 hours in individual wells of a 48 well microplate. After 24 hours the media was removed and each well was seeded with primary umbilical vein endothelial cells, normal, human at a concentration of 3×10^4 cells/mL. After 2 days the scaffolds were

moved to new 48-well plates to ensure cellular attachment to the scaffolds only. All scaffolds were incubated for 7 days at 37 °C and 5% CO2 with half the media in each well replaced every 24 hours. WST-1 reagent was then added to each well and the plates were incubated for 6 hours. 100 µl was removed at 6 hours and placed into a 96-well microplate and read by a BIO-Rad Model 680 Microplate Reader (Bio-Rad Laboratories Hercules, CA). The percent viability was calculated by normalizing the resulting values by the average absorbance of the decellularized group.

3.2.8 Mechanical Testing of Porcine Versus Bovine Tissue

Experimental Groups:

1) Native Porcine Carotid Artery: freshly harvested porcine carotid artery n=6

2) Decellularized Porcine Carotid Artery: porcine aortic tissues that underwent the decellularization protocol. n=6

3) Crosslinked Porcine Carotid Artery: decellularized porcine aortic tissues that were crosslinked as previously described. n=4

4) Native Porcine Aorta: freshly harvested porcine aorta. n=4

5) Decellularized Porcine Aorta: porcine carotid arteries that underwent the decellularization protocol. n=6

6) Crosslinked Porcine Aorta: decellularized porcine carotid arteries that were crosslinked as previously described. n=6

7) Native Bovine Carotid Artery: freshly harvested bovine carotid artery. n=10

8) Decellularized tissues: bovine carotid arteries that underwent the decellularization protocol. n=6

9) Crosslinked tissues: decellularized bovine carotid arteries that were crosslinked as previously described. n=5

AuNP conjugated tissues were not tested as no significant differences were found between tissues with and without them. That data can be found in Chapter 4 of this dissertation. The vessels were tested in the longitudinal direction. Each piece was 4 cm by 1 cm and notched to reduce the width of the specimen to approximately 0.5 cm and create a stress concentration in the center of the specimen and thus prevent failure in the grip. A mechanical testing system (Instron TA.XT2, Texture Technologies, Corporation, Scarsdale, NY) strained the specimens until failure. The tensile strength at yield was calculated by dividing the maximum load, Fmax, by the original cross-sectional area, A, of the specimen. The modulus of elasticity E, was determined from the slope of a line fit to the stress versus strain curve of each specimen.

3.2.9 Statistical Analysis

GraphPad Prism v4.0 (GraphPad Software, Inc., San Diego, CA) was used to analyze experimental data. One-way analysis of variance (ANOVA) with a 95% confidence interval was conducted followed by a Tukey-Kramer post-test to determine significant differences between means of the experimental groups for the mechanical testing and biocompatibility assays. A two-way ANOVA was used to analyze the cell proliferation assay with regards to both the differing time

points and experimental groups. Values are reported and graphed as the mean ± standard error of the mean.

3.3 Results

3.3.1 Biocompatibility of Porcine Tissue with Fibroblasts

The WST-1 assay showed no significant differences between any of the groups when the percent viability of the experimental groups were compared to the decellularized tissue, indicating no significant changes in viability with the use of crosslinking or nanoparticles. Significance was set at $P<0.05$ and for this experiment $P= 0.884$. Figure 3.1 shows percent viability of each experimental group relative to the decellularized, with specific values in Table 3.1.

Table 3.1 Summary of WST-1 Assay data with fibroblasts

Experimental Group	% Viability compared to Decell
Decellularized Porcine Tissue	100.0% ± 7.5%
Crosslinked Porcine Tissue	95.5% ± 8.7%
Crosslinked with 4x 100nm AuNPs	101.9% ± 11.1%

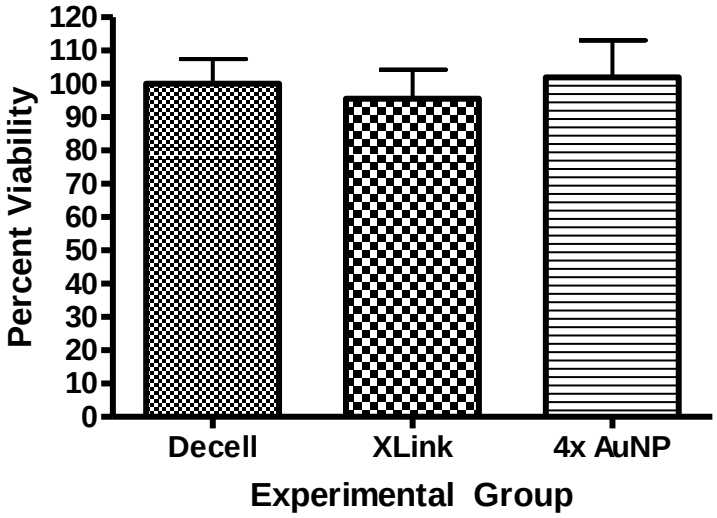

Figure 3.1 Cell Proliferation Reagent WST-1 assay on porcine aortas showing percent viability relative to the decellularized tissue, indicating no significant changes in viability with the use of crosslinking or nanoparticles.

3.3.2 Cell Proliferation of Fibroblasts on Porcine Tissue

The fluorescence intensity of the Quant-iT™ PicoGreen® dsDNA reagent quantified cell proliferation and was recorded for the experimental material digests after being cultured with L-929 mouse fibroblasts. The lamda DNA standard curve was used to calculate a curve with an r^2 value of 0.9699. The data was normalized to the dry weight of each scaffold (see Table 3.2) and the nanograms of DNA per milligram scaffold was calculated and graphed in Figure 3.2. There were no significant differences ($p<0.05$) between each group on a specific day, however there was a significant increase within groups between days 7 and 10. This increase shows that the cells continue proliferating as they should, and do not start dying out. The lack of significant differences between experimental groups at each time point shows that the crosslinking and addition of AuNPs does not have a negative effect on cell proliferation.

Table 3.2 Summary of PicoGreen Data of fibroblasts on porcine tissue showing scaffold dsDna content (ng/mg dry scaffold weight)

Experimental Group	Day 7	Day 3
Decellularized Porcine Aorta	3.90 ± 0.253	7.322 ± 0.339
Crosslinked Porcine Aorta	3.028 ± 0.591	7.683 ± 0.774
Crosslinked with 4x 100nm AuNPs	4.015 ± 0.993	7.402 ± 0.552

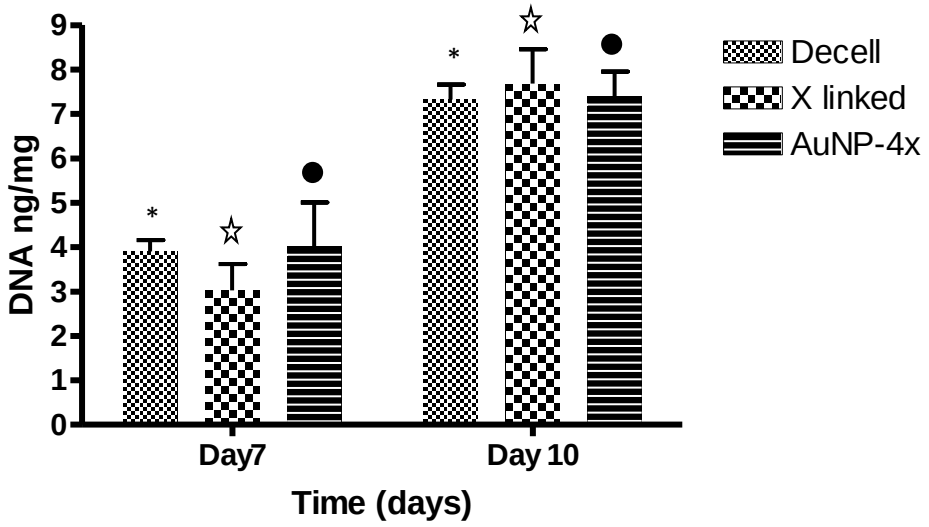

Figure 3.2 The results of the PicoGreen Assay using porcine aortas and fibroblast cells showing that each group had a significant increase ($p<0.05$) between days 7 and 10.

3.3.3 Biocompatibility of Bovine Tissue with Endothelial Cells

The WST-1 assay showed no significant differences between any of the groups when the percent viability of the experimental groups were compared to the decellularized tissue, indicating no significant changes in viability with the use of crosslinking or nanoparticles. Significance was set at $P<0.05$ and for this experiment $P= 0.624$. Figure 3.3 shows percent viability of each experimental group relative to the decellularized, with specific values in Table 3.3.

Table 3.3 Summary of WST-1 Assay data of endothelial cells on bovine tissue

Experimental Group	% Viability compared to Decell
Decellularized Bovine Carotid	100.0% ± 15.0%
Crosslinked Bovine Carotid	80.2% ± 14.2%
Crosslinked with 4x 100nm AuNPs	89.4% ± 13.7%

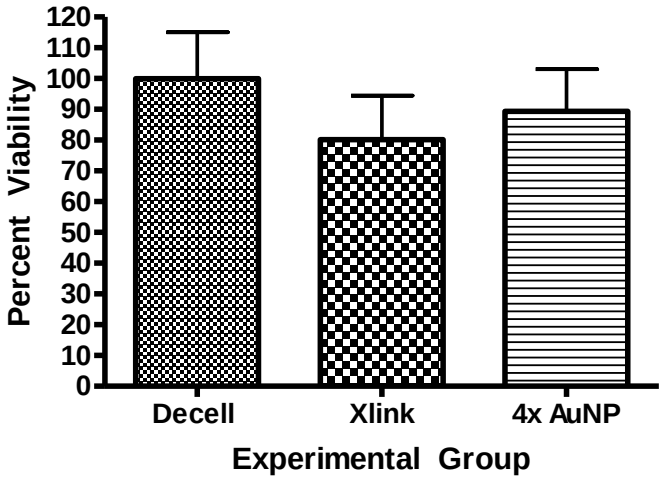

Figure 3.3 Cell Proliferation Reagent WST-1 assay on bovine tissue showing percent viability relative to the decellularized tissue, indicating no significant changes in viability with the use of crosslinking or nanoparticles.

3.3.4 Mechanical Testing of Porcine Versus Bovine Tissue

Porcine aortic and carotid tissue was compared to bovine carotid tissue to compare the mechanical properties of each. The tensile stress at maximum load, the modulus of elasticity, and the percent tensile strain at maximum load were calculated to determine how each behaved. Table 3.4 contains the values for each experimental group. For the modulus of elasticity, Porcine Decell Carotid, Porcine X link Carotid, Porcine Native Aorta, Porcine Decell Aorta, and Porcine Xlink Aorta were significantly lower ($p<0.01$) than Bovine Native Carotid. Porcine Decell Carotid was significantly ($p<0.05$) lower than Bovine Xlink Carotid. Porcine Decell Carotid, Porcine Decell Aorta, and Porcine Xlink Aorta were significantly lower ($P<0.01$) than Bovine Carotid Decell. These differences can be seen in Figure 3.4a. For tensile stress at max load, Porcine Decell Carotid and Porcine Decell Aorta were significantly lower ($p<0.01$) than Bovine Native Carotid. Porcine Native Carotid, Porcine Decell Carotid, Carotid Porcine Native Aorta, Porcine Decell Aorta, and Porcine Xlink Aorta were significantly lower ($p<0.01$) than Bovine Decell Carotid. Porcine Decell Carotid, Porcine Native Aorta, Porcine Decell Aorta, and Porcine Xlink Aorta were significantly lower ($p<0.01$) than Bovine Xlink Carotid. These differences can be seen in Figure 3.4b.

Table 3.4 Modulus of Elasticity (MPa) and Tensile Stress at Max (MPa) for each experimental group

	Modulus of Elasticity (MPa)	Tensile Stress at Max (MPa)
PCNative	15.07 ± 2.60	1.15 ± 0.17
PCDcell	3.22 ± 0.75	0.57 ± 0.07
PCXlink	9.63 ± 1.26	1.33 ± 0.43
PANative	9,74 ± 2.67	0.57 ± 0.09
PADcell	6.29 ± 2.63	0.57 ± 0.11
PAXlink	5.73 ± 0.68	0.65 ± 0.06
BCNative	26.61 ± 3.27	1.87 ± 0.27
BCDecell	22.81 ± 4.70	2.62 ± 0.41
BCXlink	17.72 ± 3.04	2.44 ± 0.30

3.4a) Modulus of Elasticity

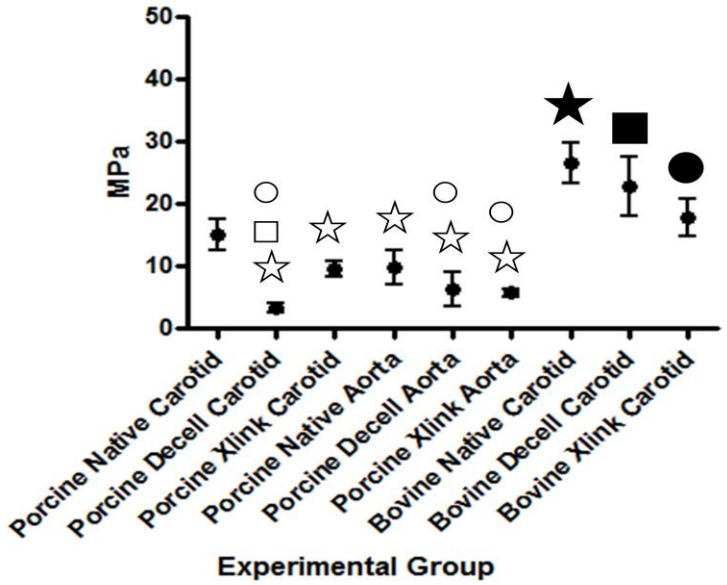

3.4b) Tensile Stress at Max Load

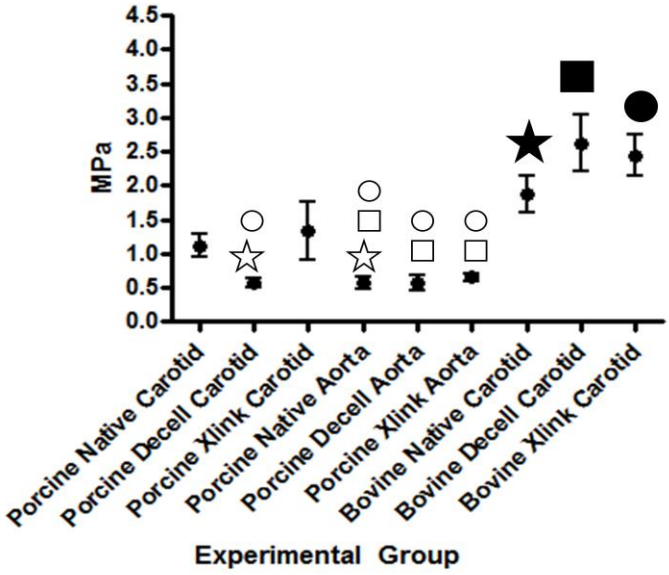

Figure 3.4 Mechanical testing on porcine and bovine tissues. White shapes denote a value significantly lower than the matching black shape on each graph.

3.4 Discussion and Conclusions

Preliminary studies were done using porcine aortic tissue and murine fibroblasts to test the basic biocompatibility of the material and its various modifications. L-929 murine fibroblasts are a very commonly used cell line and the studies done here prove that our modifications do not kill the fibroblast cells. This was the basis for our later testing with more sensitive endothelial cell line, which is the type of cell we hope will populate the surface of our biomaterial *in vivo*. While the decellularization process used here has been previously published [8, 9], cell culture studies using a basic fibroblast cell line were useful to ensure we were performing the protocol correctly and not leaving any potentially harmful chemicals in the material. Crosslinking with zero length crosslinkers has become more common as the use of glutaraldehyde crosslinkers have been shown to calcify when implanted. [11, 12] The zero length crosslinking utilized here has shown that it does not cause any cytotoxicity and allows cells to proliferate as well as experimental groups without crosslinking. The final modification tested was the use of AuNPs. AuNPs have been shown *in vitro* to enhance cellular proliferation, reduce bacterial adhesion, and reduce reactive oxygen species when conjugated to polyethylene terephthalate.[13] Here we tested them at a high concentration to make sure we wouldn't see cytotoxicity. From these preliminary tests we concluded that the material was safe enough to try with endothelial cell culture assays.

Animal tissue is used in numerous medical applications such as heart valves [14-17], blood vessels [18-20], urinary bladder [21], bovine pericardium, and many others [22]. Bovine pericardium is used as a vascular and cardiac patch material. We wanted to look at bovine carotid vessels as they are larger than the porcine carotid arteries, but still thinner than the porcine aortas. The biocompatibility study showed that the bovine carotid tissue had no detrimental effect on human endothelial cells. The mechanical studies indicate that the strengths of bovine and porcine tissue vary between animal species and artery type. However there were no significant differences between material modifications (decellularizing, crosslinking) and the native tissue within groups of the same tissue type. This indicates that our modifications are not changing the properties of the native tissue, which shows great promise for our biomaterial. A biomaterial with a higher elastic modulus will be stiffer. Overall the bovine tissue was generally stiffer than the porcine tissue. When implanted into a vessel this would allow for less stretch of the bovine patch and could indicate more deformation of the hemodynamic flow pattern. It has been shown that a more compliant graft may match mechanical and flow parameters better than a less compliant material [23]. Bovine arterial tissue might still be a promising material for other cardiovascular applications such as heart valve leaflets, though. The tensile stress at max load indicates the point at which the material fails completely. Again we saw that overall the porcine tissue failed at a lower force per unit area than the bovine tissue. This is not necessarily a negative characteristic, and later we saw that the porcine material still withstands great

vascular pressures *in vivo.* These conclusions leave the door open for further testing of the bovine vessels. Bovine and porcine vessels should be compared to human native vessels, something we were unable to do due to availability of such. Suture pullout testing of the biomaterial is included in Chapter 6 of this dissertation. The decision was made to move forward with the porcine tissue as the bovine showed no real advantage over it and was much more difficult to obtain.

Overall these preliminary studies gave us good basic information on the characteristics of our bases for a composite biomaterial as well as about the surface modifications made to that material. Further *in vitro* and *in vivo* testing of these materials is available in the next several chapters of this dissertation.

3.5 References

[1] Badylak SF. Xenogeneic extracellular matrix as a scaffold for tissue reconstruction. Transpl Immunol. 2004;12:367-77.

[2] Cartmell JS, Dunn MG. Effect of chemical treatments on tendon cellularity and mechanical properties. Journal of biomedical materials research. 2000;49:134-40.

[3] Hsu SH, Tang CM, Tseng HJ. Biocompatibility of poly(ether)urethane-gold nanocomposites. J Biomed Mater Res A. 2006;79:759-70.

[4] Castaneda L, Valle J, Yang N, Pluskat S, Slowinska K. Collagen cross-linking with Au nanoparticles. Biomacromolecules. 2008;9:3383-8.

[5] Hsu S-h, Tang C-M, Tseng H-J. Gold nanoparticles induce surface morphological transformation in polyurethane and affect the cellular response. Biomacromolecules. 2007;9:241-8.

[6] Rai A, Prabhune A, Perry CC. Antibiotic mediated synthesis of gold nanoparticles with potent antimicrobial activity and their application in antimicrobial coatings. Journal of Materials Chemistry. 2010;20:6789-98.

[7] Qu Y, Lü X. Aqueous synthesis of gold nanoparticles and their cytotoxicity in human dermal fibroblasts–fetal. Biomedical Materials. 2009;4:025007.

[8] Williams C, Liao J, Joyce EM, Wang B, Leach JB, Sacks MS, et al. Altered structural and mechanical properties in decellularized rabbit carotid arteries. Acta Biomater. 2009;5:993-1005.

[9] Amiel GE, Komura M, Shapira O, Yoo JJ, Yazdani S, Berry J, et al. Engineering of blood vessels from acellular collagen matrices coated with human endothelial cells. Tissue Eng. 2006;12:2355-65.

[10] Deeken CR, White AK, Bachman SL, Ramshaw BJ, Cleveland DS, Loy TS, et al. Method of preparing a decellularized porcine tendon using tributyl phosphate. J Biomed Mater Res B Appl Biomater. 2011;96:199-206.

[11] Ma L, Gao C, Mao Z, Zhou J, Shen J. Enhanced biological stability of collagen porous scaffolds by using amino acids as novel cross-linking bridges. Biomaterials. 2004;25:2997-3004.

[12] Duan X, Sheardown H. Crosslinking of collagen with dendrimers. J Biomed Mater Res A. 2005;75:510-8.

[13] Whelove OE, Cozad MJ, Lee BD, Sengupta S, Bachman SL, Ramshaw BJ, et al. Development and in vitro studies of a polyethylene terephthalate-gold nanoparticle scaffold for improved biocompatibility. J Biomed Mater Res B Appl Biomater. 2011;99:142-9.

[14] Bader A, Schilling T, Teebken OE, Brandes G, Herden T, Steinhoff G, et al. Tissue engineering of heart valves–human endothelial cell seeding of detergent acellularized porcine valves. European journal of cardio-thoracic surgery. 1998;14:279-84.

[15] Grauss RW, Hazekamp MG, Oppenhuizen F, van Munsteren CJ, Gittenberger-de Groot AC, DeRuiter MC. Histological evaluation of decellularised porcine aortic valves: matrix changes due to different decellularisation methods. European journal of cardio-thoracic surgery. 2005;27:566-71.

[16] Kasimir M, Rieder E, Seebacher G, Silberhumer G, Wolner E, Weigel G, et al. Comparison of different decellularization procedures of porcine heart valves. The International journal of artificial organs. 2003;26:421-7.

[17] Rieder E, Kasimir M-T, Silberhumer G, Seebacher G, Wolner E, Simon P, et al. Decellularization protocols of porcine heart valves differ importantly in efficiency of cell removal and susceptibility of the matrix to recellularization with human vascular cells. The Journal of thoracic and cardiovascular surgery. 2004;127:399-405.

[18] Conklin B, Richter E, Kreutziger K, Zhong D-S, Chen C. Development and evaluation of a novel decellularized vascular xenograft. Medical engineering & physics. 2002;24:173-83.

[19] Dahl SL, Koh J, Prabhakar V, Niklason LE. Decellularized native and engineered arterial scaffolds for transplantation. Cell transplantation. 2003;12:659-66.

[20] Uchimura E, Sawa Y, Taketani S, Yamanaka Y, Hara M, Matsuda H, et al. Novel method of preparing acellular cardiovascular grafts by decellularization with poly (ethylene glycol). Journal of Biomedical Materials Research Part A. 2003;67:834-7.

[21] Freytes DO, Badylak SF, Webster TJ, Geddes LA, Rundell AE. Biaxial strength of multilaminated extracellular matrix scaffolds. Biomaterials. 2004;25:2353-61.

[22] Badylak SF, Freytes DO, Gilbert TW. Extracellular matrix as a biological scaffold material: Structure and function. Acta Biomater. 2009;5:1-13.

[23] Wang X, Lin P, Yao Q, Chen C. Development of small-diameter vascular grafts. World J Surg. 2007;31:682-9.

Chapter Four

MECHANICAL AND IN VITRO CHARACTERIZATION OF DECELLULARIZED PORCINE ARTERIAL TISSUE CONJUGATED WITH GOLD NANOPARTICLES AS A VASCULAR REPAIR MATERIAL

4.1 Abstract

There is a need for improved vascular and cardiac repair materials. These materials must be biocompatible and resist rupture, calcification, and degradation. Materials of biological origin such as decellularized tissue have shown the most promise for achieving these characteristics; however, they still suffer from poor cellular integration and mechanical weakness as compared to the native structures. This study investigated the effects of decellularization, crosslinking, and conjugation with gold nanoparticles (AuNP) on porcine aortic tissue for use as a vascular repair material. Histology and scanning electron microscopy were performed and confirmed the removal of immunogenic nuclear remnants, confirmed little change in structure after decellularization, and confirmed the presence of the AuNPs on the material. Mechanical testing was performed which indicated no significant differences in mechanical properties between the native vessel and the modified vessels. Cell culture studies were performed which demonstrated that the modified material was biocompatible.

This study confirmed that the decellularized scaffolds maintain the important native tissue characteristics and that crosslinking and the addition of AuNPs achieves biocompatible tissue scaffolds.

4.2 Introduction

Vascular disease is one of the leading causes of morbidity and mortality in the United States [1-3]. It includes vessel occlusion due to atherosclerosis, coronary artery occlusion, peripheral artery disease, and stroke with vessel occlusion. Many of these conditions require surgical interventions such as carotid endarterectomy with patch angioplasty, which involve materials that can replace or enhance damaged vessels. There are numerous types of material available, and all have their own strengths and weaknesses. [4, 5] A repair material needs to display the same mechanical and biologic characteristics as the native tissue while not causing an immune reaction, but rather allowing for the material to be integrated into the host [1-3, 6, 7] .

Current synthetic and biologic scaffolds can cause a host reaction including inflammation, calcification, and infection [4, 8-12]. Synthetic materials such as expanded polytetrafluoroethylene (ePTFE) and Dacron (polyethylene terephthalate) are currently used for vascular patches. These materials possess good mechanical properties and have demonstrated acceptable *in vivo* durability. The problems with the synthetic materials are their inability to promote endothelial cell migration and remodeling while their foreign body response can

lead to chronic phase inflammation [13]. Another shortcoming is the inability of the synthetic material to “grow”, which is especially problematic with pediatric patients. Biological patches, such as bovine pericardium, are an alternative to synthetic materials. Biologic materials used in a vascular environment tend towards mechanical failure, re-stenosis, and calcification [13]. In particular the use of glutaraldehyde crosslinkers has been shown to promote this process. However, utilizing a natural tissue structure allows for a three-dimensional scaffold that could enhance remodeling while providing mechanical strength.

The challenge to successful graft repair is how to promote constructive remodeling without sacrificing structural integrity prior to regeneration of pressure-bearing neotissue. To maintain the necessary mechanical properties, many biologic materials are crosslinked such that they are resistant to degradation. An earlier study demonstrated longer degradation times *in vivo* with crosslinked scaffolds as compared to non-crosslinked scaffolds [14]. The increased degradation time allows the cells to infiltrate and begin building their own matrix. However, crosslinking can drastically alter the overall micro-environment, resulting in a stiffer material, and the toxicity of crosslinking agents such as glutaraldehyde is a concern [15]. Additionally, the host remodeling response is distinctly altered from constructive remodeling to fibrous encapsulation and chronic inflammation [16]. Therefore to achieve successful constructive remodeling, crosslinking must be minimized so that the patch can

undergo slow degradation while promoting tissue regeneration and maintaining structural integrity.

In recent studies, crosslinking was combined with conjugating amine functionalized gold nanoparticles (AuNP) to acellular tissue scaffold to enhance biocompatibility and mitigate not only adverse crosslinking effects but also decrease the amount of crosslinkers needed. Previous research performed in our lab has shown that AuNPs improve performance including decreasing degradation [17, 18]. Cell culture studies have shown increase cell proliferation, as well as reducing reactive oxygen species which could reduce the inflammatory response [19-21]. In a study by Chou et al., poly(ether)urethane containing gold or silver nanoparticles where shown to reduce surface degradation through free radical scavenging while also improving cellularity [22].

There is a critical need for effective vascular patches for the treatment of stenosis in diseased carotid or femoral blood vessels. The purpose of this study was to investigate the use of decellularized porcine arteries as a possible vascular patch. The use of decellularized arterial blood vessels is advantageous since improved hemodynamics is achievable by replacing part of a disease artery with an actual arterial patch which would better mimic the properties of natural arteries. To reduce the negative effects of crosslinking, AuNPs were conjugated to the decellularized arteries using a zero-length crosslinker. It was hypothesized that AuNP-conjugated blood vessels would help maintain the natural tissue properties such as strength, stiffness, and open microstructure while providing

good biocompatibility. The properties of these AuNP-blood vessels were investigated using histology, scanning electron microscopy, mechanical testing, and cell culture assays.

4.3 Materials and Methods

4.3.1 Tissue Harvest and Decellularization

Porcine aortas were harvested immediately following euthanasia of swine after a laboratory exercise at the University of Missouri School of Medicine using a protocol adapted from a previously published protocol [23, 24]. They were cleaned of blood and any excess surrounding tissue and then immersed in distilled water for 24 hours at 4 ° C to rupture cell membranes. Next, the vessels were treated with 0.025% trypsin EDTA (ATCC) diluted in Dulbecco's phosphate buffered saline (dPBS; ATCC) for 24 hours at 37 °C. The tissue was then put into a solution of 1% Triton x-100 (Sigma) and 0.1% ammonium hydroxide (Fisher) in distilled water for 72 hours at 4 °C to remove nuclear components and lyse cell membranes and cytoplasmic proteins. The tissue was then put into a solution of Eagle's Minimum Essential Medium (EMEM; ATCC) 10% (v/v) horse serum and PennStrep (200 U/mL) to deactivate any remaining trypsin for 24 hours at 37 °C. Tissue was washed for 24 hours in distilled water at 4 °C and washed for 48 hours in PBS at 4 °C, changing the PBS to fresh solution at 24 hours. All of these steps were done with mechanical agitation on a stir plate.

4.3.2 Treatment Groups

We fabricated and characterized five treatment groups as shown below:

1) Decellularized tissues: porcine aortic tissues that underwent the decellularization protocol.

2) Crosslinked tissues: decellularized porcine aortic tissues that were crosslinked with the chemical crosslinkers 1-ethyl-3-[3-dimethylaminopropyl]carbodiimide (EDC) and *N*-hydroxysuccinimide(NHS).

3) 4x 20nm AuNP tissues: decellularized porcine aortic tissues that were crosslinked with 20 nm gold nanoparticles (Ted Pella) at four times the stock solution (2.8x1012 particles/mL) in combination with EDC and NHS (sterilized using peracetic acid for SEM).

4) 4x 100nm AuNP tissues: decellularized porcine aortic tissues that were crosslinked with 100nm gold nanoparticles (Ted Pella) at four times the stock solution (2.24a1010 particles/mL) in combination with EDC and NHS and sterilized using peracetic acid.

5) Natural tissues: natural, untreated porcine aortic tissue that did not undergo decellularization or crosslinking.

The 20 and 100 nm sized gold nanoparticles were chosen based on previous experience with these sizes as biocompatible, non-cytotoxic nanoparticles [17]. Initially, only 20 nm AuNPs were tested, but concerns with their sterilization led to the use of the 100 nm AuNPs.

4.3.3 Crosslinking

Circular pieces 1 cm in diameter of decellularized tissue were placed into a crosslinking solution (50:50 (v/v) of acetone and PBS with EDC and NHS. The tissue was incubated in the solution for 15 minutes at ambient temperature. After the incubation the crosslinking solution was withdrawn and nanoparticles were added. The AuNPs were first functionalized using a solution of 2-mercaptoethylamine. The crosslinked tissue group remained in the crosslinking solution. All types of tissue were incubated for 24 hours at ambient temperature with gentle agitation followed by two 24 hours rinses with PBS.

Specimens used for cell culture, sterility testing, SEM and mechanical tests were incubated in an aqueous solution of 0.1%(v/v) peracetic acid with 1.0M NaCl for 30 minutes followed by two 24 hour sterile PBS rinses. All steps were performed at ambient temperature with shaking.

4.3.4 Cell Culture

Primary umbilical vein endothelial cells, normal, human, pooled (ATCC PCS-100-013) were cultured Vascular Cell Basal Medium (ATCC PCS-100-030) supplemented with Microvascular Endothelial Cell Growth Kit-BBE (ATCC PCS-110-040) and Penicillin (10 u/mL) –streptomycin (10 µg/mL)-amphotericin B (25 ng/mL) solution (ATCC PCS-999-002).

4.3.5 Sterilization

Sterilization of the scaffolds was tested at the University of Missouri Veterinary Medicine Diagnostic Lab. Sterilized scaffolds were tested at aerobic and anaerobic conditions, at room temperature, 35 °C, and in both brain heart infusion broth and thioglycollate broth. Samples were held for 14 days to watch for bacterial growth.

4.3.6 Histology

Longitudinal and cross-sectional samples from sample groups 1-3 and 5 were embedded in paraffin, cut with a microtome at 5 µm and stained with hematoxylin and eosin (H&E). Viewing was performed on a Zeiss Axiophot (Carl Zeiss Microimaging, Inc., Thornwood, NY) and photographs were taken using an Olympus DP70 (Olympus America Inc., Center Valley, PA) camera with DP Manager Version 1.21.107 as the acquisition software. Initially the slides were viewed at 10x and 20x to get an overall sense of the tissue. Representative areas were then photographed at a magnification of 10x.

4.3.7 Scanning Electron Microscopy

Tissue scaffolds were placed in a primary fixation in 0.1 M sodium cacodylate buffer containing 2% glutaraldehyde and 2% paraformaldehyde at 4 °C. This was followed by three five minute 0.1 M sodium cacodylate buffer rinses at ambient temperature on a rocker. Samples were then rinsed three times in

Milli-Q ultrapure water at ambient temperature and five minutes per rinse. Tissue discs were dehydrated in a series of graded ethanol rinses (20%, 50%, 70%, 90%, and three rinses in 100%). This was performed under vacuum in a microwave at 100W and 40s per rinse. They were critical point dried (Auto-Samdri 815 critical point dryer – Tousimis Research Corporation, Rockville, MD) and mounted on SEM stubs with carbon tape. They were carbon coated in a 950 Turbo Evaporator (EM Technologies, LTD., Kent, England). Scaffolds were viewed using a Quanta 600F Environmental SEM (FEI Company, Hillsboro, OR) at 15kV with backscatter imaging and gold was identified using energy dispersive X-ray spectroscopy during viewing.

4.3.8 Mechanical Testing

Specimens of groups 1 (unsterilized n=6, sterilized n=6), group 2 (unsterilized n=6, sterilized n=8), group 3 (n=3), and group 5 (n=4) were tested. Groups 1 and 2 had subsets of sterilized and unsterilized specimens. The vessels were tested in the longitudinal direction. Each piece was 4 cm by 1 cm and notched to reduce the width of the specimen to approximately 0.5 cm in order to create a stress concentration in the center of the specimen and thus prevent failure in the grip. A mechanical testing system (Instron TA.XT2, Texture Technologies, Corporation, Scarsdale, NY) strained the specimens until failure. The tensile strength at yield was calculated by dividing the maximum load, F_{max}, by the original cross-sectional area, A, of the specimen. The modulus of

elasticity, E, was determined from the slope of a line fit to the stress versus strain curve of each specimen. Group 4 was not tested for mechanical properties due to 1) Group 4 was added on after concerns with the 20 nm AuNP sterility problems (they were dissolving during sterilization) and 2) previous data demonstrated that the size of the AuNPs did not affect mechanical properties[17].

4.3.9 Biocompatibility

Cell proliferation Reagent WST-1 (Roche Diagnostics Corporation, Indianapolis, IN) was used to compare the biocompatibility of the tissue groups 1, 2, and 4. Each group had an n=11 and an additional two scaffolds that were not seeded for use as standards. Culture medium with the WST-1 reagent and no cells served as the blank. The tissue discs were incubated at 37 °C and 5% CO_2 in Vascular Cell Basal Medium (ATCC PCS-100-030) supplemented with Microvascular Endothelial Cell Growth Kit-BBE (ATCC PCS-110-040) and Penicillin (10 u/mL) –streptomycin (10 µg/mL)-amphotericin B (25 ng/mL) solution (ATCC PCS-999-002) for 24 hours in individual wells of a 48 well microplate. After 24 hours the media was removed and each well was seeded with Primary umbilical vein endothelial cells, normal, human at a concentration of 3×10^4 cells/mL. After 2 days the scaffolds were moved to new 48-well plates to ensure cellular attachment to the scaffolds only. All scaffolds were incubated for 7 days at 37 °C and 5% CO_2 with half the media in each well replaced every 24 hours. WST-1 reagent was then added to each well and the plates were incubated for 6

hours. 100 µl was removed at 6 hours and placed into a 96-well microplate and read by a BIO-Rad Model 680 Microplate Reader (Bio-Rad Laboratories Hercules, CA). The amount of formazan created in the reaction between metabolically active cells and the tetrazolium salts correlates with the number of metabolically active cells. The amount of formazan was quantified using UV-Vis absorbance measurements with higher absorbance values representing more metabolically active cells and greater biocompatibility.

4.3.10 Cell Proliferation

Quant-iT™ PicoGreen® dsDNA Reagent (Invitrogen Corporation, Carlsbad, CA) was used to assess cell proliferation between groups 1, 2, and 4 (n=9 per group per time point). This assay allows for quantification of dsDNA content which can be directly correlated to the amount of cellular growth on the scaffold. The tissue discs were incubated at 37 °C and 5% CO_2 in Vascular Basal Cell Medium (ATCC PCS-100-030) supplemented with Microvascular Endothelial Cell Growth Kit-BBE (ATCC PCS-110-040) and Penicillin (10 u/mL) – streptomycin (10 µg/mL)-amphotericin B (25 ng/mL) solution (ATCC PCS-999-002) for 24 hours in individual wells of three 48 well microplates- one for each time point. After 24 hours the media was removed and each well was seeded with 1 mL of primary umbilical vein endothelial cells, normal, human at a concentration of 3×10^4 cells/mL. All scaffolds were incubated at 37 °C and 5% CO_2 for the 7, 10, and 14 day time points. After 2 days the scaffolds were

moved to new 48-well plates to ensure cellular attachment to the scaffolds only. The media was changed out every three days. At 7, 10, and 14 days post cell seeding the appropriate scaffolds were removed, rinsed with 5mL sterile PBS, placed in 1.5 mL microcentrifuge tubes, and frozen at - 70 ®C. Samples were lypholized for 24 hours and then the dry mass of each scaffold was determined. Each sample was subjected to a papain digestion buffer of 125 µg/mL on a buffer of sterile PBS with 5mM cysteine-HCl and 5mL Na_2 EDTA for 24 hours at 60 °C. Each sample was put in 4 mL cuvettes then diluted with 1X TE buffer and the PicoGreen dsDNA reagent. The cuvettes were incubated at in the dark at ambient temperature for 5 minutes. Fluorescence readings were taken at 520 nm using 480 nm excitation on a FluoroMax-3 spectrofluorometer (HORIBA Jobin Yvon, Inc., Edison, NJ). A Lambda DNA standard curve was used to determine the DNA concentrations for the samples. Each concentration was normalized by the dry mass of the sample.

4.3.11 Statistical Analysis

Statistical analysis of the mechanical testing, WST assay, and PicoGreen Assay were performed using GraphPad Prism software, version 4.0 using a one way analysis of variance with a 95% confidence interval. Values are reported and graphed as the mean ± standard error of the mean.

4.4 Results

4.4.1 Sterilization

In scaffolds sterilized in peracetic acid for 30 minutes there was no bacterial growth under any of the conditions for two weeks.

4.4.2 Histology

The H&E staining of natural porcine aortic tissue showed typical arterial architecture. The cross-sections displayed smooth muscle cell nuclei within the layers of elastic lamellae in the tunica media. The tunica adventitia shows moderately disrupted layers of collagen and fibroblast nuclei. After decellularization no cellular nuclei or debris can be observed in the tissue. The adventitial layer has a minimal presence. The layers of elastic lamellae remain the same between tissue that is decellularized, crosslinked, and crosslinked with gold nanoparticles. No major structural changes were noted, as can be seen in Figure 4.1.

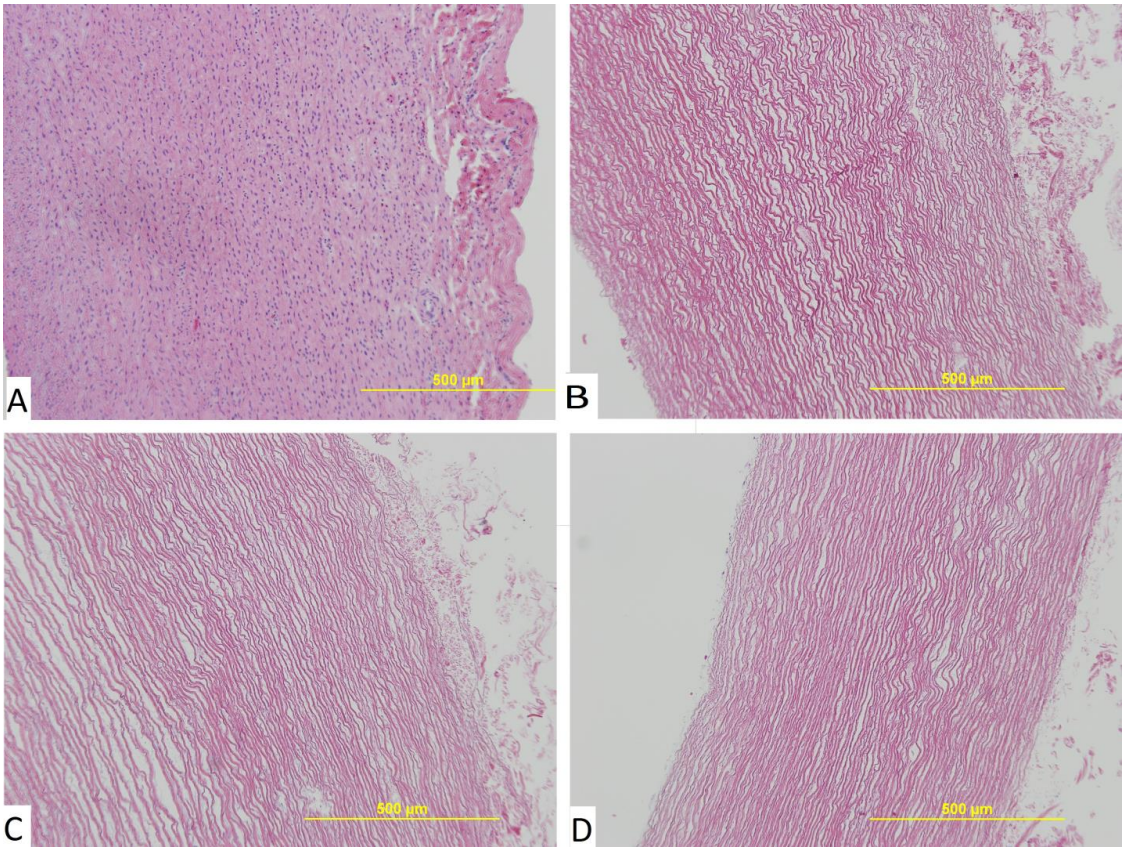

Figure 4.1 Histologic findings for porcine aortic tissue (H&E stain, original magnification 10x).

a) Native porcine aorta

b) Decellularized porcine aorta

c) Decellularized and crosslinked porcine aorta

d) Porcine aorta decellularized and crosslinked with AuNPs

4.4.3 Scanning Electron Microscopy

No major deformations in the scaffold structure were noted on SEM. Backscatter and EDS showed the presence of 20 nm and 100 nm AuNPs on tissue that was not sterilized. However after sterilization no 20 nm AuNPs could

be detected. 100nm AuNPs were present and subjectively were well dispersed over the scaffold as shown in Figure 4.2. Energy dispersive x-ray spectroscopy (EDS) indicated that areas of increased density on backscatter viewing had molecular weights equivalent to gold.

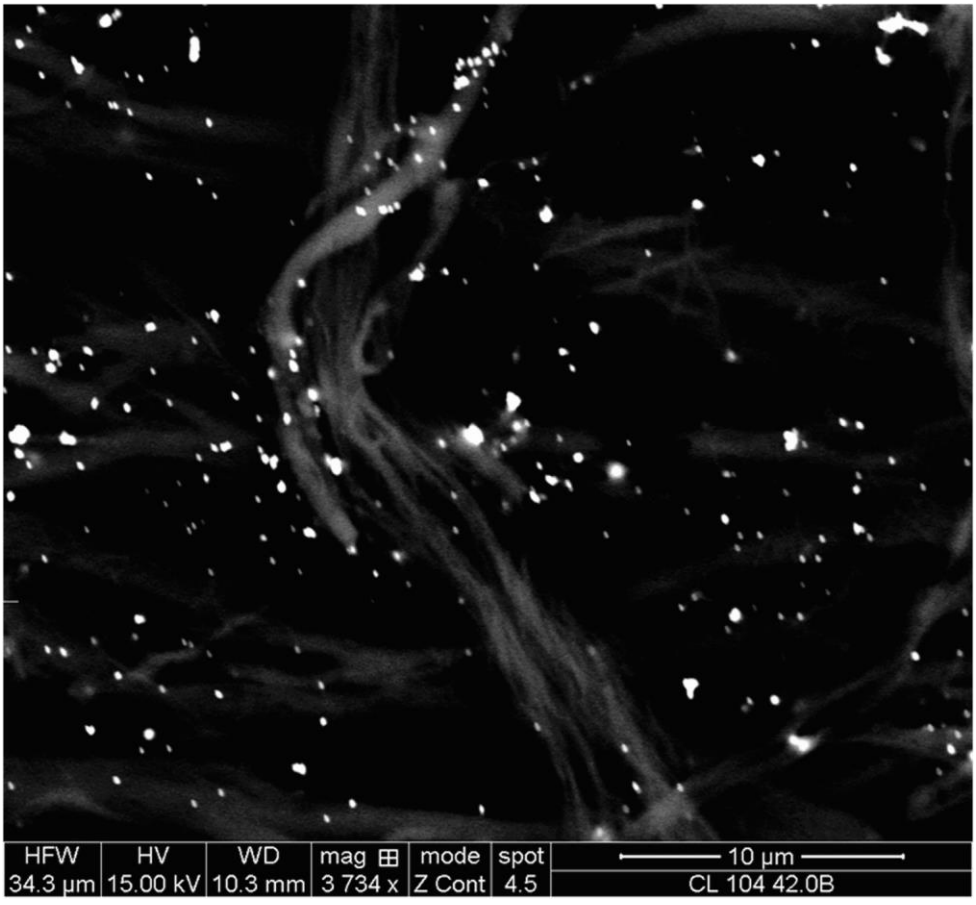

Figure 4.2 Scanning electron micrograph using backscatter imaging of 100nm AuNP crosslinked scaffold with AuNPs present.

4.4.4 Mechanical Testing

Natural porcine aorta and tissue that was decellularized, crosslinked, crosslinked with AuNPs, sterile and non-sterile were compared to one another. The tensile stress at maximum load, the modulus of elasticity, and the percent tensile strain at maximum load were calculated and are shown in Figure 4.3 with standard error of the mean. There were no significant differences in between the native tissue and the experimental groups. Specific values can be found in Table 4.1.

Table 4.1 Summary of mechanical testing data

	Modulus of Elasticity (MPa)	**Mean Tensile Strength at Yield (MPa)**	**Percent Strain at Yield (%)**
Native Aorta	9.754 ± 0.2.673	0.573 ± 0.094	19.484 ± 1.869
Unsterilized Decellularized Aorta	6.294 ± 2.632	0.571 ± 0.109	26.404 ± 2.414
Unsterilized Crosslinked Aorta	5.728 ± 0.682	0.646 ± 0.059	22.58 ± 0.957
Unsterilized AuNP Crosslinked Aorta	7.936 ± 1.368	0.505 ± 0.031	12.512 ± 1.292
Sterilized Decellularized Aorta	8.310 ± 1.181	0.603 ± 0.078	17.717 ± 0.865
Sterilized Crosslinked Aorta	11.469 ± 1.472	0.855 ± .111	15.148 ± 0.990

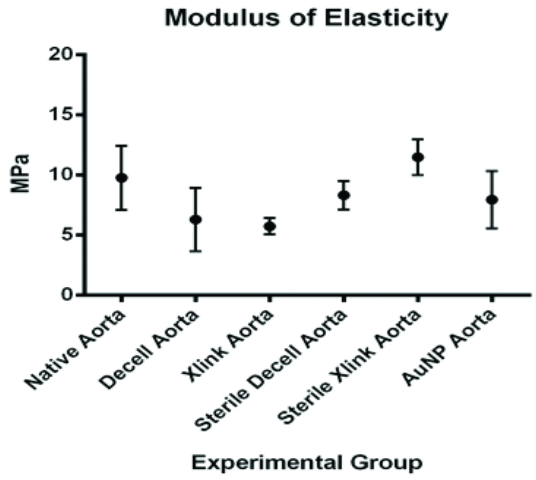

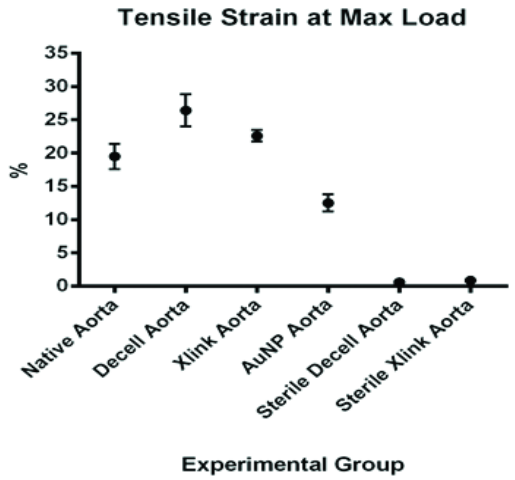

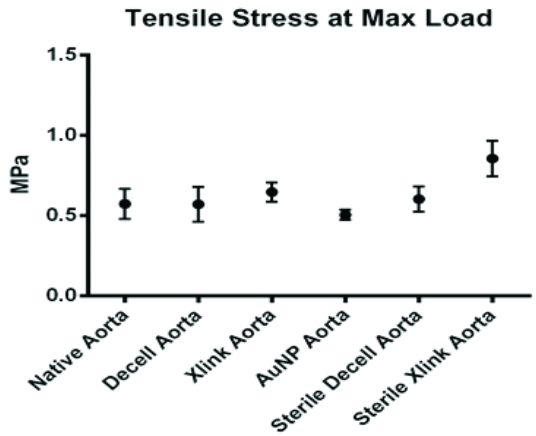

Figure 4.3 Results of mechanical testing showing no significant differences between the native and experimental.

4.4.5 Biocompatibility

The WST-1 assay showed no significant differences (P>0.05) between any of the groups when the percent viability of the experimental groups were compared to the decellularized tissue. The percent viabilities can be compared in Figure 4.4 with specific values in Table 4.2.

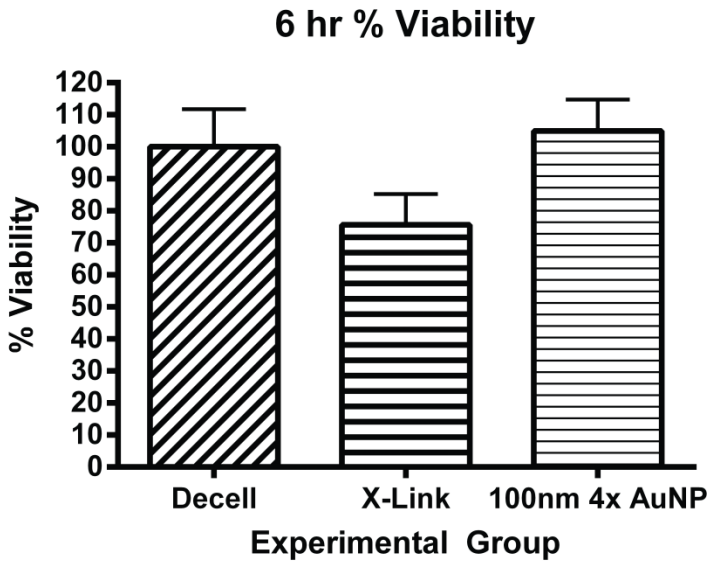

Figure 4.4 Results of WST-1 Assay showing percent viability of the experimental groups relative to the decellularized control.

Table 4.2 Summary of WST-1 Assay data

Experimental Group	% Viability at 6 hours
Decellularized Tissue	100.0 ± 3.5%
Crosslinked Tissue	75.7 ± 2.9%
Crosslinked with 4x 100nm AuNPs	104.9 ± 3.0%

4.4.6 Cell Proliferation

The PicoGreen dsDNA assay quantified cell proliferation. The data was normalized to the dry weight of each scaffold and the nanograms of DNA per milligram scaffold was calculated. The assay showed no significant differences between groups at each time point or within groups at different time points. The comparisons between groups at each time point can be found in Figure 4.5 with values for each group in Table 4.3.

Table 4.3 Summary of PicoGreen dsDNA Assay data

Scaffolds	Day 7 (ng DNA/mg scaffold)	Day 10 (ng DNA/mg scaffold)	Day 14 (ng DNA/mg scaffold)
Decellularized	36.1172 ± 6.230115	26.65453 ± 5.259623	28.83081 ± 6.065864
Crosslinked	22.15774 ± 5.872915	30.01409 ± 2.698935	24.87589 ± 3.994903
Crosslinked 4x 100nm AuNP	23.58197 ± 1.45902	20.71868 ± 1.603951	24.08586 ± 4.7469

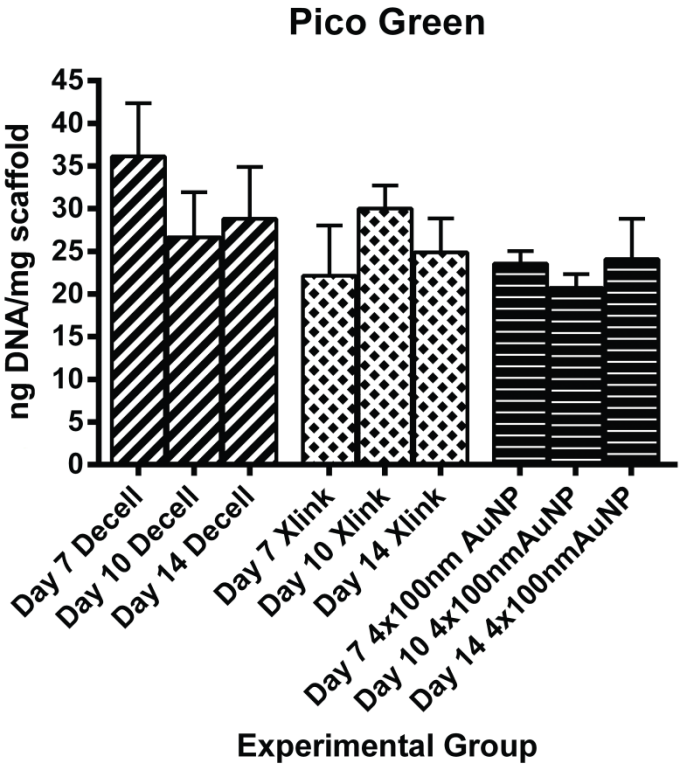

Figure 4.5 Results of the PicoGreen dsDNA assay for 7, 10, and 14 days showing the DNA content per mg scaffold weight

4.5 Discussion

This study characterized vascular patches composed of decellularized aortic tissue conjugated with AuNPs nanomaterials. The use of AuNPs should impart beneficial properties such as increase cell attachment and proliferation, reduced inflammation and antimicrobial-like features. Studies using mouse fibroblast cells have demonstrated increased cellularity on polymeric scaffolds, (polypropylene conjugated to AuNPs), while other studies have shown increased proliferation on AuNP-decellularized tissue [17, 25]. Other nanosized materials have also shown increased cellularity. In a study by Rodrigues, et al., nanosize hydroxyapatite (HA) conjugated to collagen fibrils demonstrated a significant increase in cell proliferation over non-HA collagen scaffolds [26]. Additionally, Sumbayev, et al., has demonstrated anti-inflammatory activity in gold nanoparticles while in other studies using functionalizing poly(ether)urethane (PU) with AuNPs has been shown to reduce oxidation [19, 20, 27]. Gold is an electron acceptor so it has the ability to scavenge free radicals, which may reduce the inflammatory response. Studies have also demonstrated the bacteriostatic nature of gold nanoparticles. In a study by Badwaik, et al., sugar-encapsulated gold nanoparticles were shown to exhibit bactericidal action via a disruption of the bacterial cell membrane [28]. The 60 to 120 nm AuNPs had the most beneficial effects.

The use of decellularized blood vessels should impart similar biomechanics as the native vessel and thus have similar hemodynamics.

However, crosslinking is occasionally needed to increase the biomechanics, which can affect the remodeling response. Additionally, crosslinkers have been shown to elicit cytotoxicity, such as with the glutaraldehyde crosslinker during the degradation process. To avoid these problems, we conjugated AuNPs to acellular tissue using a zero-length crosslinker, EDC, which has been shown to be more cell friendly. Conjugating AuNPs to acellular scaffolds, as well as purified collagen, slows down the degradation which provide more time for remodeling and thus maintains its biomechanical strength longer. It has been stated in recent studies that the AuNPs bond to carboxylic acid groups on the collagen fibrils which helps disrupt the collagenase binding sites [18]. Therefore, less crosslinking is needed to achieve long term stability and thus less changes in the natural tissue structure [29]. Additionally, less crosslinking leaves behind a more open structure for cellular migration. The SEM images demonstrated a very similar structure to native decellularized tissue. The intended use of AuNPs is not to improve mechanical properties, but to hinder collagenase binding sites to prevent premature degradation, as seen in our lab's previous studies [18]. Therefore it is imperative to find a correct balance of crosslinking to achieve good mechanical properties while still maintaining the native microstructure of the scaffold.

4.5.1 Histology

Histology indicates that the decellularization process is feasible; the native structure was not destroyed or altered while cells and cellular debris were effectively removed leaving behind the extracellular matrix. Decellularized tissue as biological repair material is becoming more common. Preliminary studies using swine small intestine submucosa demonstrated no evidence of patch related surgical complications in humans [30]. Successful decellularization of the arterial tissue was possible as shown through histology. Also noted was the objective lack of change in the structure of the extracellular matrix (ECM) after decellularizing and crosslinking. The removal of the nuclear material from the tissue is the first major step in creating a xenograft that will not be rejected by the host. The lack of remnant nuclear material shows the decellularization protocol works and thus can remove material that might cause an immune reaction in a human. The removal of the adventitial layer is not concerning as this was performed mostly through the removal of outer connective tissue and was moderately disrupted even before the decellularization process. A previous study had concerns about the removal of this layer, but our imaging and mechanical testing indicated no such concerns [23]. By removing the nuclear material, the extracellular matrix remains and is intact for use as a vascular patch. No damage to the structure of the ECM was noted under light microscopy or SEM, indicating the decellularization process is not damaging to the scaffold. This was also demonstrated through mechanical testing.

4.5.2 Scanning Electron Microscopy

SEM provided a technique to observe changes in the architecture of the material after decellularization and crosslinking. It also allowed for the important step of ensuring the AuNPs were present after sterilization of the tissue. Our results demonstrated that the 20 nm AuNPs did not survive the sterilization process. Most likely the peracetic acid and low pH used in the study disrupted the atomic bonding causing the dissipation of the atoms. Other studies have also shown problems with sterilization of small nanoparticles [31, 32]. While we discovered that the 20nm AuNPs could not survive, we could identify the 100nm AuNPs using EDS. Thus 100 nm AuNPs were utilized for the biocompatibility study instead of the 20 nm AuNPs. Additionally, several recent studies have indicated concerns with cytotoxicity of AuNPs at very small sizes (<20nm); we concluded that using larger nanoparticles, i.e., 100nm AuNPs would be more conducive to the design of vascular patches [32, 33]. In other studies, the 100 nm AuNPs have shown positive biocompatibility and free radical scavenging effects without cytotoxity concerns [22, 34, 35].

4.5.4 Mechanical Testing

The loss of native mechanical properties of decellularize tissue will negate the usefulness of the scaffold as a vascular repair material [36]. While previous studies have shown conflicting results regarding methods of decellularization decreasing mechanical strength [23, 37-39], we found no significant differences

between the native arteries, the decellularized arteries, crosslinked arteries, and AuNP arteries. Sterilization of the scaffolds also did not change the mechanical properties significantly from that of the native vessels. Our modifications did not have adverse effects on the mechanical properties; this is very important when considering problems such as intimal hyperplasia which may be caused when compliance mismatch occurs between the native vessel and the patch material.

4.5.6 Biocompatibility

There have been conflicting studies on the cytotoxicity of gold nanoparticles; however, many studies do agree that size plays an important role in cytotoxicity. Our lab has previously tested the effects of varying concentrations of AuNPs on cytotoxicity and noted that specimens crosslinked with AuNPs at 4x the stock solution showed the same levels of cell growth as specimens without AuNPs [40]. Therefore we chose to use a concentration of 4x to avoid wastefully repeating past experiments. The 100 nm AuNPs used in this study were conjugated to tissue and the WST-1 assay was utilized to test the biocompatibility of the material, which showed no cytotoxic effects with human umbilical endothelial cells. The decellularized, crosslinked, and crosslinked with AuNPs showed equivalent cellular viability. The 100nm AuNPs at 4 times the stock concentration showed no cytotoxic effects. This assay suggests that the 100nm AuNPs are biocompatible.

4.5.7 Cell Proliferation

Previous studies have demonstrated that the presence of AuNPs will increase cell proliferation [17, 18, 29]. The rough topography of scaffolds with nanoparticles provides attachment sites for adhesion-loving cells, such as fibroblasts. Additionally, the high surface energy of nanoparticles may also be attracting cells. Cell proliferation was quantified using a dsDNA assay. The assay showed no significant differences between groups at each time point. However the cells did continue to proliferate over time rather than dying off. Again, there is no cytotoxicity seen with the use of the AuNPs. The lack of increased proliferation shown in the study may be due to the different cell line. Typically, mouse fibroblast cells were utilized in our previous studies and many of the studies cited in literature. The use of the endothelial cell line could indicate that endothelial cells are not attracted to high surface energies materials and/or roughened surfaces.

4.6 Conclusions

This study characterized decellularized porcine aortic tissue conjugated to amine functionalized gold nanoparticles. The purpose of this study was to characterize and test the feasibility of a novel decellularized vascular patch that had been conjugated with AuNPs. It was hypothesized that AuNP-conjugated blood vessels would help maintain the natural tissue properties such as strength, stiffness, and open microstructure while providing good biocompatibility. The

results supported the hypothesis. The decellularization process removed all immunogenic material from the patch, and the decellularization and crosslinking processes did not change the mechanical properties of the native vessel. In addition it was demonstrated that crosslinking and conjugation of AuNPs did not cause significantly alter endothelial cell growth. This material has the potential to be a feasible vascular patch.

4.7 Acknowledgments

This research was sponsored in part by the University of Missouri Bioprocessing and Biosensing Center grant (BBC), and by NIH Grant T32 RR007004. The authors would like to thank Dave Grant, Aaron Wood, Matt Cozad, Carrie Schmidt, and Sarah Smith. This study would not have been possible without the excellent animal care provided by the Office of Animal Research staff.

4.8 References

[1] Bordenave L, Menu P, Baquey C. Developments towards tissue-engineered, small-diameter arterial substitutes. Expert review of medical devices. 2008;5:337-47.

[2] Ratcliffe A. Tissue engineering of vascular grafts. Matrix Biol. 2000;19:353-7.

[3] Tu JV, Pashos CL, Naylor CD, Chen E, Normand S-L, Newhouse JP, et al. Use of Cardiac Procedures and Outcomes in Elderly Patients with Myocardial Infarction in the United States and Canada. New England Journal of Medicine. 1997;336:1500-5.

[4] Muto A, Nishibe T, Dardik H, Dardik A. Patches for carotid artery endarterectomy: Current materials and prospects. Journal of Vascular Surgery. 2009;50:206-13.

[5] Schmidt CE, Baier JM. Acellular vascular tissues: natural biomaterials for tissue repair and tissue engineering. Biomaterials. 2000;21:2215-31.

[6] Lu Q, Ganesan K, Simionescu DT, Vyavahare NR. Novel porous aortic elastin and collagen scaffolds for tissue engineering. Biomaterials. 2004;25:5227-37.

[7] Zhang WJ, Liu W, Cui L, Cao Y. Tissue engineering of blood vessel. J Cell Mol Med. 2007;11:945-57.

[8] Awad IA, Little JR. Patch angioplasty in carotid endarterectomy. Advantages, concerns, and controversies. Stroke. 1989;20:417-22.

[9] Bond R, Rerkasem K, Naylor AR, AbuRahma AF, Rothwell PM. Systematic review of randomized controlled trials of patch angioplasty versus primary closure and different types of patch materials during carotid endarterectomy. Journal of Vascular Surgery. 2004;40:1126-35.

[10] Cho SW, Park HJ, Ryu JH, Kim SH, Kim YH, Choi CY, et al. Vascular patches tissue-engineered with autologous bone marrow-derived cells and decellularized tissue matrices. Biomaterials. 2005;26:1915-24.

[11] Lee WK, Park KD, Kim YH, Suh H, Park JC, Lee JE, et al. Improved calcification resistance and biocompatibility of tissue patch grafted with sulfonated PEO or heparin after glutaraldehyde fixation. Journal of biomedical materials research. 2001;58:27-35.

[12] Matsagas M, Bali C, Arnaoutoglou E, Papakostas J, Nassis C, Papadopoulos G, et al. Carotid Endarterectomy with Bovine Pericardium Patch Angioplasty: Mid-Term Results. Annals of vascular surgery. 2006;20:614-9.

[13] Li X, Guo Y, Ziegler KR, Model LS, Eghbalieh SDD, Brenes RA, et al. Current Usage and Future Directions for the Bovine Pericardial Patch. Annals of vascular surgery. 2011;25:561-8.

[14] Liang H-C, Chang Y, Hsu C-K, Lee M-H, Sung H-W. Effects of crosslinking degree of an acellular biological tissue on its tissue regeneration pattern. Biomaterials. 2004;25:3541-52.

[15] Huang-Lee LL, Cheung DT, Nimni ME. Biochemical changes and cytotoxicity associated with the degradation of polymeric glutaraldehyde derived crosslinks. Journal of biomedical materials research. 1990;24:1185-201.

[16] Reing JE, Zhang L, Myers-Irvin J, Cordero KE, Freytes DO, Heber-Katz E, et al. Degradation products of extracellular matrix affect cell migration and proliferation. Tissue Engineering Part A. 2008;15:605-14.

[17] Deeken CR, Bachman SL, Ramshaw BJ, Grant SA. Characterization of bionanocomposite scaffolds comprised of mercaptoethylamine-functionalized gold nanoparticles crosslinked to acellular porcine tissue. J Mater Sci Mater Med. 2012;23:537-46.

[18] Grant SA, Spradling CS, Grant DN, Fox DB, Jimenez L, Grant DA, et al. Assessment of the biocompatibility and stability of a gold nanoparticle collagen bioscaffold. J Biomed Mater Res A. 2013.

[19] Barathmanikanth S, Kalishwaralal K, Sriram M, Pandian SR, Youn HS, Eom S, et al. Anti-oxidant effect of gold nanoparticles restrains hyperglycemic conditions in diabetic mice. J Nanobiotechnology. 2010;8:16.

[20] Ionita P, Spafiu F, Ghica C. Dual behavior of gold nanoparticles, as generators and scavengers for free radicals. Journal of materials science. 2008;43:6571-4.

[21] Lu S, Xia D, Huang G, Jing H, Wang Y, Gu H. Concentration effect of gold nanoparticles on proliferation of keratinocytes. Colloids Surf B Biointerfaces. 2010;81:406-11.

[22] Chou CW, Hsu SH, Wang PH. Biostability and biocompatibility of poly(ether)urethane containing gold or silver nanoparticles in a porcine model. J Biomed Mater Res A. 2008;84:785-94.

[23] Williams C, Liao J, Joyce EM, Wang B, Leach JB, Sacks MS, et al. Altered structural and mechanical properties in decellularized rabbit carotid arteries. Acta Biomater. 2009;5:993-1005.
[24] Amiel GE, Komura M, Shapira O, Yoo JJ, Yazdani S, Berry J, et al. Engineering of blood vessels from acellular collagen matrices coated with human endothelial cells. Tissue Eng. 2006;12:2355-65.

[25] Grant D, Benson J, Cozad M, Whelove O, Bachman S, Ramshaw B, et al. Conjugation of gold nanoparticles to polypropylene mesh for enhanced biocompatibility. J Mater Sci: Mater Med. 2011;22:2803-12.

[26] Rodrigues SC, Salgado CL, Sahu A, Garcia MP, Fernandes MH, Monteiro FJ. Preparation and characterization of collagen-nanohydroxyapatite biocomposite scaffolds by cryogelation method for bone tissue engineering applications. Journal of Biomedical Materials Research Part A. 2013;101:1080-94.

[27] Sumbayev VV, Yasinska IM, Garcia CP, Gilliland D, Lall GS, Gibbs BF, et al. Gold Nanoparticles Downregulate Interleukin-1β-Induced Pro-Inflammatory Responses. Small. 2013;9:472-7.

[28] Badwaik VD, Vangala LM, Pender DS, Willis CB, Aguilar ZP, Gonzalez MS, et al. Size-dependent antimicrobial properties of sugar-encapsulated gold nanoparticles synthesized by a green method. Nanoscale research letters. 2012;7:1-11.

[29] Whelove OE, Cozad MJ, Lee BD, Sengupta S, Bachman SL, Ramshaw BJ, et al. Development and in vitro studies of a polyethylene terephthalate-gold nanoparticle scaffold for improved biocompatibility. J Biomed Mater Res B Appl Biomater. 2011;99:142-9.

[30] Quarti A, Nardone S, Colaneri M, Santoro G, Pozzi M. Preliminary experience in the use of an extracellular matrix to repair congenital heart diseases. Interact Cardiovasc Thorac Surg. 2011;13:569-72.

[31] França Á, Pelaz B, Moros M, Sánchez-Espinel C, Hernández A, Fernández-López C, et al. Sterilization Matters: Consequences of Different Sterilization Techniques on Gold Nanoparticles. Small. 2010;6:89-95.

[32] Johnston HJ, Hutchison G, Christensen FM, Peters S, Hankin S, Stone V. A review of the in vivo and in vitro toxicity of silver and gold particulates: particle attributes and biological mechanisms responsible for the observed toxicity. Crit Rev Toxicol. 2010;40:328-46.

[33] Pan Y, Neuss S, Leifert A, Fischler M, Wen F, Simon U, et al. Size-dependent cytotoxicity of gold nanoparticles. Small. 2007;3:1941-9.

[34] Boisselier E, Astruc D. Gold nanoparticles in nanomedicine: preparations, imaging, diagnostics, therapies and toxicity. Chem Soc Rev. 2009;38:1759-82.

[35] Hsu SH, Tang CM, Tseng HJ. Biocompatibility of poly(ether)urethane-gold nanocomposites. J Biomed Mater Res A. 2006;79:759-70.

[36] Zou Y, Zhang Y. The orthotropic viscoelastic behavior of aortic elastin. Biomech Model Mechanobiol. 2010.

[37] Roy S, Silacci P, Stergiopulos N. Biomechanical properties of decellularized porcine common carotid arteries. Am J Physiol Heart Circ Physiol. 2005;289:H1567-76.

[38] Conklin B, Richter E, Kreutziger K, Zhong D-S, Chen C. Development and evaluation of a novel decellularized vascular xenograft. Medical engineering & physics. 2002;24:173-83.

[39] Zou Y, Zhang Y. Mechanical Evaluation of Decellularized Porcine Thoracic Aorta. J Surg Res. 2011.

[40] Cozad MJ, Bachman SL, Grant SA. Assessment of decellularized porcine diaphragm conjugated with gold nanomaterials as a tissue scaffold for wound healing. J Biomed Mater Res A. 2011;99:426-34.

Chapter Five

AN *IN VIVO* STUDY OF THE EFFECTS OF A NANOMATERIAL-TISSUE PATCH FOR VASCULAR AND CARDIAC RECONSTRUCTION IN A PORCINE MODEL

5.1 Abstract

Vascular and cardiac reconstruction involves the use of biological patches to treat trauma and defects. An *in vivo* study was performed to determine the remodeling and biologic effects of novel nanostructured vascular patches with and without gold nanoparticles. Porcine vascular tissue was decellularized and conjugated with gold nanoparticles to evaluate if integration would occur while avoiding rupture and stenosis. Swine underwent a bilateral patch angioplasty of the carotid arteries with experimental patches on the right and control patches of bovine pericardium on the left. Animals were sacrificed after surgery and at 3 and 9 weeks. Ultrasound was performed during surgery, every 3 weeks, and before euthanasia. Endothelial regeneration was examined using Evans Blue dye and histology using Trichrome and H&E. There was a 100% success rate of implantation with 0% mortality. All patches were patent on ultrasound. At 3 weeks, experimental patches had regenerating endothelial cell growth and normal healing responses. At 9 weeks, the experimental patches demonstrated excellent integration, particularly the gold nanoparticle carotid vascular patch.

Histology demonstrated cellular in-growth into the experimental patches and no major immune reactions. This is one of the first studies to demonstrate the feasibility of nanomaterial-tissue patches for vascular and cardiac reconstruction.

5.2 Introduction

Cardiac and vascular materials are utilized to treat trauma and aneurysms, repair congenital defects, and patch defects in vessel and cardiac walls [1-4]. Finding a suitable material for these repairs has included research in both biologic and synthetic materials [1, 5]. The ideal material must mimic the mechanics and biocompatibility of the natural tissue as close as possible [6-11]. Current synthetic and biologic scaffolds can cause negative host reactions such as inflammation, calcification, and infection [12-17].

Synthetic materials such as expanded polytetrafluoroethylene (ePTFE) and Dacron (polyethylene terephthalate) possess good mechanical properties and have demonstrated acceptable *in vivo* durability. However synthetic materials can cause a foreign body response leading to chronic phase inflammation and thrombus formation and are often unable to promote endothelial cell migration and remodeling [18]. They often have poor flow hemodynamics and are unable to “grow”, which is especially problematic with pediatric patients. When used as small diameter vascular grafts they have a high rate of thrombosis and do not maintain long term patency [19, 20].

Biological materials, such as swine small intestine submucosa (SIS), are an alternative to synthetic materials. In a vascular environment, biologic materials tend towards mechanical failure, re-stenosis, and calcification [18]. In particular the use of glutaraldehyde crosslinkers to stabilize biologics has been shown to promote calcification as well as display cytotoxic effects upon degradation. The biologic materials do not have the durability of the synthetics. An ideal biologic would possess a natural three-dimensional tissue structure that would enhance remodeling while providing mechanical strength.

We have been investigating a biologic construct that possesses a natural 3D tissue structure while being conjugated with gold nanoparticles (AuNPs). The conjugation of AuNPs to biological constructs has been shown to improve the overall biocompatibility performance of the constructs [21, 22]. The conjugation method can increase the stability of the tissue due to the AuNPs hindering collagenase binding sites [21]. This can help prevent early degradation of the material, giving the body time to properly infiltrate and remodel the tissue. Studies have also shown that the addition of AuNPs can improve the thermal and mechanical properties of material [22].

A preliminary pilot study was performed in order to acquire early evidence that the use of decellularized porcine arteries conjugated with nanomaterials could be utilized as a possible patch material *in vivo*. It was hypothesized that the arteries conjugated with AuNPs would show enhanced cellular integration

and remodeling when compared to the currently used non-autologous patch material while also avoiding stenosis.

5.3 Materials and Methods

5.3.1 Materials

Unconjugated gold nanoparticles (100nm diameter, $5.6x10^9$ particles/ml) were purchased from Ted Pella, Inc. (Redding, CA) Trypsin EDTA, Dulbecco's phosphate buffered saline, Eagle's Minimum Essential Medium, horse serum, were obtained from ATCC (Manassas, VA). Triton X-100, peracetic acid (99.5%), 2-mercaptoethylamine (MEA), 1-Ethyl-3-[3-dimethylaminopropyl]carbodiimide hydrochloride (EDC), and phosphate buffered saline were acquired from Sigma-Aldrich (St. Louis, MO). Nydroxysulfosuccinimide (Sulfo-NHS) was obtained via Pierce, a part of Thermo Fisher Scientific in Rockor, IL. Acetone (99.5%) and formalin (10% buffered) came from Thermo Fisher Scientific (Fair Lawn, NJ). The control bovine pericardium patch was a Peri-Guard Repair Patch® from Synovis (St. Paul, MN).

5.3.2 Study Design

The study design involved the use of four different types of experimental patches:

1) Decellularized porcine abdominal aorta blood vessel patch (DBVP);

2) Decellularized and crosslinked porcine abdominal aorta blood vessel patch (CBVP);

3) Decellularized and crosslinked with 100nm gold nanoparticles attached to porcine abdominal aorta blood vessel (GBVP);

4) Decellularized and crosslinked porcine carotid artery patch with 100nm gold nanoparticles (GCVP) – (for the 9 week time point only).

The study was designed with a feasibility “acute study” component where the patches were implanted in three non-survival porcine models. For the 3 and 9 week study, the survival component comprised a total of 11 animals. The three-week time point had 3 animals - one for each type of experimental patches 1) through 3). The nine week time point had a total of 8 animals- two for each type of experimental patch groups from 1) through 4). Table 5.1 displays the experimental groups. Each animal was its own control, receiving a commercially available bovine pericardial patch on the contralateral artery.

Table 5.1 Experimental groups and time points

	Total Animals	Decellularized Aorta (DBVP)	Cross-linked Aorta(CBVP)	AuNP Aorta (GBVP)	AuNP Carotid (GCVP)
Acute Study	3	1	1	1*	1*
Three Week	3	1	1	1	0
Nine Week	8	2	2	2	2

*This was a single animal with AuNP aorta implant on the right side and the AuNP carotid on the left.

5.3.3 Tissue Harvest and Decellularization

Porcine aortas and carotids were harvested immediately following euthanasia of swine after a laboratory exercise at the University of Missouri School of Medicine. Decellularization was performed using a protocol adapted from a previously published protocol [23, 24].

5.3.4 Crosslinking

As shown in Table 1, three of the four experimental groups were crosslinked. A crosslinking solution (50:50 (v/v) solution of acetone and PBS with 1-ethyl-3-[3-dimethylaminopropyl]carbodiimide (EDC) and *N*-hydroxysuccinimide(NHS) was prepared and the decellularized tissue was incubated in this solution for 15 minutes at ambient temperature. After the incubation the crosslinking solution was withdrawn and functionalized AuNPs (100 nm in diameter) were added to allow peptide binding to the tissue. The gold nanoparticles were functionalized using a solution of 2-mercaptoethylamine. The crosslinked tissue group remained in the crosslinking solution (experimental group 1). After processing, all types of the experimental tissue were incubated for 24 hours at ambient temperature with gentle agitation followed by two 24 hours rinses with PBS.

5.3.5 Sterilization

Specimens were incubated in an aqueous solution of 0.1%(v/v) peracetic acid with 1.0M NaCl for 30 minutes followed by two 24 hour sterile PBS rinses. All steps were performed at ambient temperature with shaking. Completed patch material can be seen in Figure 5.1.

5.3.6 Animals

Female domestic swine with a starting weight of approximately 120 lbs were singly housed in accordance with the NIH guidelines for the care and use of laboratory animals (NIH Publication #85-23 Rev. 1985) and were observed under a protocol approved by the Institutional Animal Care and Use Committee. On the day preceding surgery animals were given 325 mg aspirin orally. Intramuscular (IM) telazol (4.4-6.6 mg/kg body weight), xylazine (2.2 mg/kg) and atropine (0.05 mg/kg) was given as a preanesthetic. 2-4% Isoflurane was administered via nose cone until the animal was sedated enough to be safely intubated. A surgical plane of anesthesia was maintained using 1-3% isoflurane gas and a ventilator at 6-8 breaths/minute. Prior to the surgical incision animals were given ceftiofur (5 mg/kg IM). An intravenous (IV) catheter was placed in the ear with an isotonic sodium chloride flow throughout surgery. Heparin was given IV at an initial bolus of 10,000 U/kg followed by 5,000 u/kg every hour intra op when necessary. Post operatively the animals were given carprofen (3mg/kg) subcutaneously (SQ) and buprenorphine (0.01-0.02 mg/kg) IM. The

buprenorphine dose was repeated at 6-8 hours after the animal was sternal. Animals received 325 mg aspirin PO for 3 days post op and then 81 mg/day PO until sacrifice.

At the conclusion of the study the animals were anesthetized as previously described. Three and nine week animals were given Evan Blue Dye at 2ml/kg of a 2% solution IV which was allowed to circulate for 30 minutes. The carotid arteries were ligated and excised before the animals were sacrificed using pentobarbital sodium and phenytoin sodium (Beuthanasia - 1 ml/4.5 kg IV).

5.3.7 Operative Procedure

All animals underwent a bilateral carotid patch angioplasty. Sterile technique was used throughout. A midline incision was made over the trachea and the carotid arteries were exposed. Each artery was dissected out and proximal/distal control was obtained using vessel loops. A longitudinal arteriotomy 2 cm long was created and patches were implanted over the arteriotomy using 6-0 prolene continuous running suture technique (Figure 5.1a). The experimental patch was placed on the right side (Figure 5.1b) and the control patch on the left in each animal. The muscle and the subcutaneous layers were opposed using Vicryl in a simple continuous pattern, the skin was closed with a continuous intradermal suture pattern using absorbable suture.

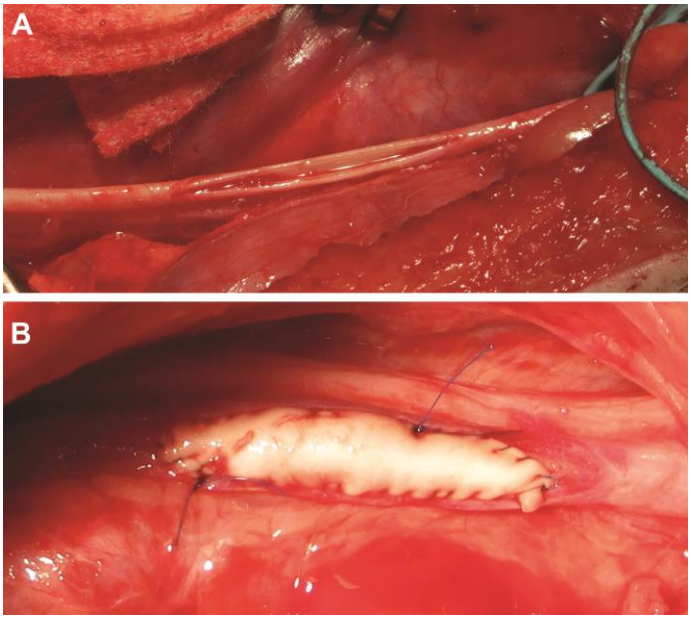

Figure 5.1 Intro-op placement of the patches

a) 2 cm longitudinal defect created on the carotid artery after the occlusion of the artery using vessel loops

b) GBVP patch sutured onto the defect in the artery, showing typical patch placement

5.3.8 Ultrasound

Doppler ultrasound (LS probe on a Logique GE ultrasound) was used to visualize the flow through the arteries. During the initial surgery the vessels were imaged before the arteriotomy as a baseline and then following patch placement. Nine week animals were sedated at three and six weeks post-op using IM telazol (4.4-6.6 mg/kg body weight), and xylazine (2.2 mg/kg) for percutaneous ultrasounds. A final reading was taken before sacrifice. In the 9 week animals color flow as well as waveform characteristics were imaged. The velocity and diameter of the vessels was recorded before the arteriotomy and at each time

point. The percentage area stenosis was calculated using the following equation which has been used in previous publications [25]:

$$(1-[D_2\times D_2\times V_2]/ [D_0\times D_0\times V_1]) \times 100\%$$

Where D_0 is the diameter of the vessel at the patch at the time of euthanasia and D_2 is the diameter of the vessel before patch placement (reference area). $V_1$is the peak velocity at the time of euthanasia and V_2 is the peak velocity at the reference area as can be seen in Figure 5.2.

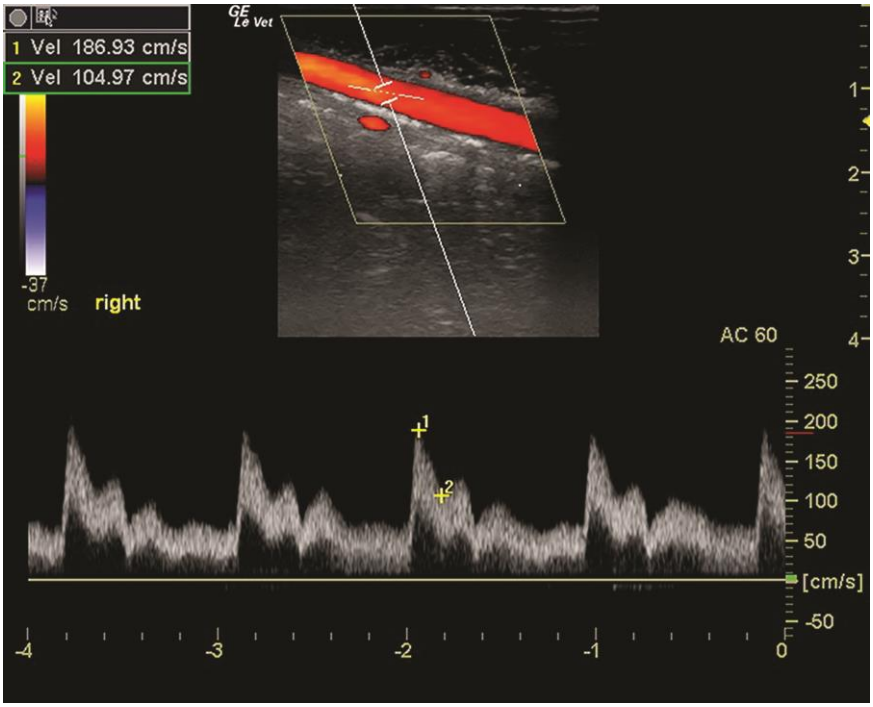

Figure 5.2 Ultrasound image of the GCVP at 9 weeks showing the pulsatile flow through the artery as well as the measurement of the systolic and diastolic flow rates. There was no vessel occlusion seen on any of the arteries at any time point. The flow rates were analyzed and there was no significant difference between control and experimental patches.

5.3.9 Gross Examination

After explantation each artery was photographed (Canon PowerShot A4000 IS) and then incised longitudinally opposite to the patch site. After exposure the level of blue staining was photographed. Each sample was cut in half and stored in 10% formalin for at least 24 hours or 70% ethanol. In all survival animals, the patches were grossly examined for bowing of the patches, Evan's Blue staining, thickening of the blood vessel wall, and fibrinous debris. Only fibrinous debris was examined in the non-survival animals.

5.3.10 Histology

Longitudinal and cross sectional samples were embedded in paraffin, cut with a microtome at 5 μm and stained with hematoxylin and eosin (H&E) for all studies and also with a Masson's trichrome stain for all survival studies. All slides were viewed at 50x, 100x, 200x, and 400x. Viewing was performed on a Zeiss Axiophot (Carl Zeiss Microimaging, Inc., Thornwood, NY) and photographs were acquired using an Olympus DP70 (Olympus America Inc., Center Valley, PA) camera with DP Manager Version 1.21.107 as the acquisition software.

5.3.11 Statistical Analysis

GraphPad Prism v4.0 (GraphPad Software, Inc., San Diego, CA) was used to analyze experimental data. One-way analysis of variance (ANOVA) with a 95% confidence interval was conducted followed by a Tukey-Kramer post-test

to determine significant differences between means of the experimental groups and control for the percentage of stenosis.

5.4 Results

5.4.1 Non-Survival Observations

The results of the non-survival, acute study demonstrated that there would be no catastrophic failure with the patch material. It also allowed for refinement of the surgical approach and indicated the size of the swine being used were acceptable substitutes for human subjects. It also allowed the surgeon to differentiate between the four experimental groups used in terms of material handling and suturing. The anesthetic and ultrasound techniques used for this particular procedure proved to be sound. No arteries were ligated for more than 30 minutes.

5.4.2 Gross Examination Results

For the non-survival acute animals red fibrinous debris was noted on the luminal side of the patches in all patches. There was a slight increase in the amount of fibrinous debris on the control patch for the second animal with the CBVP (experimental group 2), but this debris did not hinder blood flow as noted by the ultrasound.

In all survival animals, the patches were grossly examined for bowing of the patches, Evan's Blue staining, thickening of the blood vessel wall, and

fibrinous debris. In all the survival animals, both arteries demonstrated slight bowing in the area of patch placement, but this bowing did not hinder blood flow as noted by the ultrasound. Table 5.2 provides a summary of the 3-week gross examination results. The 3 week results demonstrated that there was a variety of changes. For example, Evan's Blue staining was noted as minimal to moderate amounts on all vessels. Thickened vessel walls were noted in some groups and not others.

Table 5.3 summarizes the results of the 9 week animals. Grossly the control patches were not well integrated in any of the animals. For the experimental patches, the GCVP (gold nanoparticle carotid patch, group 4) showed the best gross integration. There was variable Evans Blue dye staining of both control and experimental patches. No major clots were noted inside the vessels. Figure 5.3 displays the gross images of the explanted patches and vessels.

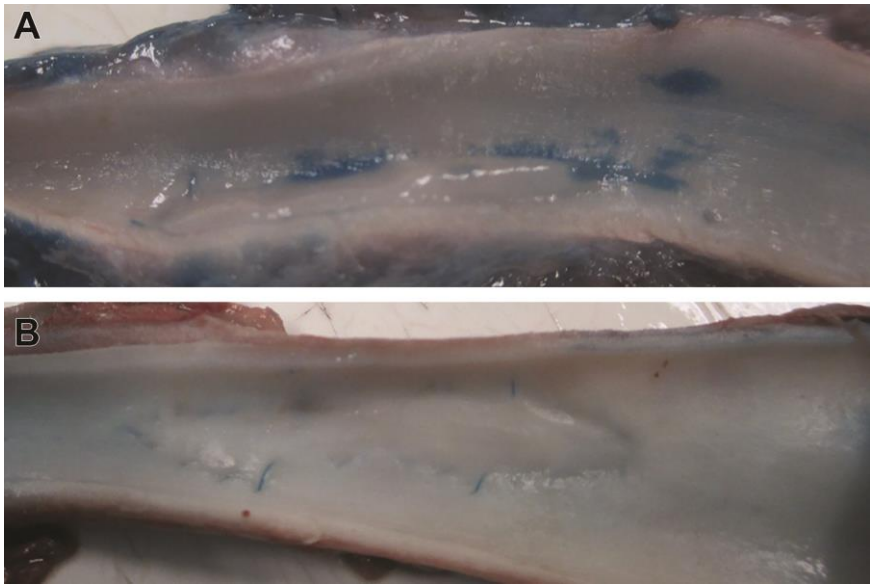

Figure 5.3 Gross images taken at the time of patch explantation

a) GBVP at nine weeks showing the gross integration of the tissue patch into the vessel.

b) GCVP at nine weeks showing the presence of the suture along the patch outline, but overall excellent gross integration of the patch

Table 5.2 Summary of 3 week gross examination results

	DBVP	Control	CBVP	Control	GBVP	Control
Evans Blue Staining	Minimal	Minimal	Moderate	Moderate	Moderate	Moderate
Integrated with host	Moderate	Poor	Moderate	Poor	Poor	Poor
Other features	No	No	No	Clotted blood, thickened vessel wall	Small mass, thickened vessel wall	Opaque, yellow crystals, clotted blood, thickened vessel wall

Table 5.3: Summary of 9 week gross examination results

	DBVP	Control	CBVP	Control	GBVP	Control	CBVP	Control
Evans Blue Staining	Minimal	Minimal	Minimal	Moderate	Minimal	Minimal	Minimal	Minimal
Host integration	Moderate	Poor	Moderate	Poor	Moderate	Poor	Excellent	Poor
Other features	No	No	No	Increased bowing of artery	Some scarring	Yellowed patch	No	Yellowed patch

5.4.3 Histologic Assessment Results

In the acute study there were no major histologic changes seen on the H&E slides. Both experimental and control patches were evident. The DBVP, CBVP, and GBVP patches were all close to the same thickness as the control

patch; between 800-1000 µm. The GCVP was thinner than the others (400 µm) and showed an infiltration of red blood cells between the collagen fibers.

Both H&E and trichrome staining were performed on the survival study patches. The results of the trichrome slides are shown in Figures 5.4-5.6. The trichrome stains highlight the collagen fibers of the patch materials better than the H&E stains.

As shown in Figure 5.4a and 5.5a, in the three-week animals the control patches were a very bright blue on the trichrome slides and showed thick wavy collagen fibers. The experimental patches have thin strands that stained lightly basophilic. Both patches of the DBVP (group 1) animal had inflammation. The control side (group 1) showed lymphocytes and multinucleated cells and a mild infiltration of cells into the patch. The experimental sides showed lymphocytes and fibroblasts, with cells penetrating further into the patch.

The CBVP (group 2) demonstrated an increased cellular layer within the lumen of the vessel, more inflammatory cells, and not as much cellular infiltration into the patch as the DBVP (group 1) as shown in Figure 5.4 and 5.5b,c. The control on this animal (group 2) had a blood clot adhered to the luminal surface.

The results of the GBVP (group 3) histology demonstrated a mass (seen grossly) which appeared to be an organized thrombus. Part of the thrombus is encapsulated with fibroblasts and contains debris, red blood cells, and hemosiderin. The area cut in without the mass has moderate cellular infiltration and inflammation as shown in Figure 5.4d and 5.5d. The control side (group 3)

showed a large inflammatory response and moderate occlusion of the vessel lumen. Both the CBVP (group 2) and the GBVP (group 3) showed mononuclear cellular infiltration into the scaffolds with some higher concentrations of inflammatory cells at the edges of the patches. The control patches (group 3) also showed cluster of lymphocytes and minimal cellular infiltration. The second GCVP (group 3) had cells growing into the scaffold, indicating infiltration. Areas of the scaffold were difficult to discern from the native structure. The control side (group 3) showed minimal cellular infiltration. See Table 5.4 for summarized results.

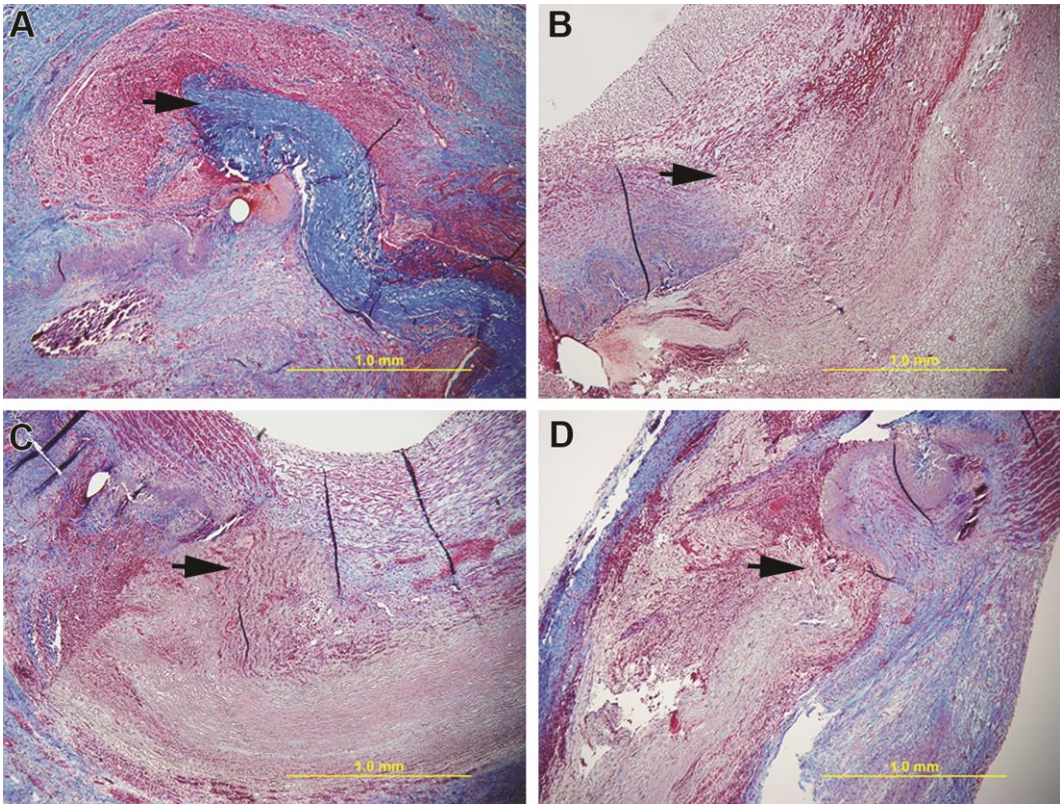

Figure 5.4 Histologic images of patches explanted at three weeks, trichrome staining, at 5x with representative control. The bar indicates 1mm.

a) The control patch is very obvious as the deeply blue stained area (arrow), indicating the distinct junction between the native tissue and control patch

b) DBVP at three weeks where the arrow indicates the experimental patch with the less distinct junction. There are red blood cells and other cells within the layers of the patch material
d) CBVP at three weeks again showing the junction between patch and native tissue with cells infiltrating the patch.

d) GBVP at three weeks with the arrow highlighting the cells infiltrating the patch. The amount of patch material present is thinner as this is the carotid patch.

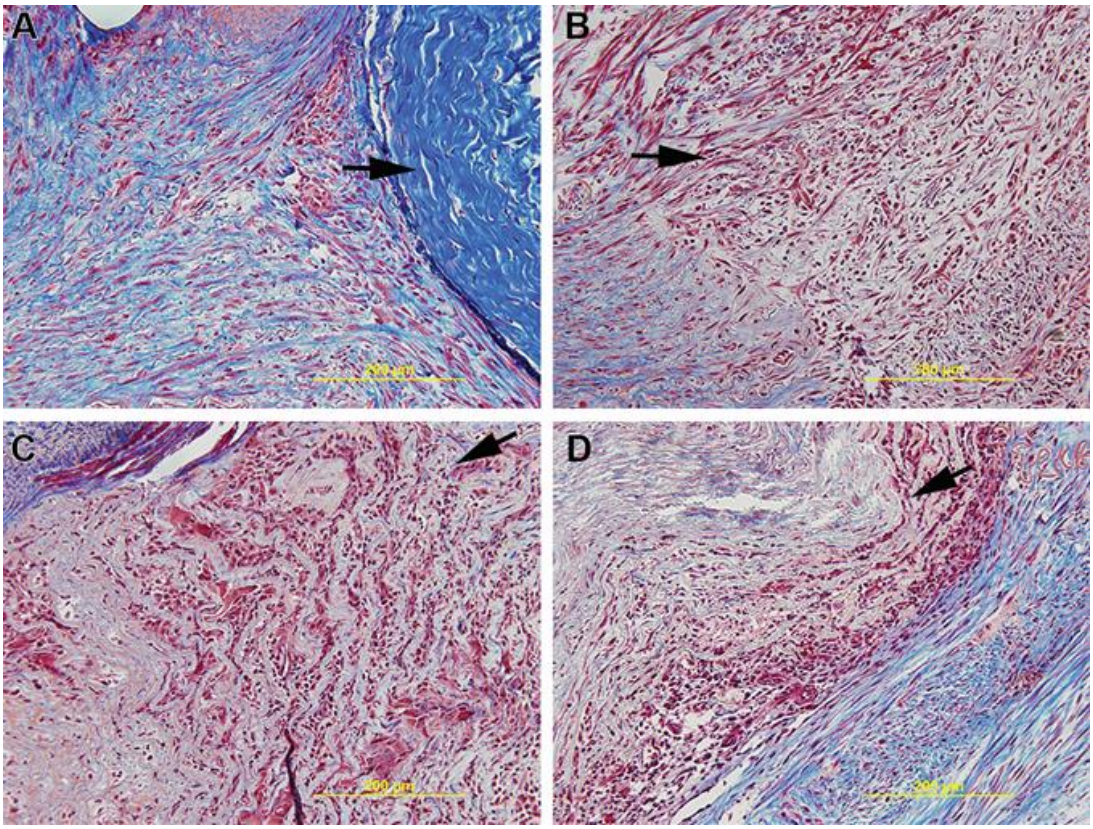

Figure 5.5 Histologic images of patches explanted at three weeks with trichrome staining at 20x with representative control

a) The control patch has a very distinct junction (arrow) with the native tissue and very minimal cellular infiltration

b) DBVP at three weeks showing a less distinct junction between host and patch with infiltration by red blood cells (arrow)

c) CBVP at three weeks showing the junction between patch and native tissue with cells (arrow) infiltrating the patch.

d) GBVP at three weeks with the arrow highlighting the cells infiltrating the patch.

Table 5.4 Summary of 3 week histology results

	DBVP	Control	CBVP	Control	GBVP	Control
Cellular infiltration/ host integration	Moderate	Mild	Mild	Mild	Moderate	Moderate
Inflammatory reaction	Mild	Mild	Moderate	Moderate	Moderate	Mild
Thrombus formation	No	No	No	Blood clot	Organized thrombus	Moderate occlusion of the vessel

At nine weeks the animals with the DBVP (group 1) showed significant cellular infiltration of mononuclear and RBCs into the scaffold material. There were also mononuclear cells lining the lumen of the vessel and an inflammatory response as shown in Figure 5.6a. The controls (group 1) showed very mild cellular infiltration and inflammatory cells could be seen along the anastomosis sites. One of the CBVP (group 2) animals had a significant immune response with dense areas of lymphocytes on the edges of the patch, infiltrating the patch as demonstrated in Figure 5.6b. The control on this animal also showed organized lymphocytes and a thick layer of fibrous tissue on the luminal side. The other CBVP animal (group 2) showed cellular infiltration of the scaffold with mononuclear cells and lymphocytes present on the periphery of the scaffold. The GBVP (group 3) had cells lining the lumen of the vessel as well as penetrating the patch and was very close to the smooth muscle cells as shown in Figure 6C. The animal with the GCVP (group 4) that had post-operative problems showed very few cells infiltrating the control or experimental patches,

with both also having lymphocytes present and numerous red blood cells. The second GCVP animal (group 4) demonstrated infiltration of blue connective tissue (on the trichrome stain) into the patch, which was at times difficult to discern from the native tissue (Figure 5.6d). See Table 5.5 for summarized results.

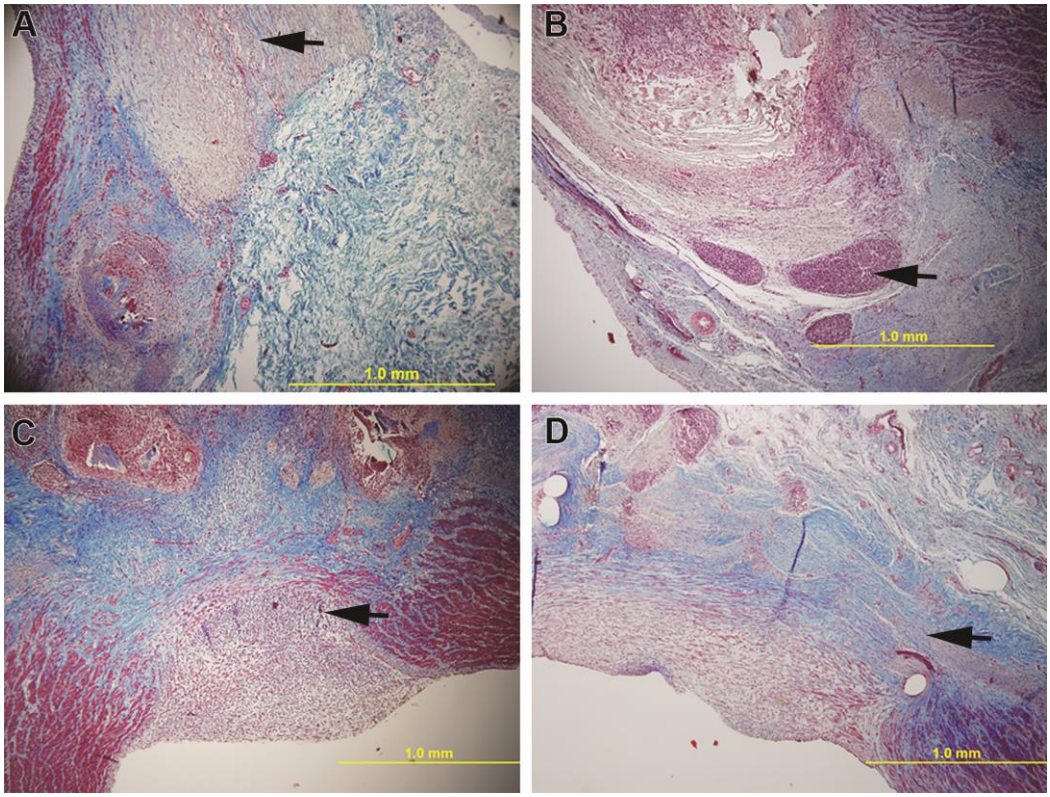

Figure 5.6 Histologic images of patches explanted at nine weeks with trichrome staining at 5x

a) DBVP at nine weeks with the arrow indicating native cells deep within the patch material

b) CBVP at nine weeks showing how the matrix of the patch has expanded to allow for host infiltration with the arrow noting the immune response to the patch (also present on the control side in this animal)

c) GBVP at nine weeks had cells lining the lumen of the vessel (arrow) as well as penetrating the patch and was very close to the smooth muscle cells

d) GCVP at nine weeks demonstrating infiltration of blue connective tissue (arrow) into the patch, which was at times difficult to discern from the native tissue

Table 5.5 Summary of 9 week histology results

	DBVP	Control	CBVP	Control	GBVP	Control	CBVP	Control
Cellular infiltration/ host integration	Significant	Mild	Moderate	Mild	Significant	Mild	Significant	Mild
Inflammatory reaction	Mild	Moderate	Mild	Moderate	Mild	Mild	Mild	Moderate
Thrombus formation	No	No	No	No	No	No	No	No

5.4.4 Ultrasound Results

The results of the ultrasound data showed no pre-existing conditions in the carotid arteries of any of the animals. In the three week animals, all arteries were patent after patch placement and at sacrifice. Gross examination of the lumen of the arteries showed varying degrees of stenosis in several of these animals, as is discussed in the gross results section, though blood flow was noted through all.

In the nine week animals, all arteries were patent at all time points. The pulsatile waveform of the GCVP patch at nine weeks is shown in Figure 5.2. The diameters and velocities of the vessels were used to compute the percentage of stenosis as described above. There were no significant differences in percentage of stenosis area between the control and experimental patches at the time of euthanasia.

5.5 Discussion

This study investigated the remodeling characteristics and biologic effects of different patch materials including a novel design which incorporated AuNPs into a decellularized blood vessel. The goal of the study was to determine how a novel nanomaterial-tissue construct design would behave *in vivo* when compared to a commercially available biologic patch. Parameters that were measured included rupture, stenosis, endothelial cell regeneration, and cellular infiltration in a swine cardiovascular model. Vascular repair materials must closely mimic the native tissue structure that is being replaced in order to avoid intimal hyperplasia (occlusion) and rupture. The use of decellularized blood vessels is advantageous because its mechanical advantage and its ability to retain structural elements, which can include stimulating growth factors that can support cell growth and differentiation [21, 26-29]. Additionally, conjugation of AuNPs to the constructs is also advantageous because AuNPs have been shown to increase stability, decrease inflammation, and slow down scaffold degradation [21, 26-29]. The results of this pilot study demonstrated that the novel AuNP-blood vessel material is biocompatible in a vascular environment; the patches presented increased tissue integration when compared to the control bovine pericardium material.

The use of arterial tissue as a vascular repair material yields a patch with characteristics very similar to that of the native tissue. The initial acute procedures showed that the patch could be easily handled in surgery and had

acceptable suture holding strength. The 100% success rate of implantation and 0% mortality rate demonstrated the ability of the material to be utilized as a vascular substitute *in vivo*. It is able to withstand the pressures and responses that occur with implantation of a vascular patch material. Nine weeks after implantation, all the experimental patches showed cellular ingrowth and the thinnest patch, the GCVP, demonstrated exceptional integration with the lumen of the vessel. It is possible that the addition of the gold nanoparticles as well as the thinner graft material enhanced cellular adhesion and migration. The dimensions of the thinner patch may be more conducive to remodeling because of the shorter migration distance of the host cells into the graft material, and thus allow for more host cells to infiltrate and vascularize the patch. It is also possible that the high surface energy of the AuNPs attracts cells and thus increased cellular migration and adhesion. These differences may lead to faster, enhanced cellular remodeling, and thus the improved integration.

The ultrasound data demonstrated that there were no initial problems within the vessels and that they remained patent throughout the experiment. The calculated percent stenosis of the vessels varied widely. Since the animals must be sedated during the ultrasound measurements, the blood velocity readings may not accurately reflect the flow of the blood pass the patches. The changes in velocity could be caused by inappropriate angle alignment or by the inherent nature of the tortuous vessels [29].

The gross examination of the vessels and the Evans Blue staining indicated that there was endothelial cell growth on the patch areas within the lumen. These events were not as evident in the nine week animals, which may indicate that the endothelial cells were no longer taking up the dye, an indication of mature cells, rather than regenerating ones since only regenerating cells will uptake the dye. The difficulty in grossly discerning the GCVP (group 4) from the native tissue at the nine week time point demonstrates excellent integration with the native tissue. The patch remained in place while allowing the native tissue to grow into and integrate with the scaffold.

The histology slides cut from this study demonstrated differences between the control and the experimental patches. At a microscopic level, the control and experimental patches have different widths of collagen strands and differences in the structure, as the control patch collagen strands tend to be thicker and closer packed than the decellularized arterial tissue. These differences can be noted by the different hues of blue found on the trichrome stained slides. Structural differences occur due to the different types of tissue being used and possibly from the crosslinking. The bovine pericardium control patch material has a different collagen orientation than the experimental blood vessel patches. Additionally, the bovine patch was crosslinked with glutaraldehyde.

The experimental patches are crosslinked in order to conjugate the AuNPs to the material. Crosslinking is typically performed in order to improve mechanical properties of acellular scaffolds; however, crosslinking has been

shown to adversely affect biocompatibility, leading to fibrous encapsulation. To avoid possible adverse biocompatibility issues but still achieving a structurally stable scaffold, we lightly crosslinked (using low molarity) the AuNPs to the acellular scaffold using a zero-length crosslinker, EDC, which has also been shown to be more cell friendly. Conjugating AuNPs to acellular scaffolds as well as to purified collagen has been shown to hinders collagenase binding sites;[21] therefore, less crosslinking is needed to achieve long term stability and thus less changes in the natural tissue structure [30]. The histology results supported the concept of increased stability and equivalent mechanical properties when the crosslinked patches are compared to the control material.

5.6 Conclusions

This was one of the first studies to demonstrate the feasibility of a vascular nano-material biological patch. The survival of all animals indicated that the patch material is compatible with a vascular environment and is capable of withstanding the mechanical forces while also enhancing cellular integration and avoiding stenosis. While the results were very encouraging it is noted that the study was a pilot study; the number of animals used was low and the time points were short. The material will be further explored with long term animal studies, as well as with other applications such as aortic patching.

5.7 Acknowledgments

This research was sponsored in part by the University of Missouri Bioprocessing and Biosensing Center grant (BBC), by NIH Grant T32 RR007004**,** and the University of Missouri Department of Surgery. The authors would like to thank Drs. Scott Korte, Erin O'Connor, Marcia Hart, and Beth Ahner for their anesthetic and surgical assistance as well as Dave Grant, Aaron Wood, and Sarah Smith. This study would not have been possible without the excellent animal care provided by the Office of Animal Research staff.

5.8 References

[1] Robinson KA, Li J, Mathison M, Redkar A, Cui J, Chronos NAF, et al. Extracellular Matrix Scaffold for Cardiac Repair. Circulation. 2005;112:I-135-I-43.

[2] David TE, Armstrong S. Surgical repair of postinfarction ventricular septal defect by infarct exclusion. Seminars in thoracic and cardiovascular surgery. 1998;10:105-10.

[3] David TE. The use of pericardium in acquired heart disease: a review article. J Heart Valve Dis. 1998;7:13-8.

[4] Fishman NH. Left ventricular aneurysm repair. Ann Thorac Surg. 1998;65:602-3.

[5] Xue L, Greisler HP. Biomaterials in the development and future of vascular grafts. J Vasc Surg. 2003;37:472-80.

[6] Bordenave L, Menu P, Baquey C. Developments towards tissue-engineered, small-diameter arterial substitutes. Expert review of medical devices. 2008;5:337-47.

[7] Ratcliffe A. Tissue engineering of vascular grafts. Matrix Biol. 2000;19:353-7.

[8] Tu JV, Pashos CL, Naylor CD, Chen E, Normand S-L, Newhouse JP, et al. Use of Cardiac Procedures and Outcomes in Elderly Patients with Myocardial

Infarction in the United States and Canada. New England Journal of Medicine. 1997;336:1500-5.

[9] Wang X, Lin P, Yao Q, Chen C. Development of small-diameter vascular grafts. World J Surg. 2007;31:682-9.

[10] Zhang WJ, Liu W, Cui L, Cao Y. Tissue engineering of blood vessel. J Cell Mol Med. 2007;11:945-57.

[11] Lu Q, Ganesan K, Simionescu DT, Vyavahare NR. Novel porous aortic elastin and collagen scaffolds for tissue engineering. Biomaterials. 2004;25:5227-37.

[12] Awad IA, Little JR. Patch angioplasty in carotid endarterectomy. Advantages, concerns, and controversies. Stroke. 1989;20:417-22.

[13] Bond R, Rerkasem K, Naylor AR, AbuRahma AF, Rothwell PM. Systematic review of randomized controlled trials of patch angioplasty versus primary closure and different types of patch materials during carotid endarterectomy. Journal of Vascular Surgery. 2004;40:1126-35.

[14] Cho SW, Park HJ, Ryu JH, Kim SH, Kim YH, Choi CY, et al. Vascular patches tissue-engineered with autologous bone marrow-derived cells and decellularized tissue matrices. Biomaterials. 2005;26:1915-24.

[15] Lee WK, Park KD, Kim YH, Suh H, Park JC, Lee JE, et al. Improved calcification resistance and biocompatibility of tissue patch grafted with sulfonated PEO or heparin after glutaraldehyde fixation. Journal of biomedical materials research. 2001;58:27-35.

[16] Matsagas M, Bali C, Arnaoutoglou E, Papakostas J, Nassis C, Papadopoulos G, et al. Carotid Endarterectomy with Bovine Pericardium Patch Angioplasty: Mid-Term Results. Annals of vascular surgery. 2006;20:614-9.

[17] Muto A, Nishibe T, Dardik H, Dardik A. Patches for carotid artery endarterectomy: Current materials and prospects. Journal of Vascular Surgery. 2009;50:206-13.

[18] Li X, Guo Y, Ziegler KR, Model LS, Eghbalieh SDD, Brenes RA, et al. Current Usage and Future Directions for the Bovine Pericardial Patch. Annals of vascular surgery. 2011;25:561-8.

[19] Roy S, Silacci P, Stergiopulos N. Biomechanical properties of decellularized porcine common carotid arteries. Am J Physiol Heart Circ Physiol. 2005;289:H1567-76.

[20] Whittemore AD. Failure of peripheral arterial reconstruction. Acta chirurgica Scandinavica Supplementum. 1988;550:74-80.

[21] Grant SA, Spradling CS, Grant DN, Fox DB, Jimenez L, Grant DA, et al. Assessment of the biocompatibility and stability of a gold nanoparticle collagen bioscaffold. J Biomed Mater Res A. 2013.

[22] Hsu SH, Tang CM, Tseng HJ. Biocompatibility of poly(ether)urethane-gold nanocomposites. J Biomed Mater Res A. 2006;79:759-70.

[23] Williams C, Liao J, Joyce EM, Wang B, Leach JB, Sacks MS, et al. Altered structural and mechanical properties in decellularized rabbit carotid arteries. Acta Biomater. 2009;5:993-1005.

[24] Amiel GE, Komura M, Shapira O, Yoo JJ, Yazdani S, Berry J, et al. Engineering of blood vessels from acellular collagen matrices coated with human endothelial cells. Tissue Eng. 2006;12:2355-65.

[25] Wong CB, Wong JC. A novel method to quantify carotid artery stenosis by Doppler ultrasound: Using the continuity principle. The International journal of angiology: official publication of the International College of Angiology, Inc. 2010;19:e86.

[26] Hodde JP, Badylak SF, Brightman AO, Voytik-Harbin SL. Glycosaminoglycan content of small intestinal submucosa: a bioscaffold for tissue replacement. Tissue Eng. 1996;2:209-17.

[27] Voytik-Harbin SL, Brightman AO, Kraine MR, Waisner B, Badylak SF. Identification of extractable growth factors from small intestinal submucosa. J Cell Biochem. 1997;67:478-91.

[28] McPHERSON TB, Badylak SF. Characterization of fibronectin derived from porcine small intestinal submucosa. Tissue Engineering. 1998;4:75-83.

[29] Voytik-Harbin SL, Brightman AO, Waisner BZ, Robinson JP, Lamar CH. Small intestinal submucosa: A tissue-derived extracellular matrix that promotes tissue-specific growth and differentiation of cells in vitro. Tissue Engineering. 1998;4:157-74.

[30] Whelove OE, Cozad MJ, Lee BD, Sengupta S, Bachman SL, Ramshaw BJ, et al. Development and in vitro studies of a polyethylene terephthalate-gold nanoparticle scaffold for improved biocompatibility. J Biomed Mater Res B Appl Biomater. 2011;99:142-9.

Chapter Six

AN *IN VIVO* STUDY OF A NOVEL GOLD NANOCOMPOSITE BIOMATERIAL FOR VASCULAR REPAIR

6.1 Abstract

Currently vascular repairs are treated using synthetic or biologic patches, however these patches have an array of complications, including calcification, rupture, re-stenosis, and intimal hyperplasia. A more effective patch material composed of decellulzarized tissue conjugated to gold nanoparticles (AuNPs) was developed and the long term biocompatibility and cellular integration was investigated. Porcine abdominal aortic tissue was decellularized and crosslinked with 100nm gold nanoparticles (AuNP). These patches were placed over a longitudinal arteriotomy of the thoracic aorta in six pigs. The animals were monitored for six months. Gross, histological, and immunohistochemical analyses of the patches were performed after euthanasia. Grossly there was minimal scar tissue with the patches still visible on the outer surface of the vessel. The inner lumen was smooth and went from patch to native tissue seamlessly. Histologically there was infiltration of host cells into the patch material. The immunohistochemical results showed that an endothelial cell layer had formed over the patch within the vessel and smooth muscle cells were

repopulating the biomaterial in all animals. These results demonstrated that the AuNP biomaterial had excellent *in vivo* feasibility. It integrated well with the host tissue and was not rejected nor failed over the six month period of time. The host cells re-populate the biomaterial's matrix appropriately and with minimal immune response. This biomaterial holds great promise as a vascular repair material.

6.2 Introduction

Vascular patch materials are used to repair and reconstruct damage to blood vessels [1-3]. These patch materials ideally mimic the native extracellular matrix, sustain and guide new cell growth, avoid intimal hyperplasia, resist infection, and degrade after new tissue has formed [4-9]. Unfortunately an ideal material has not yet been created, and currently a variety of synthetic and biologic materials are in use [10, 11]. The currently used synthetic and biological materials can cause immune reactions, infections, calcification, and neo-intimal hyperplasia [3, 12-16].

Synthetic materials such as expanded polytetrafluoroethylene are strong and long lasting *in vivo.* However they are susceptible to thrombus formation, calcification, and infection [17]. The native tissue tends to have a strong foreign body response to these types of materials and this leads to chronic inflammation. The cells have difficulty integrating into these synthetic materials which in turn

leads to their inability to continue growing when used in pediatric patients [18]. Biologic materials such as bovine pericardium better approximate characteristics of the native tissue than synthetic materials, but tend to be weaker and degrade quicker in the body [19, 20]. Both types of materials show foreign body responses, intimal hyperplasia and increased thrombogenicity when compared to native tissue [21, 22].

To counter these problems new types of materials and surface modifications are being explored. One of these surface modifications is the use of gold nanoparticles (AuNPs). AuNPs are biologically inert and can increase antimicrobial properties of biomaterials while also aiding cell proliferation [23-27]. They are being investigated in numerous medical applications such as drug delivery, imaging, biosensors, diagnostics, gene therapy, and nanocomposite biomaterials due to their biocompatibility, optical properties, and conjugation capabilities [28-33]. AuNPs have been shown to improve the thermal and mechanical properties of material and hinder collagenase binding sites to create a more stable biomaterial sites [23, 34]. This is extremely important in tissue engineering that require constructive remodeling

In this study, we developed a nanocomposite vascular patch using gold nanoparticles and decellularized arterial tissue matrices. Our objective was to perform a long term *in vivo* test of our biomaterial. The hypothesis for this experiment was that the novel nanocomposite biomaterial would show minimal immune response, endothelial and smooth muscle cell regeneration, and overall

excellent integration and biocompatibility with the host tissue. Gold nanoparticles were conjugated onto the decellularized tissue and implanted on the thoracic aorta of swine. Six months after implantation, wound healing, tissue remodeling, endothelial cell regeneration, and cellular integration were investigated by gross, histological, immunohistochemical, and electron microscopic analyses.

6.3. Materials and methods

6.3.1 Tissue Harvest and Decellularization

Decellularization was performed following a previously published protocol [35, 36]. Porcine abdominal aortas were harvested immediately following euthanasia of swine at the University of Missouri. Blood and any excess connective tissue were removed and then they were immersed in distilled water for 24 hours at 4° C. The vessels were treated with 0.025% trypsin EDTA (ATCC) diluted in Dulbecco's phosphate buffered saline (dPBS; ATCC) for 24 hours at 37 °C. The tissue was decellularized with a solution of 1% Triton x-100 (Sigma) and 0.1% ammonium hydroxide (Fisher) in distilled water for 72 hours at 4 °C. It was then washed in a solution of Eagle's Minimum Essential Medium (EMEM; ATCC) 10% (v/v) horse serum and PennStrep (200 U/mL). The material was immersed for 24 hours in distilled water at 4 °C and then for 48 hours in PBS at 4 °C, changing the PBS to fresh solution at 24 hours. All of these steps were done with agitation**.**

6.3.2 Crosslinking

Decellularized patches were incubated for 15 minutes at ambient temperature in a crosslinking solution (50:50 (v/v) solution of acetone and PBS with 1-ethyl-3-[3-dimethylaminopropyl]carbodiimide (EDC) and *N*-hydroxysuccinimide(NHS). 100 nm AuNPs at 4 times the stock solution were functionalized using a solution of 2-mercaptoethylamine and added to the tissue. The patches were incubated for 24 hours at ambient temperature with gentle agitation followed by two 24 hour PBS rinses. Sterilization occurred via immersion in an aqueous solution of 0.1%(v/v) peracetic acid with 1.0M NaCl for 30 minutes followed by two 24 hour sterile PBS rinses at ambient temperature with shaking.

6.3.3 Suture Pullout Testing

Suture pullout testing was performed on native porcine aortic tissue (n=5), decellularized porcine aortic tissue (n=7), crosslinked porcine aortic tissue (n=9), and bovine pericardium (n=5). The bovine pericardium was chosen to represent the typical biologic repair patch that would be used in human medicine. As noted in Chapter 3 the addition of AuNPs did not significantly change the mechanical properties of the material, so they were not retested here. Each piece of tissue was cut into a 10mm x 10mm strip. A piece of 6-0 prolene suture that is typically used for this type of procedure *in vivo* was tied 3mm from one edge to create a

5mm loop. The tissue was gripped with a pneumatic grip set to 52psi, and the suture was placed over an opposing hook. An Instron TA.XT2 mechanical testing system (Texture Technologies, Corporation, Scarsdale, NY) was utilized to strain the specimens at a rate of 0.2mm/s until failure. If the suture broke before pulling out of the tissue the test results were discarded. The tensile strength at yield was calculated by dividing the maximum load, Fmax, by the original cross-sectional area, A, of the specimen. The modulus of elasticity E, was determined from the slope of a line fit to the stress versus strain curve of each specimen.

6.3.4 Implantation

Female domestic swine (n=6) with a starting weight of approximately 120 lbs were housed in accordance with the *Guide for the Care and Use of Laboratory Animals* under a protocol approved by the Institutional Animal Care and Use Committee. 24 hours before surgery animals were given 325 mg aspirin orally (PO). Intramuscular (IM) telazol (4.4-6.6 mg/kg body weight), xylazine (2.2 mg/kg) and atropine (0.05 mg/kg) were given as a preanesthetic. 2-4% Isoflurane was administered via nose cone until the animal was sedated enough to be safely intubated. A surgical plane of anesthesia was maintained using 1-3% isoflurane gas and a ventilator at 6-8 breaths/minute. Prior to the incision animals were given ceftiofur (5 mg/kg IM). An intravenous (IV) catheter was placed in the ear with an isotonic sodium chloride flow throughout surgery.

Heparin was given IV at an initial bolus of 10,000 U/kg followed by 5,000 u/kg every hour intra op when necessary. Pancuronium (0.1 mg/kg IV) was given at the time of the incision.

The aorta was reached through the fourth rib space via a left lateral thoracotomy. The aorta was partially clamped and opened in the longitudinal direction. Patch material was sutured over the defect using 6-0 prolene.

Post operatively a 75 µg/hr fentanyl patch was placed on the dorsum for pain relief and carprofen (3mg/kg) subcutaneously (SQ) and buprenorphine (0.01-0.02 mg/kg) IM were given to bridge the gap until the fentanyl became effective. Animals received 325 mg aspirin PO for 3 days post op and then 81 mg/day PO until sacrifice.

6.3.5 Gross Examination

Each artery was photographed (Canon PowerShot A4000 IS) *in vivo* after the thorax of the animal had been re-opened. The lumen was photographed after the artery was explanted.

6.3.6 Histology

All slides were prepared by IDEXX Bioresearch (Columbia, MO). Samples were fixed in 10% (v/v) buffered formalin, dehydrated with a graded ethanol

series, embedded in paraffin and cut to a thickness of 5 µm with a microtome. The histology slides were stained with hematoxylin and eosin (H&E), as well as van Gieson's method to look at elastin and collagen was stained for using Masson's trichrome. All slides were viewed at 50x, 100x, 200x, and 400x on a Zeiss Axiophot (Carl Zeiss Microimaging, Inc., Thornwood, NY) and photographs were acquired using an Olympus DP70 (Olympus America Inc., Center Valley, PA) camera with DP Manager Version 1.21.107 as the acquisition software.

6.3.7 Immunohistochemistry

All slides were prepared by IDEXX Bioresearch (Columbia, MO). Samples were fixed in 10% (v/v) buffered formalin, dehydrated with a graded ethanol series, embedded in paraffin and cut to a thickness of 5 µm with a microtome. The slides were deparaffinized using a standard protocol of xylene, to absolute alcohol, 95% alcohol to water. They were then immersed in 5% bovine serum albumin (Sigma A3294-50) for 20 minutes followed by CD31 (Abcam ab28364) at a 1:50 ratio for one hour. They were rinsed using a Dako wash buffer (Dako K1492). Next the slides were submerged in the goat anti-rabbit IgG Alexafluor 594 red (Invitrogen A11037) at a 1:500 ratio for 30 minutes followed by another Dako rinse and then put in bovine serum albumin for 20 minutes. They were dyed with Actin Smooth Muscle (Dako M0851) at a 1:400 ratio for an hour, rinsed, and immersed in goat anti-mouse IgG Alexafluor 288 green (Molecular

Probes A11001). Slides were rinsed again in Dako, then a coverslip with MoWiol(polyvinyl alcohol mounting medium with DABCO antifade - Fluka Cat #10981) was applied. They were viewed on a Leica TCP SP8 MP Inverted spectral confocal microscope with tunable white light laser at the University of Missouri Cytology Core. Images were taken using Leica software.

6.3.8 Statistical Analysis

GraphPad Prism v4.0 (GraphPad Software, Inc., San Diego, CA) was used to analyze experimental data. One-way analysis of variance (ANOVA) with significance set at $p<0.05$ was conducted followed by a Tukey-Kramer post-test to determine significant differences between means of the experimental groups for the mechanical testing and biocompatibility assays. Values are reported and graphed as the mean ± standard error of the mean.

6.4 Results

6.4.1 Suture Pullout Testing

The suture pullout testing showed that the bovine pericardial patch had a significantly higher Modulus of Elasticity and Tensile Stress at the maximum load when compared to any of the porcine tissue. The values for each group can be found in Table 6.1 with the results graphed noting the significance in Figure 6.1.

Table 6.1 Modulus of Elasticity (MPa) and Tensile Stress at Max (MPa) for each experimental group

	Modulus of Elasticity (MPa)	Tensile Stress at Max (MPa)
Native Porcine	3.28 ± 0.48	0.33 ± 0.05
Decell Porcine	3.63 ± 0.49	0.36 ± 0.06
Crosslink Porcine	3.99 ± 0.55	0.36 ± 0.04
Bovine Pericaridum	15.74 ±1.15	0.89 ± 0.05

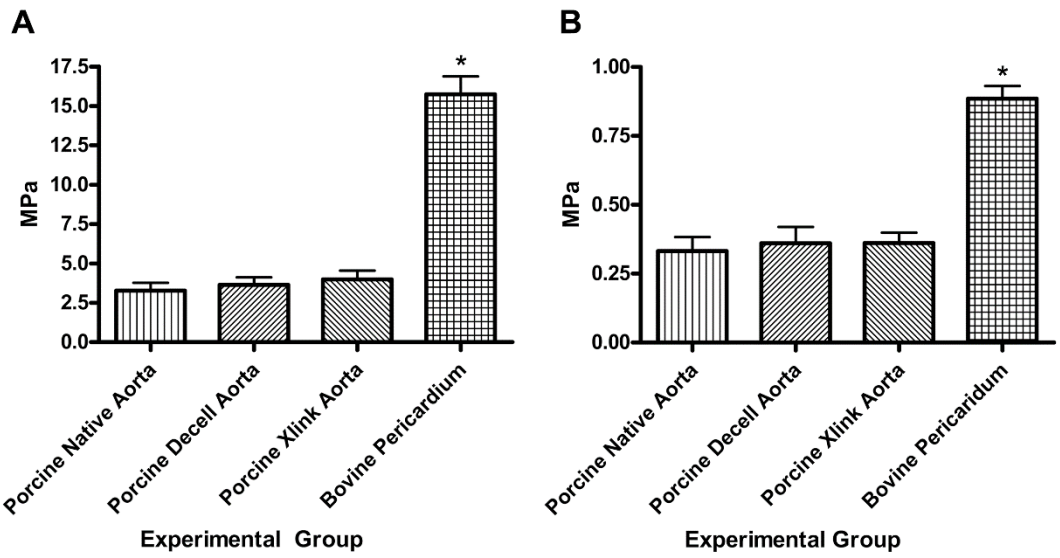

Figure 6.1 Suture Pullout testing on porcine and bovine tissues. The asterisk denotes a significantly higher value than the other experimental groups. a) Modulus of Elasticity, b) Tensile Stress at Max Load

6.4.2 Implantation

Overall, implantation went smoothly for 5 of the 6 animals. The sixth animal was awakening from the anesthetic when she experienced a cardiac event and could not be revived. The thoracic cavity was reopened and the patch was still in place and not the cause of death. All other animals survived to their time point of 6 months. Figure 6.2 shows the approach, isolation, and implantation of the patch into the aorta.

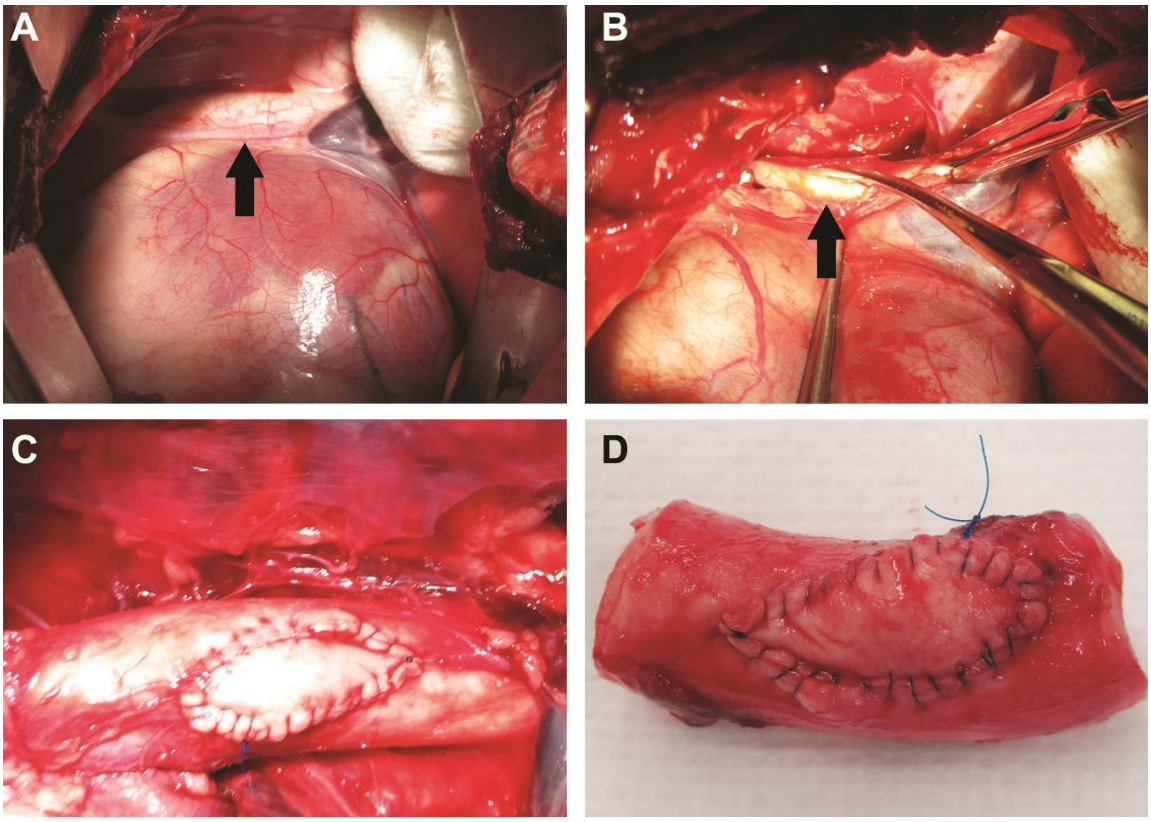

Figure 6.2 Implantation of the material on the thoracic aorta

a) Access to the thoracic aorta (black arrow) was done through the 5th and 6th rib space

b) The aorta was isolated and partially clamped before a defect (black arrow) was made into the lumen

c) The material *in vivo* just after implantation

d) The material explanted less than 3 hours post implantation (non-survival animal)

6.4.3 Gross Examination

After 6 months the aortas were removed from the animals. Upon approach minimal scar tissue was seen within the thoracic cavity of most of the animals (Figure 6.3). The patch integrated smoothly on the luminal side with the native tissue.

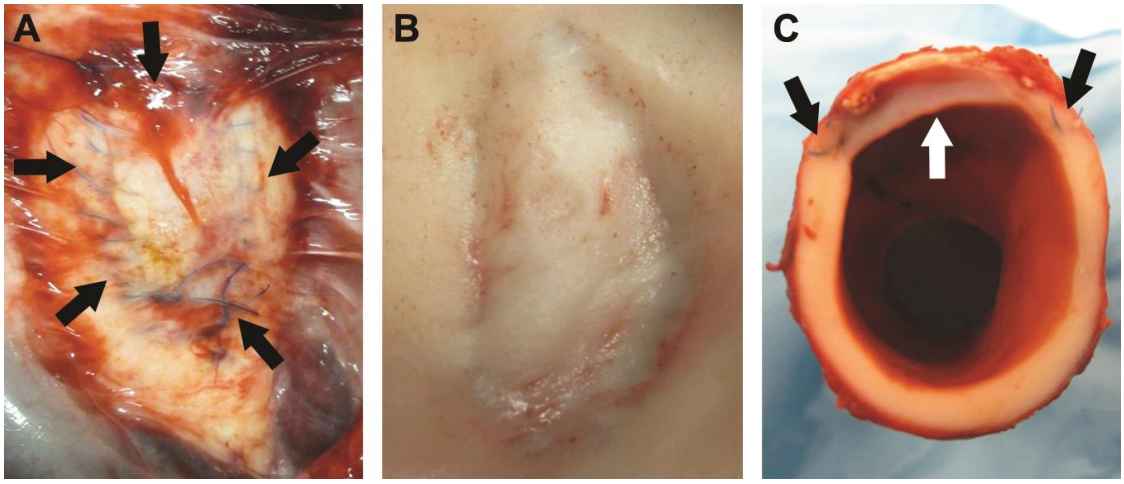

Figure 6.3 Thoracic aorta patched with the biomaterial after 6 months of implantation.

a) The patch still *in vivo*. The suture material can still be seen on the adventitial layer of the vessel. There is minimal scar tissue such that the patch is visible through it. The arrows indicate the outline of the patch

b) The lumen of the aorta with the patch. There are no blood clots associated with the patch and grossly is has integrated smoothly with the host tissue.

c) A cross sectional view of the aorta through the patch showing the smooth transition between patch and native tissue.

6.4.4 Histology

Figure 6.4a shows the patch before the decellularization process and the nuclei of the cells are clearly visible. After decellularization the histology shows that the nuclear remnants have been removed (Figure 6.2 b-d). The Masson's trichrome staining and van Gieson's staining highlight the elastin and collagen tissue present in the exctracellular matrix. Figure 6.2e shows the presence of gold nanoparticles on the material before implantation.

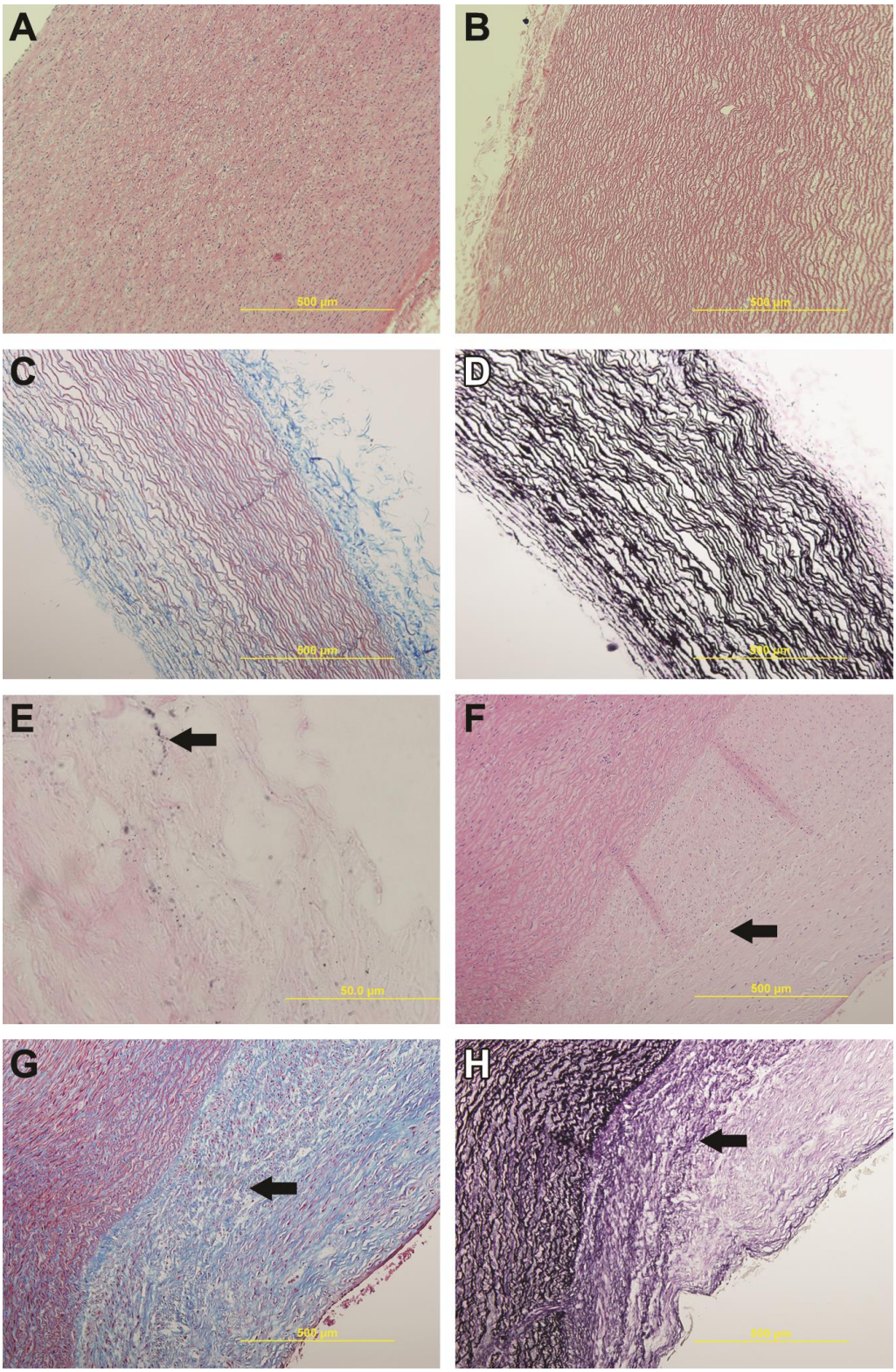

Figure 6.4 Histology of native control tissue and pristine biomaterial

a) 100x H&E staining of native porcine aorta with cell nuclei present

b) 100x H&E staining of decellularized aorta showing removal of cellular components

c) 100x Masson's trichrome staining of the biomaterial with a black arrow indicating collagen and the white arrow indicating lighter staining collagen

d) 100x van Geison's stain of the biomaterial showing the presence of the black elastin fibers.

e) 1000x H&E staining of the biomaterial showing the presence of the AuNPs.

f) 100x H&E staining of native tissue and the biomaterial at 6 months. Arrow indicates the nuclei of cells that have moved into the patch area.

g) 100x Masson's trichrome staining of the biomaterial at 6 months with a black arrow the transition zone between the biomaterial and native tissue.

h) 100x van Geison's stain of the biomaterial at 6 monthsshowing the presence of the black elastin fibers. The black arrow indicates that the area of biomaterial closest to the native tissue has characteristics more similar to the native tissue.

After six months the explanted patch material showed cellular integration, though there is still a difference between the biomaterial and the native tissue. Using H&E staining (Figure 6.5a) we can note that cells have infiltrated into the patch material. There are no major congregations of immune cells, nor signs of infection or fibrosis around the patch. The trichrome (Figure 6.5b) shows that the biomaterial has a higher amount of collagen when compared to the native tissue. There is red staining areas within the biomaterial though, indicating smooth muscle cell integration. The van Gieson's stain (Figure 6.5c) shows that the patch stains less for elastin than the native tissue. The arrow in Figure 6.5c

points to a transition zone though, where it appears the biomaterial is becoming more similar to the native tissue.

6.4.4 Immunohistochemistry

Immunohistochemical analysis showed that the cells present on the lumen side of the patches stained positively for CD31(red fluorescence labeled) which indicates endothelial cell regeneration (Figure 6.6b). The vessel has repaired the area over the patch appropriately and is comparable to the control animal's endothelial cell layer in Figure 6.6a. The green fluorescence labeled SM actin stain showed that smooth muscle cells (SMCs) have re-populated the graft (Figure 6.6a, b). Figure 6.6d is the patch just after implantation (non-survival animal) and highlights how much cellular integration occurred during the 6 months. In Figure 6.6a the native vessel is seen, and compared to Figure 6.6b which represents just the area associated with the patch. Figure 6.6c shows the transition zone between the native tissue and the patch, highlighting that while there are still some differences in the way the smooth muscle cells are oriented, they are rebuilding within the extracellular matrix of the patch.

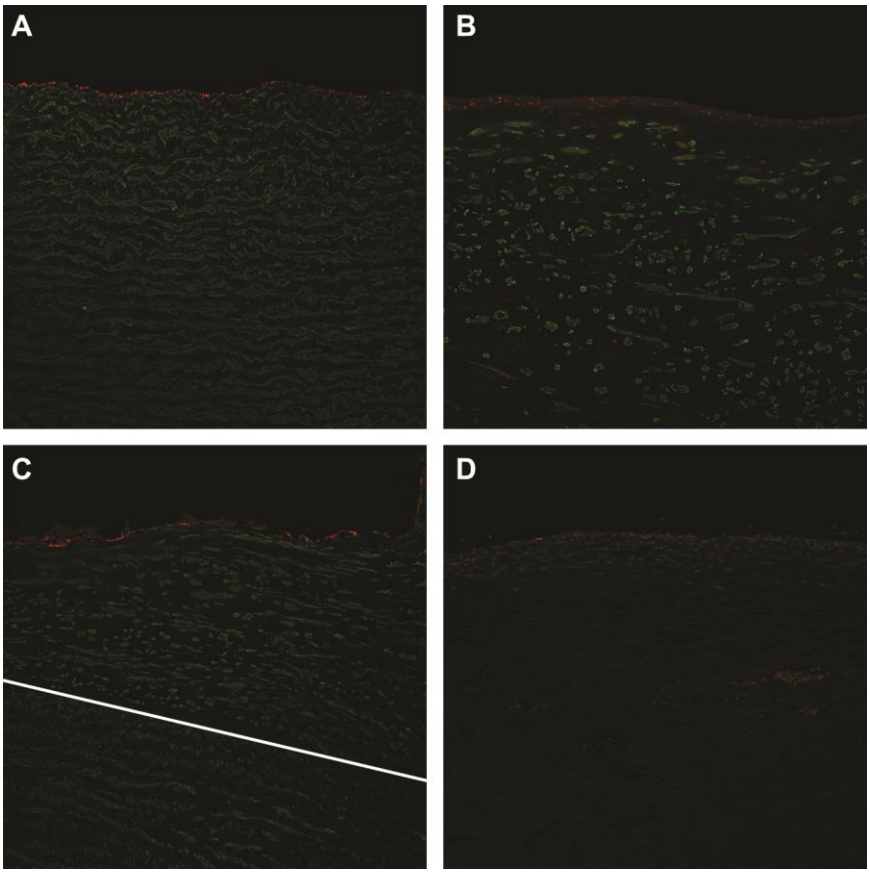

Figure 6.6 Immunohisotchemical staining of endothelial (red) and SMCs (green) taken at 200x.

a) Native aortic tissue taken from a control animal (no surgical intervention). There is a smooth line of endothelial cells present on the lumen of the vessel with typical SMC patterning below it.

b) The nanocomposite biomaterial 6 months after implantation showing a smooth, single layer of endothelial cells (red) comparable to the control tissue. There are also SMCs present throughout the area below the endothelial cells.

c) The white line indicates the transition between native tissue and the implanted biomaterial. The SMCs have integrated the biomaterial and are forming patterns much like the native tissue. There is a smooth layer of endothelial cells present on the luminal side.

d) This image is of a patch that was implanted only briefly. It shows a lack of SMCs or endothelial cell growth, indicating what is present in the other images is not autofluorescence, but evidence of true cellular integration and remodeling.

6.5 Discussion

A more intelligently engineered biomaterial could conquer the negative attributes associated with the currently available biologic and synthetic solutions. Previously extracellular matrices have been explored as a base material for wound healing [37]. Porcine arterial tissue has an extracellular matrix that allows for cellular in growth and wound healing. In this study the decellularized arterial tissue was crosslinked and had AuNPs conjugated to it. The material was studied mechanically compared to a commercially available biological patch. The biomaterial was then subjected to a long term *in vivo* study to determine how the native tissue would respond.

There were significant mechanical differences between the porcine aortic tissue when compared with the bovine pericardium. The bovine pericardium showed a higher strength before failing, but was significantly stiffer than the porcine tissue. *In vivo* the porcine tissue withstood the blood pressure of the thoracic aorta, so the strength at failing is not truly a concern. Instead this data shows that the porcine aorta may mimic the native arterial tissue much better than the bovine pericardium does. Wang et al. showed that more compliant graft may match mechanical and flow parameters better than a less compliant material [8]. As the suture pulls out more easily from the porcine tissue, surgeons may need to slightly change their methods to account for this. However the porcine tissue may allow for better healing and a lower chance of thrombosis when compared to stiffer materials.

The implantation process of this material went smoothly, with the exception of one animal lost to anesthetic complications and the aorta was still intact at death. The surgeon did note that there was more hemorrhage around the suture bites in our material when he compared it to biomaterials he has previously implanted in humans. While this is a concern, the bleeding was moderate and controlled quickly. The initial physical attributes of the patch during surgery can be accounted for and given the integration and the wound healing response with the biomaterial; it is definitely worth making a change. After explantation the gross photos show that there was minimal scar tissue in the chest. The animal did not try to wall it via the immune system as can be seen with some other materials. The gross view of the lumen shows a smooth, well integrated patch. There were no thrombi seen as can occur when the body contacts a foreign material [38-40]. Typically the contact of blood will with an unknown material will lead to adhesion and aggregation of platelets and a coagulation response, which was not seen with this material [41].

The decellularized porcine aortic tissue showed that the native extracellular matrix remains after decellularization (Figure 6.4). The collagen and elastin that are present in the biomaterial's matrix can provide an organized scaffold for cells to adhere and proliferate onto [42]. The AuNPs that are present (Figure 6.4e) have been shown to increase stability, decrease inflammation, and slow down scaffold degradation [34, 43-46]. The lack of thrombosis and other

inflammatory and immune reactions may indicate that the biomaterial's surface modifications are aiding in the healing process.

The histologic images show that while the biomaterial is integrated with native cells, there are still structural differences between the native vessel and the biomaterial. The trichrome and van Geison's stains show the biomaterial has less collagen and elastin still than the native tissue, but does have a zone where it appears to be remodeling into something more like the native tissue. With the H&E staining we see minimal immune response and no signs of infection. The body often responds to foreign materials with an inflammatory response including neutrophils, macrophages, and multi-nucleated giant cells [47]. This was not noted in our study. Often when a vascular wall repairs itself there is a generalized thickening of the media due to over proliferation of smooth muscle cells known as intimal hyperplasia [48, 49]. On the histologic and gross images for this study there is no thickening of the intimal layer between the native tissue and the biomaterial. Intimal hyperplasia is evident at six months if it is going to occur. It was not seen in any of the animals here, another indicator of biocompatibility.

The results of the immunohistochemical staining were particularly promising. They show definitive evidence that the vessel has appropriately begun to remodel into the biomaterial. The CD31 stain highlighted the layer of endothelial cells that has covered the patch. It is not overly thickened and comparable to the control tissue. The presence of an endothelial cell layer is

important as decreases in endothelial derived substances result in a decreased ability to regulate coagulation [50]. When compared to the patch that had only been briefly implanted, the six months patches had excellent integration of smooth muscle cells in the extracellular matrix. As previously discussed, smooth muscle cells can over proliferate during vascular repair. However they must be present to properly rebuild the vessel as they also play a role in synthesizing extracellular matrix [51-54]. The immunohistochemical staining shows that they are infiltration the biomaterial in a pattern similar to the native tissue. A longer term study might show total integration of the material.

6.6 Conclusions

This long term study examines the potential of a novel nanocomposite biomaterial for vascular repair and blood contacting applications. The biomaterial did not fail in any of the animals tested and the long term survival of five of the animals indicated the *in vivo* durability of the biomaterial. It was able to withstand the pressure of the aorta while allowing for endothelial and smooth muscle cell re-growth. The integration and healing seen during this study highlight the potential of this biomaterial to give the body a chance to correctly rebuild injured tissue. The reaction of the body to the biomaterial supports our thesis that there would be minimal immune response, endothelial and smooth muscle cell regeneration, and overall excellent integration and biocompatibility. Further studies should be done utilizing diseased animal models to see how the

biomaterial performs when attached to a more friable tissue in an environment that is not as capable of healing itself. This nanocomposite biomaterial shows great promise as a vascular repair material.

6.7 Acknowledgments

This research was sponsored in part by the University of Missouri by NIH Grant T32 RR007004**,** and the University of Missouri Departments Bioengineering and Surgery. The authors would like to thank Dr. Raja Gopaldas and Jan Ivey for their surgical work, as well as Drs. Scott Korte, Erin O'Connor, Marcia Hart, Sarah Hansen, Mike Fink, and Beth Ahner for their anesthetic and surgical assistance. The University of Missouri Cytology Core was integral in the capture of the confocal images. Dr. Cindy Besch-Williford, Jan Adair, and Jill Hansen at IDEXX Bioresearch ensured the success of all histological and immunohistochemical slide staining. Dave Grant and Sarah Smith aided greatly with lab work. This study would not have been possible without the excellent animal care provided by the Office of Animal Research staff.

6.8 References

[1] Rhodes VJ. Expanded polytetrafluoroethylene patch angioplasty in carotid endarterectomy. Journal of Vascular Surgery.22:724-31.

[2] AbuRahma AF, Hannay RS, Khan JH, Robinson PA, Hudson JK, Davis EA. Prospective randomized study of carotid endarterectomy with polytetrafluoroethylene versus collagen-impregnated Dacron (Hemashield) patching: perioperative (30-day) results. Journal of Vascular Surgery. 2002;35:125-30.

[3] Cho SW, Park HJ, Ryu JH, Kim SH, Kim YH, Choi CY, et al. Vascular patches tissue-engineered with autologous bone marrow-derived cells and decellularized tissue matrices. Biomaterials. 2005;26:1915-24.
[4] Bordenave L, Menu P, Baquey C. Developments towards tissue-engineered, small-diameter arterial substitutes. Expert review of medical devices. 2008;5:337-47.

[5] Ratcliffe A. Tissue engineering of vascular grafts. Matrix Biol. 2000;19:353-7.

[6] Tu JV, Pashos CL, Naylor CD, Chen E, Normand S-L, Newhouse JP, et al. Use of Cardiac Procedures and Outcomes in Elderly Patients with Myocardial Infarction in the United States and Canada. New England Journal of Medicine. 1997;336:1500-5.

[7] Zhang WJ, Liu W, Cui L, Cao Y. Tissue engineering of blood vessel. J Cell Mol Med. 2007;11:945-57.

[8] Wang X, Lin P, Yao Q, Chen C. Development of small-diameter vascular grafts. World J Surg. 2007;31:682-9.

[9] Zwirner K, Thiel C, Thiel K, Morgalla MH, Konigsrainer A, Schenk M. Extracellular brain ammonia levels in association with arterial ammonia, intracranial pressure and the use of albumin dialysis devices in pigs with acute liver failure. Metab Brain Dis. 2010;25:407-12.

[10] Robinson KA, Li J, Mathison M, Redkar A, Cui J, Chronos NAF, et al. Extracellular Matrix Scaffold for Cardiac Repair. Circulation. 2005;112:I-135-I-43.

[11] Xue L, Greisler HP. Biomaterials in the development and future of vascular grafts. J Vasc Surg. 2003;37:472-80.

[12] Awad IA, Little JR. Patch angioplasty in carotid endarterectomy. Advantages, concerns, and controversies. Stroke. 1989;20:417-22.

[13] Bond R, Rerkasem K, Naylor AR, AbuRahma AF, Rothwell PM. Systematic review of randomized controlled trials of patch angioplasty versus primary closure and different types of patch materials during carotid endarterectomy. Journal of Vascular Surgery. 2004;40:1126-35.

[14] Lee WK, Park KD, Kim YH, Suh H, Park JC, Lee JE, et al. Improved calcification resistance and biocompatibility of tissue patch grafted with sulfonated PEO or heparin after glutaraldehyde fixation. Journal of biomedical materials research. 2001;58:27-35.

[15] Matsagas M, Bali C, Arnaoutoglou E, Papakostas J, Nassis C, Papadopoulos G, et al. Carotid Endarterectomy with Bovine Pericardium Patch Angioplasty: Mid-Term Results. Annals of vascular surgery. 2006;20:614-9.

[16] Muto A, Nishibe T, Dardik H, Dardik A. Patches for carotid artery endarterectomy: Current materials and prospects. Journal of Vascular Surgery. 2009;50:206-13.

[17] Lee WK, Park KD, Kim YH, Suh H, Park JC, Lee JE, et al. Improved calcification resistance and biocompatibility of tissue patch grafted with sulfonated PEO or heparin after glutaraldehyde fixation. Journal of biomedical materials research. 2001;58:27-35.

[18] Li X, Guo Y, Ziegler KR, Model LS, Eghbalieh SDD, Brenes RA, et al. Current Usage and Future Directions for the Bovine Pericardial Patch. Annals of vascular surgery. 2011;25:561-8.

[19] Bolland F, Korossis S, Wilshaw S-P, Ingham E, Fisher J, Kearney JN, et al. Development and characterisation of a full-thickness acellular porcine bladder matrix for tissue engineering. Biomaterials. 2007;28:1061-70.

[20] Southgate J, Cross W, Eardley I, Thomas DFM, Trejdosiewicz LK. Bladder reconstruction—from cells to materials. Proceedings of the Institution of Mechanical Engineers, Part H: Journal of Engineering in Medicine. 2003;217:311-6.

[21] Frost MC, Reynolds MM, Meyerhoff ME. Polymers incorporating nitric oxide releasing/generating substances for improved biocompatibility of blood-contacting medical devices. Biomaterials. 2005;26:1685-93.

[22] Sefton MV, Gemmel CH, Gorbet MB. What really is blood compatibility? Journal of Biomaterials Science -- Polymer Edition. 2000;11:1165.

[23] Hsu SH, Tang CM, Tseng HJ. Biocompatibility of poly(ether)urethane-gold nanocomposites. J Biomed Mater Res A. 2006;79:759-70.

[24] Castaneda L, Valle J, Yang N, Pluskat S, Slowinska K. Collagen cross-linking with Au nanoparticles. Biomacromolecules. 2008;9:3383-8.

[25] Hsu S-h, Tang C-M, Tseng H-J. Gold nanoparticles induce surface morphological transformation in polyurethane and affect the cellular response. Biomacromolecules. 2007;9:241-8.

[26] Rai A, Prabhune A, Perry CC. Antibiotic mediated synthesis of gold nanoparticles with potent antimicrobial activity and their application in antimicrobial coatings. Journal of Materials Chemistry. 2010;20:6789-98.

[27] Qu Y, Lü X. Aqueous synthesis of gold nanoparticles and their cytotoxicity in human dermal fibroblasts–fetal. Biomedical Materials. 2009;4:025007.

[28] Freese C, Gibson MI, Klok H-A, Unger RE, Kirkpatrick CJ. Size-and coating-dependent uptake of polymer-coated gold nanoparticles in primary human dermal microvascular endothelial cells. Biomacromolecules. 2012;13:1533-43.

[29] Sperling RA, Rivera Gil P, Zhang F, Zanella M, Parak WJ. Biological applications of gold nanoparticles. Chemical Society Reviews. 2008;37:1896-908.

[30] Lim Z-ZJ, Li J-EJ, Ng C-T, Yung L-YL, Bay B-H. Gold nanoparticles in cancer therapy. Acta Pharmacologica Sinica. 2011;32:983-90.

[31] Whelove OE, Cozad MJ, Lee BD, Sengupta S, Bachman SL, Ramshaw BJ, et al. Development and in vitro studies of a polyethylene terephthalate-gold nanoparticle scaffold for improved biocompatibility. J Biomed Mater Res B Appl Biomater. 2011;99:142-9.

[32] Gu Y-J, Cheng J, Lin C-C, Lam YW, Cheng SH, Wong W-T. Nuclear penetration of surface functionalized gold nanoparticles. Toxicology and applied Pharmacology. 2009;237:196-204.

[33] Everts M, Saini V, Leddon JL, Kok RJ, Stoff-Khalili M, Preuss MA, et al. Covalently linked Au nanoparticles to a viral vector: potential for combined photothermal and gene cancer therapy. Nano Letters. 2006;6:587-91.

[34] Grant SA, Spradling CS, Grant DN, Fox DB, Jimenez L, Grant DA, et al. Assessment of the biocompatibility and stability of a gold nanoparticle collagen bioscaffold. J Biomed Mater Res A. 2013.

[35] Amiel GE, Komura M, Shapira O, Yoo JJ, Yazdani S, Berry J, et al. Engineering of blood vessels from acellular collagen matrices coated with human endothelial cells. Tissue Eng. 2006;12:2355-65.

[36] Williams C, Liao J, Joyce EM, Wang B, Leach JB, Sacks MS, et al. Altered structural and mechanical properties in decellularized rabbit carotid arteries. Acta Biomater. 2009;5:993-1005.

[37] Badylak SF, Freytes DO, Gilbert TW. Extracellular matrix as a biological scaffold material: Structure and function. Acta Biomater. 2009;5:1-13.

[38] Courtney J, Lamba N, Sundaram S, Forbes C. Biomaterials for blood-contacting applications. Biomaterials. 1994;15:737-44.

[39] Mason R, Sharp D, Chuang H, Mohammad S. The endothelium: roles in thrombosis and hemostasis. Archives of pathology & laboratory medicine. 1977;101:61-4.

[40] Mason R, Mohammad S, Saba H, Chuang H, Lee E, Balis J. Functions of endothelium. Pathobiology annual. 1979;9:1.

[41] Bloom AL. Haemostasis and thrombosis: Churchill Livingstone; 1994.

[42] Bader A, Steinhoff G, Strobl K, Schilling T, Brandes G, Mertsching H, et al. Engineering of human vascular aortic tissue based on a xenogeneic starter matrix. Transplantation. 2000;70:7-14.

[43] Hodde JP, Badylak SF, Brightman AO, Voytik-Harbin SL. Glycosaminoglycan content of small intestinal submucosa: a bioscaffold for tissue replacement. Tissue Eng. 1996;2:209-17.

[44] Voytik-Harbin SL, Brightman AO, Kraine MR, Waisner B, Badylak SF. Identification of extractable growth factors from small intestinal submucosa. J Cell Biochem. 1997;67:478-91.

[45] McPHERSON TB, Badylak SF. Characterization of fibronectin derived from porcine small intestinal submucosa. Tissue Engineering. 1998;4:75-83.

[46] Voytik-Harbin SL, Brightman AO, Waisner BZ, Robinson JP, Lamar CH. Small intestinal submucosa: A tissue-derived extracellular matrix that promotes tissue-specific growth and differentiation of cells in vitro. Tissue Engineering. 1998;4:157-74.

[47] Velnar T, Bailey T, Smrkolj V. The wound healing process: an overview of the cellular and molecular mechanisms. Journal of International Medical Research. 2009;37:1528-42.

[48] Glagov S, Zarins C, Giddens D, Ku DN. Hemodynamics and atherosclerosis. Insights and perspectives gained from studies of human arteries. Archives of pathology & laboratory medicine. 1988;112:1018-31.

[49] Rodbard S. Negative feedback mechanisms in the architecture and function of the connective and cardiovascular tissues. Perspectives in biology and medicine. 1969;13:507-27.

[50] Weber KT. Vascular Wound Healing and Restenosis Following Revascularization. In: Weber KT, editor. Wound Healing in Cardiovascular Disease. Armonk , NY: Futura Publishing Company; 1995. p. 137-47.

[51] Thyberg J, Blomgren K, Roy J, Tran PK, Hedin U. Phenotypic modulation of smooth muscle cells after arterial injury is associated with changes in the distribution of laminin and fibronectin. Journal of Histochemistry & Cytochemistry. 1997;45:837-46.

[52] Chamley-Campbell JH, Campbell GR. What controls smooth muscle phenotype? Atherosclerosis. 1981;40:347-57.

[53] Campbell GR, Campbell JH. Smooth muscle phenotypic changes in arterial wall homeostasis: implications for the pathogenesis of atherosclerosis. Experimental and molecular pathology. 1985;42:139-62.

[54] Newby AC, Zaltsman AB. Molecular mechanisms in intimal hyperplasia. The Journal of Pathology. 2000;190:300-9.

Chapter 7

FUTURE WORK

7.1 Future Studies

Worldwide, people are three times more likely to die from cardiovascular disease than infectious and parasitic diseases combined [1]. Cardiovascular disease is a direct cause of mortality and morbidity, and improved treatments must be continually developed and refined [2-4]. The research presented in this dissertation demonstrates the viability of a novel nanomaterial tissue patch as a vascular repair device. However, there are still questions about the long-term effects of the material and its components *in vivo,* as well as its effectiveness in diseased tissue.

In order to continue optimizing blood contacting materials, there needs to be further research into the molecular aspects of the interaction between the native cells and the biomaterial. The first step in future work with this material is to perform more *in vitro* work regarding the reaction between the blood and the nanoparticle coated material. Siminescu et al. showed that certain macrophage phenotypes play a role in the degradation of bioprosthetic heart valves crosslinked with glutaraldehyde, and McDade et al. demonstrated that the use of zero length crosslinkers like EDC allow for a better immune response [5, 6]. Using these types of cell assays, future studies can determine the effects of

AuNPs on the immune response. Cell migration studies can also be used to examine how AuNPs in conjunction with the base material affect different types of immune response cells and various cells associated with long-term wound healing.

All materials used in medicine must be completely explored. Implanting a foreign material with nanoparticles leads to the question of how the nanoparticles will distribute or accumulate within the tissues. It is highly likely they will stay in the immediate area of the biomaterial. However, they might also be up taken by cells and enter the blood stream, and either be excreted or remain in the host tissue. The biocompatibility of AuNPs has been discussed at length in the literature review of this dissertation, and this research did not see a loss of biocompatibility with the use of AuNPs. A study performed by De Jong et al. demonstrated that 100 nm AuNPs were detected only in the blood, liver, and spleen 24 hours after being injected [7]. This indicates where the AuNPs from our biomaterial would go should they disassociate from the material. Future studies should examine the lingering presence of the AuNPs at the implant site as well as the organ distribution and excretion route of 100 nm AuNPs. The degradation of the base material- the porcine decellularized artery- should be studied along with the distribution of the AuNPs. The ECM of the biomaterial should naturally degrade over time. This could be studied using long-term studies and tagging the implant material. Thein et al. showed that a green

fluorescent protein–collagen fusion could be used to tag ECMs [8]. This method could be used to tag our material before implantation in another *in vivo* study.

There are numerous arguments for further *in vivo* testing. The studies contained here show that the material is feasible long-term in a healthy cardiovascular model. An initial concern is that this is a porcine product being tested in swine. Nonfunctional studies using the material as a xenograft in other species should be performed before it is used in humans. Porcine tissue is currently used in human medical applications, so this is not a major concern. A more pressing concern is that the material will be used in diseased individuals with vasculature more fragile than healthy swine. In addition, these studies did not challenge the material with stresses such as increased blood pressure or a high fat diet.

Swine are an excellent cardiovascular model for human medicine since they naturally develop atherosclerosis similar to humans. Reitman et al. demonstrated that Yucatan pigs fed a high fat, high cholesterol diet for 10-12 months had elevated serum cholesterol levels and developed accelerated atherosclerosis [9]. Other swine disease models include partial surgical ligation of the carotid arteries [10]. Our biomaterial could be implanted in one of these models to test its feasibility in diseased vessels. Once implanted, the material could be further stressed by increasing blood pressure through exercise. Emter et al. showed that swine can be trained to exercise on treadmills [11]. The use of exercise would stress the biomaterial and also allow studies to be performed

examining the effects of exercise and vascular remodeling. The results of these studies will further bolster the biomaterial's positive attributes.

` The final aspect of future work to be performed is that of medical applications for this material. In Chapters 5 and 6 we demonstrate the feasibility of this material *in vivo,* and its benign long-term response within the host. These are all positive attributes of the material and should be considered not only for vascular repair, but for heart valve leaflets and cardiac wall repairs. The blood compatibility of the material, as well as its integration abilities make it an excellent candidate for a wide variety of applications.

In conclusion, this dissertation has begun the extensive research needed to characterize, optimize, and discover the *in vivo* feasibility of a novel nanomaterial-tissue patch. The research supports the conclusion that a biomaterial comprised of decellularized, crosslinked porcine arterial tissue conjugated with gold nanoparticles is biocompatible as well as blood compatible and can integrate into host vascular tissue with minimum of scar formation and other negative effects. There is still much research that needs to be performed in order to understand how the material is interacting with the host tissue at a molecular level, as well as further *in vivo* studies to test it in diseased animal models. The further development of this material has the potential to advance a state-of-the-art class of biomaterials.

7.2 References

[1] Yusuf S, Reddy S, Ôunpuu S, Anand S. Global Burden of Cardiovascular Diseases: Part I: General Considerations, the Epidemiologic Transition, Risk Factors, and Impact of Urbanization. Circulation. 2001;104:2746-53.

[2] Weber KT. Vascular Wound Healing and Restenosis Following Revascularization. In: Weber KT, editor. Wound Healing in Cardiovascular Disease. Armonk , NY: Futura Publishing Company; 1995. p. 137-47.

[3] Bordenave L, Menu P, Baquey C. Developments towards tissue-engineered, small-diameter arterial substitutes. Expert review of medical devices. 2008;5:337-47.

[4] Tu JV, Pashos CL, Naylor CD, Chen E, Normand S-L, Newhouse JP, et al. Use of Cardiac Procedures and Outcomes in Elderly Patients with Myocardial Infarction in the United States and Canada. New England Journal of Medicine. 1997;336:1500-5.

[5] McDade JK, Brennan-Pierce EP, Ariganello MB, Labow RS, Michael Lee J. Interactions of U937 macrophage-like cells with decellularized pericardial matrix materials: Influence of crosslinking treatment. Acta biomaterialia. 2013;9:7191-9.

[6] Simionescu D, Simionescu A, Deac R. Detection of remnant proteolytic activities in unimplanted glutaraldehyde-treated bovine pericardium and explanted cardiac bioprostheses. Journal of biomedical materials research. 1993;27:821-9.

[7] De Jong WH, Hagens WI, Krystek P, Burger MC, Sips AJ, Geertsma RE. Particle size-dependent organ distribution of gold nanoparticles after intravenous administration. Biomaterials. 2008;29:1912-9.

[8] Thein MC, McCormack G, Winter AD, Johnstone IL, Shoemaker CB, Page AP. Caenorhabditis elegans exoskeleton collagen COL-19: An adult-specific marker for collagen modification and assembly, and the analysis of organismal morphology. Developmental Dynamics. 2003;226:523-39.

[9] Reitman JS, Mahley RW, Fry DL. Yucatan miniature swine as a model for diet-induced atherosclerosis. Atherosclerosis.43:119-32.

[10] Ishii A, Viñuela F, Murayama Y, Yuki I, Nien YL, Yeh DT, et al. Swine Model of Carotid Artery Atherosclerosis: Experimental Induction by Surgical Partial

Ligation and Dietary Hypercholesterolemia. American Journal of Neuroradiology. 2006;27:1893-9.

[11] Emter CA, Tharp DL, Ivey JR, Ganjam VK, Bowles DK. Low-intensity interval exercise training attenuates coronary vascular dysfunction and preserves Ca2+-sensitive K+ current in miniature swine with LV hypertrophy. American Journal of Physiology-Heart and Circulatory Physiology. 2011;301:H1687-H94.

VITA

Allison M. Ostdiek was born in Maywood, IL to Thomas and Lynda Ostdiek and grew up in Villa Park, IL. She did her undergraduate work in Animal Sciences at the University of Minnesota-Minneapolis/St. Paul, MN. Allison then attended veterinary school at the University Of Illinois College Of Veterinary Medicine where she graduated with her DVM in the spring of 2010.

In the fall of 2010 Allison began a comparative medicine residency and Ph.D program at the University of Missouri, supported by NIH T32 grant funding. She pursued a Doctorate of Philosophy in Veterinary Pathoiology in the lab of Dr. Sheila Grant characterizing and optimizing a novel nanocomposite vascular repair material in addition to performing her clinical laboratory animal duties. Besides biomaterials research Allison also enjoys working with large laboratory animals, performing surgery, and clinical veterinary medicine.